2-13-2014

Wideband Autonomous Cognitive Radios: Spectrum Awareness and PHY/MAC Decision Making

Yang Li

Yang Li

Candidate

Department of Electrical and Computer Engineering

Department

This dissertation is approved, and it is acceptable in quality and form for publication:

Approved by the Dissertation Committee:

Dr. Sudharman K. Jayaweera , Chairperson

Dr. Christos G. Christodoulou

Dr. Wei Wennie Shu

Dr. Guoyi Zhang

Wideband Autonomous Cognitive Radios: Spectrum Awareness and PHY/MAC Decision Making

by

Yang Li

B.E., Electrical Engineering, Beijing University of Aeronautics and Astronautics, 2005

M.S., Electrical Engineering, New Mexico Tech, 2009

DISSERTATION

Submitted in Partial Fulfillment of the

Requirements for the Degree of

Doctor of Philosophy

Engineering

The University of New Mexico

Albuquerque, New Mexico

December, 2013

Submitted by: Yang Li

Advisor: Dr. Sudharman K. Jayaweera
Department of Electrical and Computer Engineering
University of New Mexico

Committee Members: Dr. Christos G. Christodoulou
Department of Electrical and Computer Engineering
University of New Mexico

Dr. Wei Wennie Shu
Department of Electrical and Computer Engineering
University of New Mexico

Dr. Guoyi Zhang
Department of Mathematics and Statistics
University of New Mexico

Dedication

To my wife, Yi, my mother, Shanlin, and my wife's parents, Anyu and Fengying, for their encouragement and support.

"The real voyage of discovery consists not in seeking new landscapes but in seeing with new eyes."
– Marcel Proust

Acknowledgments

First, I would like to thank my advisor, Professor Sudharman K. Jayaweera, for his support and guidance over the past 4 years at UNM. His insightful advices were essential in achieving this work and in helping me to develop my career. Working with Professor Jayaweera has been a great learning experience for me. I am very grateful for his efforts and encouragement during this work. I would like also to thank my committee members, Professor Christos G. Christodoulou, Professor Wei Wennie Shu, and Professor Guoyi Zhang, for their help and support. I am very thankful for them serving as my committee members.

I would like to also thank my lab colleagues for making the work environment at UNM a more friendly place. I am so grateful for their collaboration and the time we spent together throughout our journey at UNM.

Last, but not least, I would like to thank my extended family for their encouragement and support.

Wideband Autonomous Cognitive Radios: Spectrum Awareness and PHY/MAC Decision Making

by

Yang Li

B.E., Electrical Engineering, Beijing University of Aeronautics and Astronautics, 2005

M.S., Electrical Engineering, New Mexico Tech, 2009

Ph.D., Engineering, University of New Mexico, 2013

Abstract

The cognitive radios (CRs) have opened up new ways of better utilizing the scarce wireless spectrum resources. The CRs have been made feasible by recent advances in software-defined radios (SDRs), smart antennas, reconfigurable radio frequency (RF) front-ends, and full-duplex RF front-end architectures, to name a few. Generally, a CR is considered as a dynamically reconfigurable radio capable of adapting its operating parameters to the surrounding environment. Recent developments in spectrum policy and regulatory domains also allow more flexible and efficient utilization of wider RF spectrum range in the future. In line with the future directions of CRs, a new vision of a future autonomous CR device, called Radiobots, was previously proposed. The goals of the proposed Radiobot surpass the dynamic spectrum access (DSA) to achieve wideband operability and the main features of cognition. In order to ensure the practicality and robust operation of the Radiobot

structure, the research focus of this dissertation includes the following aspects: 1) robust spectrum sensing and operability in a centralized CR network setup; 2) robust multivariate non-parametric quickest detection for dynamic spectrum usage tracking in an alien RF environment; 3) joint physical layer and medium access control layer (PHY/MAC) decision-making for wideband bandwidth aggregation (simultaneous operation over multiple modes/networks); and 4) autonomous spectrum sensing scheduling solutions in an alien ultra wideband RF environment.

The major contribution of this dissertation is to investigate the feasibility of the autonomous CR operation in heterogeneous RF environments, and to provide novel solutions to the fundamental and crucial problems/challenges, including spectrum sensing, spectrum awareness, wideband operability, and autonomous PHY/MAC protocols, thus bringing the autonomous Radiobot one step closer to reality.

Contents

List of Figures

List of Tables

Publications

In the following, we present a list of journal and conference publications that have resulted from the work in this dissertation.

Journal Publications

1. Y. Li, S. K. Jayaweera, M. Bkassiny, and C. Ghosh, "Learning-aided Sub-band Selection Algorithms for Spectrum Sensing in wideband Cognitive Radios", IEEE Transaction on Wireless Communications, 2013 [In review].

2. M. Bkassiny, S. K. Jayaweera, and Y. Li, "Multidimensional Dirichlet Process-based Non-Parametric Signal Classification for Autonomous Self-Learning Cognitive Radios", *IEEE Transaction on Wireless Communications*, vol.PP, no.99, pp.1-11, Aug 2013.

3. Y. Li, S. K. Jayaweera, "Dynamic Spectrum Tracking using Energy and Cyclostationarity based Multivariate Non-parametric Quickest Detection For Cognitive Radios", *IEEE Transaction on Wireless Communications*, vol.12, no.7, pp.3522-3532, July 2013.

4. Y. Li, S. K. Jayaweera, M. Bkassiny, and K. A. Avery, "Optimal myopic sensing and dynamic spectrum access in cognitive radio networks with low-complexity

implementations", *IEEE Transactions on Wireless Communications*, vol.11, no.7, pp.2412-2423, July 2012.

5. M. Bkassiny, Y. Li and S. K. Jayaweera, "A survey on machine-learning techniques in cognitive radios", *IEEE Communications Surveys and Tutorials*, vol.15, no.3, pp.1136-1159, Third Quarter 2013.

6. M. Bkassiny, Y. Li, G. El-Howayek, S. K. Jayaweera and C. G. Christodoulou, "Recent Patents on Spectrum Sensing Methods and RF Architectures for Cognitive Radios", *Journal of Recent Patents on Computer Science, Special Issue on Recent Advances in Cognitive Radio Communications, Bentham Science Publishers Ltd.*, vol.5, no.2, pp.83-92, Aug. 2012.

7. M. Bkassiny, S. K. Jayaweera, Y. Li, and K. A. Avery, "Wideband Spectrum Sensing and Non-Parametric Signal Classification for Autonomous Self-Learning Cognitive Radios", *IEEE Transactions on Wireless Communications*, vol.11, no.7, pp.2596-2605, July 2012.

Conference Publications

1. Y. Li, S. K. Jayaweera, C. Ghosh and M. Bkassiny, "Learning-aided Sensing Scheduling for wideband Cognitive Radios", *Workshop on Wideband Cognitive Radio Communications and Networks (WCRCN) at IEEE Vehicular Technology Conference (VTC-Fall 13)*, Las Vegas, NV, USA, Sept. 2013.

2. M. Bkassiny, S. K. Jayaweera, Y. Li and K. A. Avery, "Blind cyclostationary feature detection based spectrum sensing for autonomous self-learning cognitive radios", *IEEE International Conference on Communications (ICC '12)*, Ottawa, Canada, June 2012.

Publications

3. Y. Li, S. K. Jayaweera and C. G. Christodoulou, "Wideband PHY/MAC Bandwidth Aggregation Optimization for Cognitive Radios", *3rd International Workshop on Cognitive Information Processing (CIP '12)*, Parador de Baiona, Spain, May, 2012.

4. S. K. Jayaweera, Y. Li, M. Bkassiny, C. G. Christodoulou and K. A. Avery, "Radiobots: Architecture, Algorithms, and Realtime Reconfigurable Antenna Designs for Autonomous, Self-learning Future Cognitive Radios", *IEEE International Symposium on Intelligent Signal Processing and Communication Systems (ISPACS '11)*, Chiangmai, Thailand, Dec. 2011.

5. Y. Li, S. K. Jayaweera, M. Bkassiny and K. A. Avery "Optimal Myopic Sensing and Dynamic Spectrum Access with Low-Complexity Implementations," *IEEE Vehicular Technology Conference (VTC-spring 2011)*, Budapest, Hungary, May 2011.

6. M. Bkassiny, S. K. Jayaweera, Y. Li, and K. A. Avery "Optimal and Low-complexity Algorithms for Dynamic Spectrum Access in Centralized Cognitive Radio Networks with Fading Channels," *IEEE Vehicular Technology Conference (VTC-spring 2011)*, Budapest, Hungary, May 2011.

Glossary

3GPP	Third Generation Partnership Project
ACS	Almost-cyclostationary
ADC	Analog-to-digital converter
ARL	Average run length
BAG	Bandwidth aggregation
CA	Carrier aggregation
CC	Component carrier
CR	Cognitive radio
DSA	Dynamic spectrum access
DSS	Dynamic spectrum sharing
FCC	Federal communications commission
FFT	Fast Fourier transform
HMM	Hidden Markov model
i.i.d.	independent identically distributed

ISM	Industrial, Scientific and Medical
LTE	Long Term Evolution
LTE-A	Long Term Evolution-Advanced
LTV	Linear time-variant
MAC	Medium access control
MAP	Maximum *a posteriori* probability
MDP	Markov decision process
MMSE	Minimum mean-squared error
NP	Neyman-Pearson
NBP	National broadband plan
OSA	Opportunistic spectrum access
pdf	Probability density function
PLL	phase-locked loop
pmf	Probability mass function
PHY	Physical layer
POMDP	Partially observable Markov decision process
PSD	Power spectral density
PU	Primary user
QD	Quickest detection

Glossary

QoS	Quality of Service
RF	Radio frequency
RL	Reinforcement learning
SCF	Spectral correlation function
SDR	Software-defined radio
SNR	Signal-to-noise ratio
SSDC	Secondary system decision center
SU	Secondary user
TD	Temporal difference
WSS	Wide-sense stationary
WSSUS	Wide-sense stationary uncorrelated scattering

Chapter 1

Introduction

The increasing demand for mobile wireless services, including web browsing, video telephony, and video streaming, with various constraints on delay and bandwidth requirements, challenges the future generation wireless communication networks. Unfortunately, on the other hand, recent radio frequency (RF) spectrum measurement studies have shown that the licensed spectrum bands are severely under-utilized at any given time and location [1, 2], mainly due to the traditional static spectrum regulation. Under such a spectrum regulation, each spectrum band is assigned to a designated party, which is given an exclusive spectrum usage right for a specific type of service and radio device. This has resulted in an awkward situation, in which, radio devices with high demands of bandwidth are not allowed to utilize the under-utilized spectrum bands, if they are not licensed to those bands. This situation has naturally led us to consider whether it is possible to make changes to the regulation rules of the limited wireless spectrum resource.

Cognitive radio (CR) has opened up a new way of better utilizing the scarce wireless spectrum resource. The concept of CR was first proposed in 1999 by Joseph Mitola III, in his pioneering work [3]. The CRs are proposed to help mitigate the

spectrum scarcity problem by enabling dynamic spectrum access (DSA), which allows unlicensed users/devices to identify the under-utilized portions of licensed spectrum and utilize them opportunistically as long as they do not cause any harmful interference to the communications of the licensed users. A CR may accomplish this goal if it is capable of dynamically adapting its operating parameters according to the surrounding dynamic RF environment. The temporarily unused portions of spectrum are called spectrum white spaces that may exist in time, frequency, and space domains. In the context of DSA, the licensed users are called primary users (PUs) and the CR users are called secondary users (SUs). There has been a rapidly increasing interest in CR due to its potential for reshaping the way of utilizing spectrum resources. The CR has also been made feasible by recent advances such as software-defined radio (SDR), smart/reconfigurable antennas, and reconfigurable radio frequency (RF) front-ends.

On the other hand, recent developments in spectrum policy and regulatory domains, notably the release of the National Broadband Plan (NBP) [4] from the Federal communications commission (FCC), the publication of final rules for TV white spaces, and the ongoing proceeding for secondary use of the 2360-2400 MHz band for medical body area networks, will allow more flexible and efficient use of spectrum in the future. These important changes open up exciting opportunities for CR to enable and support a variety of emerging applications [5], ranging from smart grid, public safety and broadband cellular, to medical applications. To address the pressing shortage of spectrum to meet the ever increasing communication demands, the NBP recommends further freeing up 500MHz of spectrum for broadband use in the next 10 years with 300MHz being made available for mobile use in the next five years [4]. The plan proposes to achieve this goal in a number of ways: incentive auctions, repacking spectrum, and enabling innovative spectrum access models that take advantage of opportunistic spectrum access (OSA) and cognitive techniques. The plan urges the FCC to initiate further developments on OSA beyond the already

completed TV white space allocation.

In-line with the above vision of wideband application of CRs, the *Radiobot* architecture proposed in [6–11] envisions broadband CRs that are not limited to a single radio network. The Radiobot is defined as: *an intelligent wireless communication device that has the ability to autonomously reason and learn from the observed RF environment to self-decide optimal communications mode for existing conditions and to achieve current performance objectives, and can optimally self-reconfigure its hardware to physically realize the selected mode of communication.* The Radiobot is envisioned to be able to evaluate and choose among many optimality criteria, such as communication delay constraints, power consumption constraints, sensing accuracy requirements, and security requirements, etc. Also, we do not rule out the possibility that a Radiobot may develop its own optimality criteria by trading off pros and cons of multiple conflicting requirements. The Radiobot concept aims at future autonomous and self-reconfigurable wideband CRs, which indeed puts up challenges to RF hardware, analog/digital circuits, and signal processing software industries.

In order to achieve the desired goals of the wideband operable Radiobot, we may project the following five fundamental challenges of the Radiobot: 1) spectrum sensing; 2) spectrum decision; 3) spectrum sharing; 4) wideband operability; and 5) Autonomous cognition. The spectrum sensing refers to the capability of identification of spectrum opportunities (or white spaces) and the onset of other radio activities in the operating frequency range. The spectrum decision refers to the capability of selecting and utilizing the most appropriate available spectrum band to fulfill the communication demands, as well as the capability of adjusting the physical layer and/or medium access control layer (PHY/MAC) in order to communicate more reliably and efficiently. The spectrum sharing involves the actions of cooperation with other radios in order to maintain an organized and efficient spectrum access fashion, in either a centralized network or a decentralized network. The wideband operability

involves both RF hardware reconfigurations and signal processing capabilities, with which, the Radiobot may achieve flexible and robust wideband operations. Finally, the autonomous cognition refers to the capabilities of self learning and reasoning in order to autonomously and effectively perform all the previously mentioned functionalities to survive in an alien RF environment. Although some self-learning aspects are indeed present in this dissertation, the research focus is mainly on the first four aforementioned challenges.

In the following, we introduce each of the covered topics in this dissertation. Note that the aforementioned challenges/functionalities of the Radiobot closely interact with each other and the interaction among the functionalities itself is, in fact, of our research interest. As a result, each of the topics covered in this dissertation is essentially scenario-based and may address multiple or all of the aforementioned challenges/functionalities.

1.1 Myopic Spectrum Sensing in Centralized CR networks

Spectrum sensing has been identified as a major task for CRs in order to achieve awareness of their dynamic RF environments and to capture the spectrum opportunities [12, 13]. Many sensing techniques have been proposed over the last decade based on matched filter, energy detection, cyclostationary detection, wavelet detection and covariance detection [13–20]. Cooperative spectrum sensing was also proposed as a means of improving the sensing accuracy and relaxing the sensing burdens of each individual CR.

In this topic, we consider a DSA problem in a centralized CR network with multiple cognitive SUs. The network of the SUs are supposed to perform spectrum

sensing cooperatively in order to find spectrum opportunities. In this CR network, we assume a central unit, named the secondary system decision center (SSDC), that is responsible for organizing the rest of the SUs in the same network. In particular, the SSDC is responsible for making decisions on which SUs should sense which channels, as well as the decisions on which SUs should access which channels, based on the sensing history and the dynamics of the RF environment. The individual sensing results from each and every SUs are supposed to be transmitted to the SSDC through control channels to facilitate the above mentioned decision-making at the SSDC. The objective of the SSDC is to maximize the overall network communication throughput. The centralized optimal myopic channel sensing and access policy are derived based on the assumption of the Markov properties of the communication channels. Note that, by *optimal myopic* policy, we refer to the policy that is optimal within the class of myopic policies. By *myopic policies*, we refer to the class of policies that aim at maximizing the instantaneous rewards (or in our case, the communication throughput) as opposed to the long term reward by considering the impacts of current action to future reward. Note that, although this DSA problem can be formulated as a a Partially observable Markov decision process (POMDP) problem [21] if one desires the optimal solution, the motivation of finding the optimal myopic solution rather than the optimal solution is due to the high computational complexity because of the continuum of the state space in a POMDP formulation, as also noted in [22–26].

Many schemes presented in literature such as in [22–26] have previously proposed and derived the *myopic* channel sensing solutions under certain assumptions and conditions. For example, assuming that the state transition probabilities are partially known, [22, 23, 25] developed a myopic channel sensing strategy and proved that this *myopic* policy is the optimal POMDP solution under the assumption of a certain ordering of the state transition probabilities. However, this *myopic* policy was derived for a single SU without explicitly considering multiple SUs with transmission collisions and their possible cooperations. In [24], as a follow-up work of [22, 23],

the proposed myopic policy is extended to any number of primary channels with no limitation on the number of the primary channels the SU can sense at each time, which means that multiple channel selection is considered. However, possible SU cooperations and SU allocation issues are not discussed. On the contrary, our proposed optimal myopic solution is applicable to any number of primary channels, any number of SUs, and any primary channel Markov model parameters. Our proposed solution is more realistic since our solution explicitly assigns SUs to sense specific primary channels by taking into account the spatial and temporal variations of channel fading on different primary channels. Moreover, to support our optimal myopic sensing solution, we also proposed an effective Markov parameter estimation algorithm when the channel Markov properties are unknown.

1.2 Cyclostationarity-based Spectrum Sensing

In this topic, we propose a cyclostationarity-based signal feature extraction algorithm for spectrum sensing. In particular, this signal feature extraction algorithm is used to detect the signal cyclic frequency components in a communication channel or multiple signal features in a set of communication channels. Compared to other existing cyclostationarity-based spectrum sensing algorithms [], our proposed algorithm does not require any *a priori* signal knowledge, which makes it a suitable technique for autonomous Radiobots that is assumed to be able to operate in alien RF environments. Note that the extracted cyclostationary signal features may correspond to the symbol duration, and coding rates, etc. The robustness of this proposed signal feature extraction algorithm is evaluated under multi-path channel fading and Doppler effects. For a set of communication channels, we show analytically that the proposed feature extraction algorithm can potentially capture the features of multiple superposed signals.

Note that the proposed cyclostationarity-based signal feature extraction algorithm also plays an important role in the topic discussed in Chapter 4, the multivariate non-parametric quickest detection.

1.3 Multivariate Non-parametric Quickest detection

Spectrum awareness is one of the most critical elements of any CR system [6]. Previous work on CRs and dynamic spectrum sharing (DSS) often assumes that the CR networks are time-slotted as assumed in Chapter 2 (also see [27] and references therein). In time-slotted CR networks, the primary users (PUs) become active or idle at the start of a time slot. During one time slot, the PUs state is not changed. Therefore, the secondary users (SUs) can spend a short sensing period at the beginning of each time slot to determine the spectrum availability. At the end of the sensing period, SUs may transmit their data if the inferred spectrum state is idle, otherwise they must remain silent. However, in more general cases, primary networks may not be time-slotted. Even when they are time-slotted, autonomous CRs may not be able to be synchronized with the primary networks due to the absent of the knowledge of the primary signaling. As a result, the PUs may change their states at any time from the point of view of autonomous CRs, and thus the CR networks are non-time-slotted. Performing traditional periodic spectrum sensing is no longer sufficient to keep track of the state changes of the communication channels in non-time-slotted CR networks. Instead, one may have to resort to the quickest detection (QD) methods.

In this topic, a novel non-parametric, multi-variate QD method is proposed for CRs using both energy and cyclostationary features. The proposed approach can

be used to track state dynamics of communication channels. This capability can be useful for both DSS and future CRs, as in practice, centralized channel synchronization may not be always valid and the prior information of the statistics of channel usage can be sometimes hard to obtain. The proposed multi-variate non-parametric average sample power and cyclostationarity-based QD scheme is shown to achieve better performance compared to traditional energy-based QD schemes. We also develop a parallel on-line QD/off-line change-point detection algorithm to achieve self-awareness of detection delays and false alarms for higher level automation. Compared to traditional energy-based QD schemes, the proposed multi-variate non-parametric QD scheme has comparable computational complexity. The simulated performance shows improvements in terms of small detection delays and significantly higher percentage of spectrum utilization.

Note that, the proposed non-parametric QD scheme in this topic can be used for detecting both state transitions from idle to busy, and those from busy to idle. Since the only transmission opportunities for a CR happen when the channel is idle, it is desirable to actually utilize the channel while the QD is in progress detecting a state change from idle to busy. However, this may not be possible when a CR uses traditional half-duplex radio front-ends since they do not support simultaneous transmission and reception of different signals in the same channel. As a result, it is advantageous to consider a possible full-duplex RF front-end in this context. Several full-duplex proposals haven been shown in literature [28–31] due to recent advances in RF front-ends. Note that although the full-duplex radio front-ends can provide benefits in terms of transmission, the proposed QD method does not depend on the full-duplex radio front-ends and works equally well with traditional half-duplex front-ends. In this topic, full-duplex radio front-ends are not discussed any further. The incorporation is left as a future task.

1.4 Wideband PHY/MAC Bandwidth Aggregation Optimization For CRs

The simultaneous transmission over multiple radio interfaces by a single mobile terminal has been previously discussed in the literature under the term of the bandwidth aggregation (BAG) [32–37] (also known as channel aggregation), which aims at performing simultaneous use of multiple interfaces to improve transmission quality or throughput depending on specific architectural designs. A similar idea called Carrier aggregation (CA) can also be found in recent literature on the Third Generation Partnership Project Long Term Evolution-Advanced (3GPP LTE-A) [38–41]. With CA, mobile users can access a much wider transmission bandwidth up to 100 MHz compared with LTE Release 8 standard (up to 20 MHz) [38]. This is achieved by aggregating two or more individual component carriers (CCs) belonging to contiguous or non-contiguous frequency bands [38], essentially scheduling a mobile user on multiple CCs simultaneously.

In [32] the authors proposed the Earliest Delivery Path First (EDPF) scheduling algorithm that partitions the traffic onto different interfaces such that the quality of service (QoS) requirements of the application are met. In [33] an adaptive medium access control (A-MAC) layer was proposed to address the heterogeneities posed by the next generation wireless networks. The proposed A-MAC introduced a two-layered MAC framework that performs medium access to multiple networks without requiring any additional modifications in the existing network structures. In [34] the authors proposed a multi-path transmission control scheme combining BAG and packet scheduling for real-time streaming in a multi-path environment, in which the packet scheduling scheme was aimed at arranging the transmission sequence in order to effectively minimize the impact of packet reordering at the receiver. In [35], the authors investigated the BAG problem under certain practical limitations and cost

issues such as switching delays and transmission delays, but without considering the power consumption. It is not realistic, however, to ignore the power consumption of the CR since it can be a crucial limitation for many radio devices operating on limited energy sources such as batteries. Moreover, the practical issue of time-varying channel coefficients was also not considered in [35]. In [36], the BAG problem was studied without considering hardware limitations, switching costs and delays, channel coefficients, and power consumptions. In [37], a spectrum assignment strategy was proposed to increase the BAG-aware access capacity and to decrease channel switching times. However, this was again obtained without considering essential practical issues such as power consumption and channel fading.

In this topic, in order to develop the wideband operability of the Radiobot, we propose a CR PHY/MAC decision-making strategy that may simultaneously utilize multiple radio networks across a wide spectrum band. The whole spectrum range is assumed to be divided into several sub-bands in performing spectrum sensing. Each of the sub-bands may have an arbitrary bandwidth, depending on the spectrum sensing capability of the CR. We derive an optimal wideband bandwidth aggregation (BAG) strategy for the energy and frequency efficient communication problem: a multi-objective optimization problem is formulated, one objective is the communication throughput of the mobile cognitive radio device and the other is energy consumption of the device. The proposed multi-objective optimization problem takes into account the essential practical issues including imperfect spectrum sensing, time varying channel coefficients, hardware reconfiguration time delay, hardware reconfiguration power consumptions, and communication power consumptions. The optimal BAG strategy is solved using a combination of the Hungarian algorithm and convex optimization. In this topic, we show that by self-adjusting the weighting coefficients of two objectives, the CR may achieve autonomous operation. The formulation can also be easily extended to multi-objective problems that have more than two objectives.

1.5 Learning aided scheduling for wideband spectrum sensing

In order to achieve wideband operability, we propose, in this topic, the wideband spectrum sensing scheduling solutions for CRs that are equipped with reconfigurable RF front-ends. The wide frequency spectrum of interest is assumed to be segmented into frequency sub-bands due to software and hardware limitations. These sub-bands can be non-contiguous, and each may contain an arbitrary number of channels from an arbitrary number of systems. It is assumed that the CR can only sense one sub-band at a time.

Note that many schemes presented in CR literature, such as in [25, 27, 42], have previously proposed and derived the channel sensing algorithms for narrow-band scenarios. As opposed to the wideband spectrum sensing, in narrow-band spectrum sensing problems, hardware reconfigurations are generally not considered. For example, the authors in [27] developed an optimal myopic[1] sensing scheduling policy in a centralized multi-agent setup for a group of traditional narrow-band CRs with a given set of channels. In [25], assuming that the channel state transition probabilities are partially known, the authors developed a myopic channel sensing strategy for the narrow-band CRs and proved that this myopic policy is the optimal Partially Observable Markov Decision Process (POMDP) solution under the assumption of a certain ordering of the state transition probabilities of individual channels. In [42], the authors developed stationary optimal spectrum sensing and access policies under the framework of POMDP to maximize the CRs throughput on a given set of channels in a narrow-band setup with battery life constraints. However, these spectrum sensing

[1]Myopic policies aims at maximizing an instantaneous reward at each time step, as opposed to a long-term reward as considered in a Partially Observable Markov Decision Process (POMDP) setup [21,43]. The optimal myopic solution refers to the optimal solution within the class of myopic policies.

policies cannot be easily applied in a wideband spectrum sensing scenario since the reconfigurable RF front-end is not considered and the reconfiguration costs (both energy and the incurred time delays by performing RF front-end reconfiguration) are not taken into account to jointly optimize the performance. As a result, we propose the wideband spectrum sensing scheduling policies with realistic reconfigurable RF front-end considerations. In [44], the authors investigated optimal sensing time and power allocation strategies in order to maximize the transmission throughput in a wideband sensing setup. However, there is a fundamental difference between our system setup and the one in [44]. In particular, what is meant by 'wideband' in our system is different from that of [44], and all similar previous work. In [44], wideband sensing refers to simultaneous sensing of a frequency band containing multiple narrowband channels. The term wideband is justified because the spectrum spanned by these channels can be larger compared to a single narrowband channel. However, the wideband system assumed in this work is conceivably much wider than that of [44]. In fact, the wide spectrum band considered in [44] is somewhat equivalent to a single sub-band assumed in our setup. In [44] and other similar previous work, the wideband operation is limited by the RF front-end and the A/D circuits, whereas our wideband CRs are presumed to be equipped with real-time reconfigurable RF front-ends covering a set of wide spectrum ranges in each mode of operation, and each of these spectrum ranges are divided into a set of sub-bands that are still wide and may contain multiple (narrowband) channels [6, 8, 45]. Clearly, given the state-of-the-art wideband antenna/RF front-end designs [46–49], and the signal processing burdens, the wideband assumption in those previous proposals can only imply something akin to one of the sub-bands assumed in our work. As a result, while spectrum sensing decisions in many of the previous proposals are concerned with channel selection, our focus is on the problem of which subset of channels (i.e. the sub-band) to sense.

Three sub-band selection policies are proposed to find spectrum opportunities taking into account realistic hardware reconfiguration energy consumptions and time

delays. Two of the proposed policies rely on the individual channel Markov properties and the sub-band Markov properties, respectively. Although these two policies may achieve good performance, they rely on complete knowledge of RF environment dynamics and thus may become computationally demanding. The third sub-band selection policy based on Q-learning is proposed to circumvent this. Performance of the three policies are compared and discussed against a performance upper-bound of the optimal solution to the corresponding partially observable Markov decision process formulation. The suitability of the Q-learning technique is validated by showing that it achieves good performance through numerical results in both simulated and real measured RF environments.

1.6 Dissertation Contributions

The main contributions of this dissertation can be summarized as follows:

- 1) The formulation of a centralized spectrum sensing/access architecture that allows exploitation of all available primary spectrum opportunities; 2) proposing the optimal myopic spectrum sensing policy; and 3) proposing sub-optimal myopic sensing policies with low-complexity implementations and performance close to the myopic policy. We also show that our proposed sensing/access policies are close to the optimal POMDP solution and outperforms other existing strategies. We also propose a Hidden Markov Model based algorithm to estimate the parameters of primary channel Markov models when the knowledge is absent. This parameter estimation algorithm runs with a *linear* complexity.

- The propose of a non-parametric cyclostationarity-based signal feature extraction algorithm that is able to extract multiple superposed RF signals and identify their associated cyclostationary features. Unlike existing cyclostationarity-

based spectrum sensing algorithms, the proposed algorithm does not rely on the prior knowledge of the target signals. The robustness of this algorithm is also evaluated under the impact of channel fading and the Doppler effect.

- 1) The proposal of the average sample power and cyclostationarity-based multivariate non-parametric quickest detection (QD) strategy for CRs; and 2) the proposal of the parallel on-line QD/off-line change-point detection strategy that is used to provide information of detection delays and false alarm rates as feedback for possible machine learning techniques to achieve future autonomous operation. Note that originally multivariate non-parametric QD strategy was proposed in [50]. The computational complexities of the energy-based univariate non-parametric QD method and the multivariate non-parametric QD method are also compared. We show that the multivariate QD method has a comparable complexity to the uni-variate case, depending on the choice of time window length of each sensing step. The simulation also shows that the proposed multivariate QD method outperforms the energy-based uni-variate case, in terms of the detection delays and the percentage of idle channel usage.

- We propose a CR PHY/MAC decision-making strategy that may simultaneously utilize multiple radio networks across a wide spectrum band. We derive an optimal *wideband* bandwidth aggregation (BAG) strategy for the energy and frequency efficient communication problem: a multi-objective optimization problem is formulated, one objective is the communication throughput of the mobile CR device and the other one is energy consumption of the device. The proposed multi-objective optimization problem takes into account the practical issues including imperfect spectrum sensing, time varying channel coefficients, hardware reconfiguration time delay, hardware reconfiguration power consumptions, and communication power consumptions. The optimal BAG strategy is solved using a combination of the *Hungarian* algorithm and

convex optimization. We show that by self-adjusting the weighting coefficients of two objectives, the CR may achieve autonomous operation. The formulation can also be easily extended to similar optimization problems with more than two objectives.

- We propose wideband spectrum sensing scheduling solutions for CRs that are equipped with reconfigurable RF front-ends. Three sub-band selection policies are proposed to find spectrum opportunities taking into account realistic hardware reconfiguration energy consumptions and time delays. Two of the proposed policies rely on the individual channel Markov properties and the sub-band Markov properties, respectively. Although these two policies may achieve good performance, they rely on complete knowledge of RF environment dynamics and thus may become computationally demanding. The third sub-band selection policy based on Q-learning is proposed to circumvent this. Performance of the three policies are compared and discussed against a performance upper-bound of the optimal solution to the corresponding POMDP formulation. The suitability of the Q-learning technique is validated by showing that it achieves good performance through numerical results in both simulated and real measured RF environments.

1.7 Structure of the Dissertation

The remainder of this dissertation is organized as follows: Chapter 2 proposes an optimal myopic spectrum sensing policy in centralized CR networks. In Chapter 3, we present the proposed cyclostationarity-based signal feature extraction algorithm. We also evaluate its robustness under channel fading and Doppler effect. In Chapter 4, we propose the multivariate non-parametric quickest detection algorithm for CRs. In Chapter 5, we present the general framework and solution for the wideband band-

width aggregation problem. In Chapter 6, we present the proposed Machine-learning aided sub-band selection scheduling in wideband spectrum sensing problems. Finally, we conclude the dissertation in Chapter 7.

1.8 Notation

Throughout this dissertation, we use bold characters to refer to vector and matrix quantities.

Chapter 2

Optimal Myopic Sensing and Dynamic Spectrum Access in CR Networks

2.1 Introduction

In this chapter, we consider a centralized CR network in which multiple cognitive secondary users (SUs) with limited spectrum sensing capabilities cooperatively find and access spectrum white-spaces on multiple primary channels. The objective is to design the combined optimal channel sensing and access policy. This combined optimal policy maximizes the total secondary system throughput accrued over time over all primary channels. This policy is also required to satisfy a constraint on the probability of collisions with licensed transmissions. We assume that the decision-making (both sensing and access) in the CR network is centralized: a central unit, called the *secondary system decision center* (SSDC), gathers all channel sensing results from SUs over a dedicated control channel; the decisions of sensing and access are made

at the SSDC and informed to the distributed SUs over the same dedicated control channel. We model each primary channel occupancy dynamics as a two-state (*idle* and *busy*) independent identically distributed (i.i.d.) Markov chain. This Markov model, also known as the Gilbert-Elliot model [51], has been commonly used to abstract physical primary channels with memory (see, for example [22–26, 52, 53]). Note that under our formulation, primary channels can easily be generalized to be non-identical in terms of their Markov parameters.

Although this DSA problem can be formulated as a Partially Observable Markov Decision Process (POMDP) problem, as was discussed previously in [22–26], the optimal solution to the POMDP is *computationally prohibitive* because of the continuum of the state space. Many schemes presented in literature such as in [22–26] have previously proposed and derived the *myopic* channel sensing solutions under certain assumptions and conditions. For example, assuming that the state transition probabilities are partially known, [22,23,25] developed a myopic channel sensing strategy and proved that this *myopic* policy is the optimal POMDP solution under the assumption of a certain ordering of the state transition probabilities. However, this *myopic* policy was derived for a single SU without explicitly considering multiple SUs with transmission collisions and their possible cooperations. In [24], as a follow-up work of [22,23], the proposed myopic policy is extended to any number of primary channels with no limitation on the number of the primary channels the SU can sense at each time, which means that multiple channel selection is considered. However, possible SU cooperations and SU allocation issues are not discussed.

In this chapter, we derive the centralized *optimal myopic* channel sensing policy and the access policy that jointly maximize *instantaneous* total secondary system throughput on the primary channels, without considering the impact on future expected total secondary system throughput. Note that, by *optimal myopic* policy we refer to the policy that is optimal within the class of myopic policies. The proposed

myopic channel sensing policy is applicable for any number of primary channels, any number of SUs, and any channel state transition probabilities. To support our solutions, we also propose a Hidden Markov Model (HMM) based algorithm that efficiently estimates the channel transition probabilities when they are assumed unknown, with a *linear* complexity only in the number of primary channels. Under the formulation in our paper, we show that the optimal *myopic* channel sensing policy depends on the probability of white-space detections. Thus, we explicitly characterize the channel access policy based on a Neyman-Pearson (NP) detector, taking into account the interference constraint imposed by the primary users (PUs).

The remainder of this chapter is organized as follows: In Section 2.2 we introduce the system model. In Section 2.3, the access and sensing decisions are derived. The algorithm with linear complexity that is used to estimate the primary channel state transition probabilities is introduced in Section 2.4. In Section 2.5 we show the simulation results. In Section 2.6 we conclude by summarizing our results.

2.2 Problem Formulation

2.2.1 Primary channel state model

We denote by $k = \{0, 1, 2, \cdots\}$ the indices of a semi-infinite slotted time horizon. We assume a group of N SUs, and a collection of M primary channels. The primary channels are modeled as statistically identical and independent two-state Markov chains. As shown in Fig. 2.1, the state *busy* (state 1) indicates the channel is occupied by PUs; the state *idle* (state 0) indicates no PU transmissions over that channel and it is available for SUs to access. We denote by $S_m(k) \in \{0, 1\}$ the true state of the m-th primary channel in time slot k. We assume that the state of a primary channel does not change within a single time slot. The stationary transition probability of

the Markov model from state i to state j is defined as

$$p_{ij} = \Pr\{S_m(k+1) = j \mid S_m(k) = i\}, \ \ \forall i, j \in \{0, 1\}. \tag{2.1}$$

The *transition probability matrix* of the Markov model is denoted by

$$\mathbf{P} = \begin{pmatrix} p_{00} & p_{01} \\ p_{10} & p_{11} \end{pmatrix}. \tag{2.2}$$

We denote the vector $\pi = [\pi_0, \pi_1]$ as the stationary distribution vector, such that $\pi = \pi\mathbf{P}$ with π_0 and π_1 being the stationary distribution of idle and busy, respectively. When a SU successfully accesses a primary channel that is *actually free* during a given time slot, the SU is assumed to receive a reward proportional to the bandwidth of that channel. If a SU accesses a primary channel that is in state *busy*, it causes a collision with PU transmission and the SU gets a zero reward. The accumulated total reward of all SUs is used as a measure of the secondary system throughput over the primary channels.

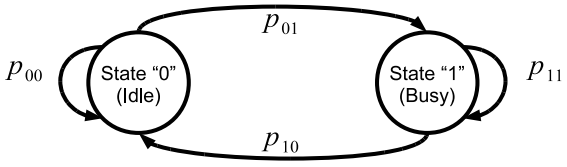

Figure 2.1: Model for primary channel state dynamics: Two-state Markov chain

2.2.2 Secondary system sensing and access decisions

In order to detect spectrum opportunities, SUs perform spectrum sensing. We assume that each SU is equipped with a single antenna, such that when a SU is performing channel sensing, no simultaneous communication can be performed. Also

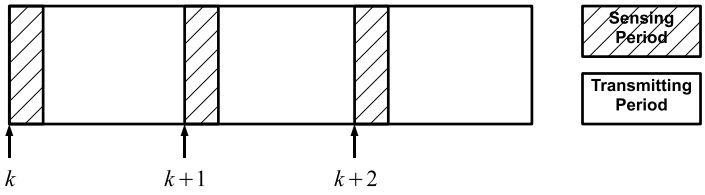

Figure 2.2: Slotted time horizon with Sensing Periods and Transmitting Periods.

assume that a single SU can only sense one primary channel at a time, but multiple SUs may simultaneously sense the same primary channel. As shown in Fig. 2.2, SUs sense primary channels during the designated sensing periods at the beginning of each time slot and we assume that if a PU intends to use its channel during a transmitting period, it starts to transmit from the beginning of that time slot.

The SSDC collects all channel sensing results from the SUs over a dedicated control channel to decide whether to access each of the channels and to make decisions on future sensing allocations. This centralized structure may incur some delay due to the need for exchanging sensing reports and decisions. There is a tradeoff between allocating a larger bandwidth for control channels to achieve a smaller delay and the bandwidth available for actual communications. However, this is not addressed due to the focus of this work. We use the $M \times N$ matrix $\mathbf{Y}_k$ to denote the sensing reports from SUs at time k with $\mathbf{Y}_k(m,n) = y_{m,n}(k)$, where $y_{m,n}(k)$ denotes the sensing report from n-th SU of the state of m-th primary channel at time k. We use the $M \times N$ matrix $\mathbf{A}_k$ to denote the sensing decision made by the SSDC at time k, where $\mathbf{A}_k(m,n) \in \{0,1\}$, with $\mathbf{A}_k(m,n) = 1$ or 0 representing n-th SU should or should not sense primary channel m at time k respectively. Since we assume that one SU can only sense one channel at a time, we have the constraint $\sum_{m=1}^{M} \mathbf{A}_k(m,n) = 1, \forall n$. We denote by $\mathcal{N}_m(k) = \{n : \mathbf{A}_k(m,n) = 1\}$ the set of indices of SUs that are assigned to sense the m-th channel at time k. We assume that whenever a particular channel is identified as *idle* at the SSDC, one SU is assigned to access that chan-

nel. The SSDC is responsible for balancing accessing opportunities among the SUs (fairness), or assigning SUs with any particular priorities. These fairness issues are not addressed due to the focus of this work, although they can be integrated into our decision-making framework as an optimization problem with constraints. The sensing and access decisions at the SSDC are further derived in Section III.

2.2.3 Secondary user sensing models and local sensing reports

For all (m, n) pairs such that $\mathbf{A}_k(m, n) = 1$, we denote by $\mathbf{r}_{m,n}(k)$ the L-length complex-valued observation vector on the m-th channel, from SU n in time slot k:

$$\mathbf{r}_{m,n}(k) = S_m(k)h_{m,n}(k)\mathbf{x}_m(k) + \mathbf{w}, \tag{2.3}$$

where $S_m(k) \in \{0, 1\}$ is the m-th channel state in time slot k, $\mathbf{x}_m(k) \in \mathbb{C}^L$ is the complex-valued primary signal vector, $\mathbf{w} = [w_1, \cdots, w_L]^T \in \mathbb{C}^L$ is a complex random vector of L zero-mean i.i.d. Gaussian random variables with real and imaginary parts, each $\mathcal{N}(0, \sigma_w^2/2)$. Thus, each $w_i \in \mathbf{w}$ is circularly symmetric and denoted by $\mathcal{CN}(0, \sigma_w^2)$. Denote $h_{m,n}(k) = \alpha_{m,n}(k)e^{j\theta_{m,n}(k)}$, the complex channel gain of the primary channel between the primary transmitter on the m-th primary channel and the n-th SU in time slot k, with amplitude $\alpha_{m,n}(k)$ and phase $e^{j\theta_{m,n}(k)}$. We assume that each SU has perfect knowledge of their own channel gain in each time slot for each of the primary channels. In practice, it can be assumed that the primary transmitter, if active, would periodically send training sequences/preambles to primary receivers for the purpose of synchronization and channel estimation [54]. The SUs may overhear and make use of these training sequences to estimate the fading coefficients between the primary transmitters and the secondary receivers. When a primary channel is idle, the secondary system may rely on the database service [55] maintained through learning at the SSDC to obtain the channel knowledge. We consider two models for

$\mathbf{x}_m(k)$ which can be considered as two extreme cases: 1) secondary system has *no* knowledge about the primary signaling; 2) secondary system has *perfect* knowledge about the primary signaling.

In the CR context, when communication opportunities are scarce (limited bandwidth and large amount of SUs), it is reasonable to assume that instead of transmitting raw data vector $\mathbf{r}_{m,n}(k)$'s, the SUs can only transmit quantized versions as reports to the SSDC. Without loss of generality, we assume the simplest case: the reports from SUs to the SSDC are compressed/quantized to 0's and 1's which can also be considered as estimates of the state of primary channels. For both aforementioned $\mathbf{x}_m(k)$ models, we use $y_{m,n}(k) \in \{0, 1\}$ to denote the report of the m-th primary channel state from the n-th SU to the SSDC, in time slot k. We assume that these $y_{m,n}(k)$'s are received error free at the SSDC. As shown in Fig. 2.3, the m-th channel true state $S_m(k)$ and the report $y_{m,n}(k)$ can be modeled as the input and output of a *Binary Asymmetric Channel* (BAC), respectively.

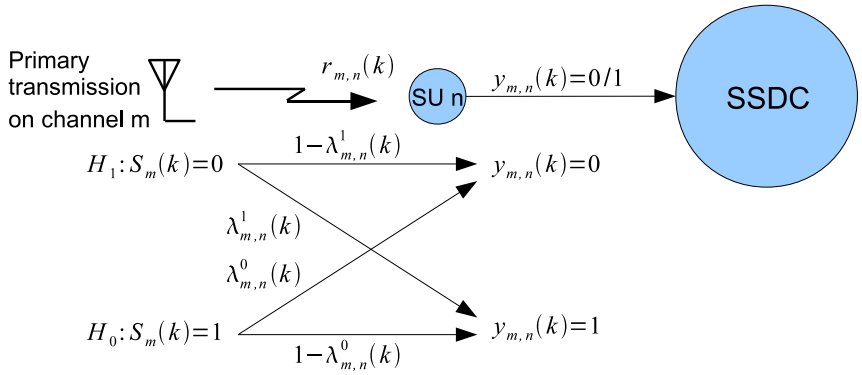

Figure 2.3: SUs' reports of observations on primary channels can be modeled as Binary Asymmetric Channels.

The two hypotheses on the m-th channel are $\mathcal{H}_1 : S_m(k) = 0$, and $\mathcal{H}_0 : S_m(k) = 1$, respectively. We use $\lambda^1_{m,n}(k)$, and $\lambda^0_{m,n}(k)$ to denote the crossover probabilities under

$\mathcal{H}_1$, and $\mathcal{H}_0$, respectively. The *maximum a posteriori probability* (MAP) decision rule used to determine $y_{m,n}(k)$ is given by

$$y_{m,n}(k) = \arg \max_{i \in \{0,1\}} \Pr\{S_m(k) = i \mid \mathbf{r}_{m,n}(k))\}, \tag{2.4}$$

which can be shown to be equivalent to the following likelihood ratio test:

$$\mathcal{L}(\mathbf{r}_{m,n}(k)) = \frac{f_{\mathbf{r}|0}(\mathbf{r}_{m,n}(k) \mid S_m(k) = 0)}{f_{\mathbf{r}|1}(\mathbf{r}_{m,n}(k) \mid S_m(k) = 1)} \underset{\mathcal{H}_0}{\overset{\mathcal{H}_1}{\gtrless}} \eta_m(k) = \frac{\Pr\{S_m(k) = 1\}}{\Pr\{S_m(k) = 0\}} = \frac{\pi_1}{\pi_0}, \tag{2.5}$$

where $f_{\mathbf{r}|s}$ denotes the conditional likelihood function of the complex-valued vector $\mathbf{r}$ given the state s.

1)When the secondary system has no knowledge about the primary signaling In general, we assume that the elements of $\mathbf{x}_m(k)$ are correlated and having a complex zero-mean Gaussian distribution with an unknown covariance matrix $\Sigma_{\mathbf{x}}$. We denote:

$$\mathbf{x}'_m(k) = \left[\Re\{\mathbf{x}_m^T(k)\}\ \Im\{\mathbf{x}_m^T(k)\}\right]^T \tag{2.6}$$

and

$$\tilde{\mathbf{x}}_{m,n}(k) = \left[\Re\{h_{m,n}(k)\mathbf{x}_m^T(k)\}\ \Im\{h_{m,n}(k)\mathbf{x}_m^T(k)\}\right]^T, \tag{2.7}$$

where $\mathbf{x}_m(k) \sim \mathcal{CN}(\mathbf{0}, \Sigma_{\mathbf{x}})$. It can be shown that $\tilde{\mathbf{x}}_{m,n}(k)$ is Gaussian and thus we denote $\tilde{\mathbf{x}}_{m,n}(k) \sim \mathcal{N}(\mathbf{0}, \Sigma_{\tilde{\mathbf{x}}})$, where $\Sigma_{\tilde{\mathbf{x}}}$ denotes the unknown covariance matrix of $\tilde{\mathbf{x}}_{m,n}(k)$. We also denote $\mathbf{R}_{m,n}(k) = [\Re\{\mathbf{r}_{m,n}^T(k)\}\ \Im\{\mathbf{r}_{m,n}^T(k)\}]^T$, and $\mathbf{W} = [\Re\{\mathbf{w}^T\}\ \Im\{\mathbf{w}^T\}]^T$. Then the complex-valued observation vector model (2.3) can be written as: $\mathbf{R}_{m,n}(k) = S\tilde{\mathbf{x}}_{m,n}(k) + \mathbf{W}$, where $\mathbf{W} \sim \mathcal{N}\left(\mathbf{0}, \frac{\sigma_w^2}{2}\mathbf{I}\right)$ and $\mathbf{R}_{m,n}(k) \sim \mathcal{N}\left(\mathbf{0}, S\Sigma_{\tilde{\mathbf{x}}} + \frac{\sigma_w^2}{2}\mathbf{I}\right)$. In this case, the MAP rule can be shown [56] to be equivalent to the following decision rule:

$$y_{m,n}(k) = \begin{cases} 0 & \text{, if } \mathbf{R}_{m,n}^T(k)\mathbf{Q}_{m,n}(k)\mathbf{R}_{m,n}(k) \le \eta_{m,n}^*(k) \\ 1 & \text{, if } \mathbf{R}_{m,n}^T(k)\mathbf{Q}_{m,n}(k)\mathbf{R}_{m,n}(k) > \eta_{m,n}^*(k) \end{cases}, \tag{2.8}$$

where $\mathbf{Q}_{m,n}(k) = \frac{2|h_{m,n}(k)|^2\sigma_x^2}{\sigma_w^2(\sigma_w^2+|h_{m,n}(k)|^2\sigma_x^2)}\mathbf{I}$ and $\eta^*_{m,n}(k) = 2\left(\ln\frac{\eta_m(k)(\sigma_w^2+|h_{m,n}(k)|^2\sigma_x^2)^L}{\sigma_w^{2L}}\right)$ in case the elements of $\mathbf{x}_m(k)$ are assumed i.i.d. [1]. Then, we have

$$\mathbf{R}_{m,n}(k)^T\mathbf{Q}_{m,n}(k)\mathbf{R}_{m,n}(k) = \mathbf{Q}_{m,n}(k)\mathbf{r}^H_{m,n}(k)\mathbf{r}_{m,n}(k),$$

where the superscript H denotes the conjugate transpose and

$$\mathbf{r}_{m,n}(k) \sim \mathcal{CN}\left(\mathbf{0}, \frac{S|h|^2\sigma_x^2+\sigma_w^2}{2}\mathbf{I}\right). \tag{2.9}$$

Then, the MAP rule can be shown to be equivalent to the following decision rule:

$$y_{m,n}(k) = \begin{cases} 0 & \text{, if } \mathbf{r}^H_{m,n}(k)\mathbf{r}_{m,n}(k) \le \eta'_{m,n}(k) \\ 1 & \text{, if } \mathbf{r}^H_{m,n}(k)\mathbf{r}_{m,n}(k) > \eta'_{m,n}(k) \end{cases}, \tag{2.10}$$

where $\eta'_{m,n}(k) = \eta^*_{m,n}(k)\frac{\sigma_w^2\left(\sigma_w^2+|h_{m,n}(k)|^2\sigma_x^2\right)}{2|h_{m,n}(k)|^2\sigma_x^2}$. The quantity $\frac{2\mathbf{r}^H_{m,n}(k)\mathbf{r}_{m,n}(k)}{\sigma_w^2}$ (under $\mathcal{H}_1$), and $\frac{2\mathbf{r}^H_{m,n}(k)\mathbf{r}_{m,n}(k)}{\sigma_w^2+|h_{m,n}(k)|^2\sigma_x^2}$ (under $\mathcal{H}_0$) can be shown distributed as χ^2_{2L}, thus the crossover probabilities can be obtained as

$$\lambda^1_{m,n}(k) = 1-\frac{1}{\Gamma(L)}\gamma\left(L, \frac{\eta'_{m,n}(k)}{\sigma_w^2}\right),\ \lambda^0_{m,n}(k) = \frac{1}{\Gamma(L)}\gamma\left(L, \frac{\eta'_{m,n}(k)}{\sigma_w^2+|h_{m,n}(k)|^2\sigma_x^2}\right) \tag{2.11}$$

where the gamma function $\Gamma(z) = \int_0^\infty t^{z-1}e^{-t}dt$ and the lower incomplete gamma function $\gamma(s,x) = \int_0^x t^{s-1}e^{-t}dt$. We assume that the threshold $\eta_m(k) = \frac{\pi_1}{\pi_0}$ is informed from the SSDC.

2) When the secondary system has perfect knowledge about the primary signaling It is assumed that $\mathbf{x}_m(k) = \mathbf{x}$ is known and the matched-filter [56] based sensing is

[1]Note that the assumption of the components of $\mathbf{x}_m(k)$ being i.i.d. is shown to be optimal for detecting zero-mean constellation signals when there is no knowledge about the primary signal [57]. In this case, the matrix $\mathbf{Q}_{m,n}(k)$ is found to be a scalar and the sufficient test statistic $\mathbf{R}_{m,n}(k)^T\mathbf{R}_{m,n}(k)$ can be considered as a measure of the primary signal energy, also known as the energy detection [56].

employed. The optimal MAP rule (2.4) can then be derived as [56]

$$y_{m,n}(k) = \begin{cases} 0 & \text{, if } \Re(\mathbf{r}_{m,n}(k)\mathbf{x}'^{H}_{m,n}(k)) \leq \frac{\mathbf{x}'_{m,n}(k)\mathbf{x}'^{H}_{m,n}(k) - \sigma_w^2 \ln(\eta_m(k))}{2} \\ 1 & \text{, if } \Re(\mathbf{r}_{m,n}(k)\mathbf{x}'^{H}_{m,n}(k)) > \frac{\mathbf{x}'_{m,n}(k)\mathbf{x}'^{H}_{m,n}(k) - \sigma_w^2 \ln(\eta_m(k))}{2} \end{cases} \tag{2.12}$$

where $\Re(\cdot)$ denotes the real part operation, and $\mathbf{x}'_{m,n}(k) = h_{m,n}(k)\mathbf{x}$. Now, given $S_m(k) = 0$,

$$\frac{\Re(\mathbf{r}_{m,n}(k)\mathbf{x}'^{H}_{m,n}(k))}{\sqrt{\mathbf{x}'_{m,n}(k)\mathbf{x}'^{H}_{m,n}(k)}} \sim \mathcal{N}(0, \sigma_w^2/2), \tag{2.13}$$

whereas given $S_m(k) = 1$,

$$\frac{\Re(\mathbf{r}_{m,n}(k)\mathbf{x}'^{H}_{m,n}(k))}{\sqrt{\mathbf{x}'_{m,n}(k)\mathbf{x}'^{H}_{m,n}(k)}} \sim \mathcal{N}\left(\sqrt{\mathbf{x}'_{m,n}(k)\mathbf{x}'^{H}_{m,n}(k)}, \sigma_w^2/2\right). \tag{2.14}$$

Thus, the resulting crossover probabilities are given as

$$\lambda^1_{m,n}(k) = Q\left(\frac{|h_{m,n}(k)|^2\mathbf{x}^H\mathbf{x} - \sigma_w^2 \ln(\eta_m(k))}{\sqrt{2}|h_{m,n}(k)|\sigma_w\sqrt{\mathbf{x}^H\mathbf{x}}}\right), \tag{2.15}$$

$$\lambda^0_{m,n}(k) = Q\left(\frac{|h_{m,n}(k)|^2\mathbf{x}^H\mathbf{x} + \sigma_w^2 \ln(\eta_m(k))}{\sqrt{2}|h_{m,n}(k)|\sigma_w\sqrt{\mathbf{x}^H\mathbf{x}}}\right), \tag{2.16}$$

where function $Q(\cdot)$ is the tail probability of the standard normal distribution and the superscript H denotes the conjugate transpose.

2.3 Channel Access and Sensing Decisions at the SSDC

2.3.1 Channel access decisions at the SSDC

To meet the constraint of collision probability with PUs on *every* channel, the optimal access decisions at the SSDC must be based on a classical NP detector [56]. Note

that we refer to the '*access decision*' as the decision at the SSDC about whether a primary channel is idle or not, whereas the decision on which SU should access which primary channel is called the '*access assigning decision*'. Let the variable length vector $\mathbf{y}_k(m,:) = \{y_{m,n}(k) : \forall n \in \mathcal{N}_m(k)\}$ denote all channel sensing reports corresponding to the m-th channel at time k and the variable length vector $\mathbf{y}_{0:k}(m,:) = \{\mathbf{y}_0(m,:), \cdots, \mathbf{y}_k(m,:)\}$ denote the sensing history on the m-th primary channel, from time 0 to k. Let $\mathbf{S}^m_{0:k}$ denote the historic state of m-th channel from time 0 to k. The set of all possible historic channel state vectors is denoted by $\mathcal{S}_c = \{0,1\}^{k+1}$.

At time k, for the m-th primary channel, the SSDC chooses one of the two possible hypotheses based on $\mathbf{y}_{0:k}(m,:)$:

$$\mathcal{H}_1(\text{ channel } \textit{idle}, \mathbf{y}_{0:k}(m,:) \sim P_{m,1}) \tag{2.17}$$

$$\mathcal{H}_0(\text{ channel } \textit{busy}, \mathbf{y}_{0:k}(m,:) \sim P_{m,0}) \tag{2.18}$$

where $P_{m,1}$, and $P_{m,0}$ denote the conditional distributions of $\mathbf{y}_{0:k}(m,:)$ given $S_m(k) = 0$, and $S_m(k) = 1$, respectively. The likelihood ratio for the m-th channel is given by $\mathcal{L}(\mathbf{y}_{0:k}(m,:)) = \frac{P_{m,1}(\mathbf{y}_{0:k}(m,:))}{P_{m,0}(\mathbf{y}_{0:k}(m,:))}$, which is generally difficult to obtain as a useful closed-form expression due to the fact that at each time k, the number of SUs on m-th channel changes and thus as time evolves, the complexity increases. To simplify the access decision structure, we assume that the access decisions regarding the m-th channel are based only on the current observations $\mathbf{y}_k(m,:)$. The likelihood ratio at the SSDC can then be found as

$$\begin{aligned}\mathcal{L}(\mathbf{y}_k(m,:)) &= \frac{P_{m,1}(\mathbf{y}_k(m,:))}{P_{m,0}(\mathbf{y}_k(m,:))} \\ &= \prod_{n\in\mathcal{N}_m(k)} \left[\left(\frac{\lambda^1_{m,n}(k)}{1-\lambda^0_{m,n}(k)} \right)^{y_{m,n}(k)} \left(\frac{1-\lambda^1_{m,n}(k)}{\lambda^0_{m,n}(k)} \right)^{1-y_{m,n}(k)} \right]. \end{aligned} \tag{2.19}$$

Note that in order to obtain the knowledge of $\lambda^0_{m,n}(k)$ and $\lambda^1_{m,n}(k)$ at the SSDC, the SUs are required to send the quantity $|h_{m,n}(k)|$ to the SSDC in each time slot. Along

with the sensing report $y_{m,n}(k)$, a total number of $2N$ messages are needed at the SSDC in each time slot k, where N is the number of SUs in the secondary system. The log-likelihood ratio can be found as

$$\mathcal{LLR}(\mathbf{y}_k(m,:)) = \sum_{n\in\mathcal{N}_m(k)} y_{m,n}(k)c_{m,n}(k) + d_m(k), \tag{2.20}$$

where

$$c_{m,n}(k) = \ln\left(\frac{\lambda^1_{m,n}(k)}{1-\lambda^0_{m,n}(k)} \cdot \frac{\lambda^0_{m,n}(k)}{1-\lambda^1_{m,n}(k)}\right), \tag{2.21}$$

and

$$d_m(k) = \sum_{n\in\mathcal{N}_m(k)} \ln\left(\frac{1-\lambda^1_{m,n}(k)}{\lambda^0_{m,n}(k)}\right). \tag{2.22}$$

The sufficient statistic for access decision at the SSDC regarding the m-th channel is then given by

$$\mathcal{T}_m(k) = \sum_{n\in\mathcal{N}_m(k)} y_{m,n}(k)c_{m,n}(k), \tag{2.23}$$

and the test is equivalent to

$$\mathcal{T}_m(k) \underset{\mathcal{H}_0}{\overset{\mathcal{H}_1}{\gtrless}} \tau_m(k) - d_m(k) = \tau'_m(k), \tag{2.24}$$

where $\tau_m(k)$ and $\tau'_m(k)$ are the thresholds for the log-likelihood ratio test and the test of the sufficient statistic $\mathcal{T}_m(k)$, respectively. Let $f^i_{m,k}$ and $F^i_{m,k}$ denote the conditional probability mass function (pmf) and the conditional cumulative distribution function (cdf) of the random variable $\mathcal{T}_m(k)$ under hypothesis $\mathcal{H}_i$, respectively. We denote the variable set $\mathcal{C}_m(k)$ as the set of discrete values that $\mathcal{T}_m(k)$ takes at time k. The

optimal access-decision regarding the m-th channel is then given by the randomized decision rule:

$$\tilde{\delta}_{NP}(\mathbf{y}_k(m,:)) = \begin{cases} 1 & \\ \gamma_m(k) & \text{if } \mathcal{T}_m(k) \gtreqless \tau'_m(k) \\ 0 & \end{cases} . \tag{2.25}$$

This randomized decision rule says: 1) access the m-th channel if $\mathcal{T}_m(k) > \tau'_m(k)$; 2) do not access the m-th channel if $\mathcal{T}_m(k) < \tau'_m(k)$; and 3) access the m-th channel with probability $\gamma_m(k)$ if $\mathcal{T}_m(k) = \tau'_m(k)$. We denote by ζ the collision probability constraint on each individual primary channel. It can be shown that the threshold $\tau'_m(k)$ must be chosen such that $\Pr\{\mathcal{T}_m(k) > \tau'_m(k) \mid \mathcal{H}_0\} \leq \zeta < \Pr\{\mathcal{T}_m(k) > \tau'^{-}_m(k) \mid \mathcal{H}_0\}$, where we denote by $\Pr\{\mathcal{T}_m(k) > \tau'_m(k) \mid \mathcal{H}_0\}$ the probability of colliding with primary user on the m-th channel at time k. The quantity $\tau'^{-}_m(k) = \max\{\tau : \tau \in \mathcal{C}_m(k), \tau < \tau'_m(k)\}$ is defined to be the maximum value in $\mathcal{C}_m(k)$ that is less than $\tau'_m(k)$. The choice of $\tau'_m(k)$ is illustrated in Fig. 2.4 where it can be seen that $\tau'_m(k)$ is unique, given the monotonicity of the complementary cdf $\Pr\{\mathcal{T}_m(k) > \tau \mid \mathcal{H}_0\}$. We can see that this is equivalent to choosing $\tau'_m(k)$ such that $1 - F^0_{m,k}(\tau'_m(k)) \leq \zeta < 1 - F^0_{m,k}(\tau'^{-}_m(k))$ (note that $\Pr\{\mathcal{T}_m(k) > \tau \mid \mathcal{H}_0\} = 1 - F^0_{m,k}(\tau)$). The randomization variable $\gamma_m(k)$ is then given by

$$\gamma_m(k) = \frac{\zeta - \left(1 - F^0_{m,k}(\tau'_m(k))\right)}{F^0_{m,k}(\tau'_m(k)) - F^0_{m,k}(\tau'^{-}_m(k))}. \tag{2.26}$$

Note that, the structure of the optimal access decision at the SSDC is independent of what type of local sensing rules were used at the distributed SUs. In turn, the above access decision rule at the SSDC is valid for any assumptions on the knowledge of primary signals by the SUs, including the considered two extreme cases, since as long as the local sensing decisions are quantized as 0 or 1 before transmitting to the SSDC, all that matters are the crossover probabilities $\lambda^1_{m,n}(k)$ and $\lambda^0_{m,n}(k)$ in

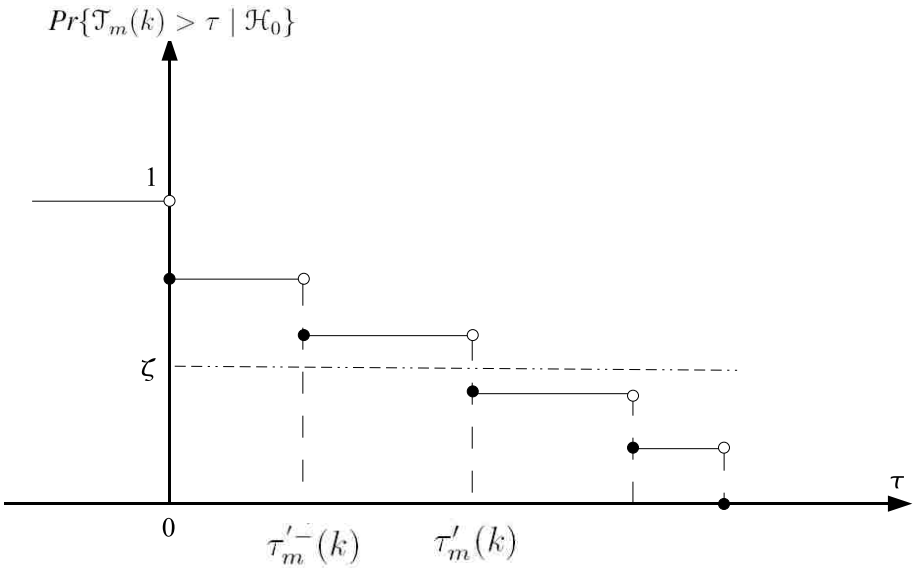

Figure 2.4: The choice of of the threshold $\tau'_m(k)$, given a false alarm probability ζ.

terms of the access decision-making at the SSDC. The probability of detection of white-spaces is then given by

$$\begin{aligned} P_{D,m}(k, \mathbf{A}_k) &= \Pr\{\mathcal{T}_m(k) > \tau'_m(k) \mid \mathcal{H}_1\} + \gamma_m(k)\Pr\{\mathcal{T}_m(k) = \tau'_m(k) \mid \mathcal{H}_1\} \\ &= 1 - F^1_{m,k}(\tau'_m(k)) + \gamma_m(k) \cdot f^1_{m,k}(\tau'_m(k)), \end{aligned} \tag{2.27}$$

Note that this is used in the sensing decision-making at the SSDC as described next.

2.3.2 Optimal and sub-optimal myopic sensing decisions at the SSDC

The sensing decision at the SSDC determines which primary channel each SU should sense at each time. We define $b_0(m,k) = \Pr\{S_m(k) = 0 \mid \mathbf{y}_{0:k-1}(m,:)\}$ and $b_1(m,k) =$

$1 - b_0(m,k)$ as the belief of the m-th channel being *idle* and *busy* at time k respectively. We denote the belief vectors as $\mathbf{b}_0(k) = [b_0(1,k), \cdots, b_0(M,k)]^T$ and $\mathbf{b}_1(k) = [b_1(1,k), \cdots, b_1(M,k)]^T$.

Assuming the sensing observations of SUs at time k are mutually independent, the belief that the m-th channel being *idle* in next time slot $k+1$ is updated at the SSDC using the Bayes' formula:

$$b_0(m,k+1) = \frac{\sum_{i\in\{0,1\}} p_{i0} \left[\prod_{n\in\mathcal{N}_m(k)} f_i(y_{m,n}(k))\right] b_i(m,k)}{\sum_{i\in\{0,1\}} \left[\prod_{n\in\mathcal{N}_m(k)} f_i(y_{m,n}(k))\right] b_i(m,k)}, \tag{2.28}$$

where $f_i(y_{m,n}(k)) = \Pr\{Y_{m,n}(k) = y_{m,n}(k) \mid S_m(k) = i\}, \forall i \in \{0,1\}$ is the conditional pmf of the local decisions from the n-th SU and $Y_{m,n}(k)$ is a random variable denoting the report from the n-th SU about the m-th channel at time k (note that $y_{m,n}(k)$ is a realization of the random variable $Y_{m,n}(k)$). For those primary channels that were not sensed by any SU, the belief is updated simply based on the Markovian evolution of primary channels: $[b_0(m,k+1), b_1(m,k+1)] = [b_0(m,k), b_1(m,k)]\mathbf{P}$, where $\mathbf{P}$ is the state transition probability matrix. The belief vectors $\mathbf{b}_0(1)$, and $\mathbf{b}_1(1)$ are initialized with the stationary distribution $\pi = [\pi_0\,, \pi_1]$ of the Markov model.

We denote by the random vector $\hat{\mathbf{S}}(k) = \left[\tilde{\delta}_{NP}(1,k), \cdots, \tilde{\delta}_{NP}(M,k)\right]^T$ the vector of NP detector outcomes at the SSDC at time k. Given a sensing assignment $\mathbf{A}_k$, the probability of $\hat{\mathbf{S}}(k) = \mathbf{s} \in \{0,1\}^M$ can be found as

$$\Pr\{\hat{\mathbf{S}}(k) = \mathbf{s}\} = \prod_{m=1}^{M} \frac{\{b_0(m,k)P_{D,m}(k,\mathbf{A}_k) + (1-b_0(m,k))\zeta\}^{\mathcal{I}_{\{\mathbf{s}(m)=0\}}}}{\{b_0(m,k)(1-P_{D,m}(k,\mathbf{A}_k)) + (1-b_0(m,k))(1-\zeta)\}^{-\mathcal{I}_{\{\mathbf{s}(m)=1\}}}}, \tag{2.29}$$

where $\mathcal{I}_E$ is the indicator function of event E and ζ is the predefined collision probability. We define the M by N matrix $\mathbf{H}'_k$ such that $\mathbf{H}'_k(m,n) = h'_{m,n}(k)$, $\forall\ m,n$, where $h'_{m,n}(k)$ denotes the channel coefficient of the channel between the n-th SU and its desired receiver on channel m. Note that the optimal secondary access assigning decisions can be obtained by an integer programming problem which can

be solved using a graph matching algorithms[2], as suggested in [58]. Due to space limitations, we omit details of the algorithm. Let us denote by $n_m(\mathbf{s}, \mathbf{A_k}, \mathbf{H}'_k)$ the index of the SU that is assigned to access the m-th channel, after sensing in time slot k, according to this optimal secondary access assigning decisions. We denote by $h'_m(\mathbf{s}, \mathbf{A}_k, \mathbf{H}'_k) \triangleq h'_{m,n_m(\mathbf{s},\mathbf{A_k},\mathbf{H}'_k)}(k)$ the channel coefficient on the m-th channel from the SU that is assigned to access that channel. Let $r_m(k, \hat{\mathbf{S}}(k), \mathbf{A}_k, \mathbf{H}'_k)$ be the secondary transmission rate on the m-th channel which can be written as:

$$r_m(k, \hat{\mathbf{S}}(k), \mathbf{A}_k, \mathbf{H}'_k) = B_m \log_2 \left(1 + \frac{P_{n_m(\hat{\mathbf{S}}(k),\mathbf{A_k},\mathbf{H}'_k)} |h'_m(\hat{\mathbf{S}}(k), \mathbf{A}_k, \mathbf{H}'_k)|^2}{N_0 B_m}\right), \quad (2.30)$$

if $\sum_n \mathbf{A}_k(m,n) \geq 1$, $S_m(k) = 0$, and $\tilde{\delta}_{NP}(m,k) = 1$, and $r_m(k, \hat{\mathbf{S}}(k), \mathbf{A}_k, \mathbf{H}'_k) = 0$ otherwise, with B_m being the bandwidth of the m-th primary channel, P_n being the transmit power of the n-th SU and N_0 is the single-sided power spectrum density of the secondary receiver noise. The expected total transmission rate/reward on all the primary channels in time slot k is then:

$$\begin{aligned} &\mathbb{E} \quad \left\{\sum_{m=1}^{M} r_m(k, \hat{\mathbf{S}}(k), \mathbf{A}_k, \mathbf{H}'_k)\right\} \\ &= \sum_{m=1}^{M} B_m \mathbb{E}_{\hat{\mathbf{S}}(k)} \left\{\log_2 \left(1 + \frac{P_{n_m(\hat{\mathbf{S}}(k),\mathbf{A_k},\mathbf{H}'_k)} |h'_m(\hat{\mathbf{S}}(k), \mathbf{A}_k, \mathbf{H}'_k)|^2}{N_0 B_m}\right)\right\} \times \\ &\qquad \times P_{D,m}(k, \mathbf{A}_k) b_0(m,k), \end{aligned} \quad (2.31)$$

where $\mathbb{E}_{\hat{\mathbf{S}}(k)}$ denotes the expectation with respect to the vector $\hat{\mathbf{S}}(k)$ so that

$$\begin{aligned} &\mathbb{E}_{\hat{\mathbf{S}}(k)} \quad \left\{\log_2 \left(1 + \frac{P_{n_m(\hat{\mathbf{S}}(k),\mathbf{A_k},\mathbf{H}'_k)} |h'_m(\hat{\mathbf{S}}(k), \mathbf{A}_k, \mathbf{H}'_k)|^2}{N_0 B_m}\right)\right\} \\ &= \sum_{\hat{\mathbf{S}}(k)=\mathbf{s}} \log_2 \left(1 + \frac{P_{n_m(\mathbf{s},\mathbf{A_k},\mathbf{H}'_k)} |h'_m(\mathbf{s}, \mathbf{A}_k, \mathbf{H}'_k)|^2}{N_0 B_m}\right) \Pr\{\hat{\mathbf{S}}(k) = \mathbf{s}\}. \end{aligned} \quad (2.32)$$

[2] A graph matching problem finds the optimal *one-to-one* matching between the elements of two bipartite sets such that it optimizes the sum-weights of the connecting edges.

Let $\mathbf{S}(k) = [S_1(k), \cdots, S_M(k)] \in \mathcal{S} = \{0,1\}^M$ denote the state of the system at time k. Then the value of state $\mathbf{s} \in \mathcal{S}$ at time 0 is

$$V^{\mathbf{A}_{0:\infty}}(\mathbf{s}) = \mathbb{E}\left\{\sum_{k=0}^{\infty}\sum_{m=1}^{M}\gamma^k r_m(k, \hat{\mathbf{S}}(k), \mathbf{A}_k, \mathbf{H}'_k) \mid \mathbf{S}(0) = \mathbf{s}\right\}, \tag{2.33}$$

which can also be expressed as

$$\mathbb{E}\left\{\sum_{m=1}^{M} r_m(0, \hat{\mathbf{S}}(0), \mathbf{A}_0, \mathbf{H}'_0) \mid \mathbf{S}(0) = \mathbf{s}\right\} + \gamma \sum_{\mathbf{s}' \in \mathcal{S}} P(\mathbf{s}, \mathbf{s}') V^{\mathbf{A}_{0:\infty}}(\mathbf{s}'), \tag{2.34}$$

where $\mathbf{A}_{0:\infty}$ denotes the SSDC sensing decisions from time $k = 0$ to ∞, $\gamma \in (0,1)$ is a discount factor and $P(\mathbf{s}, \mathbf{s}')$ is the probability of state transition from $\mathbf{s}$ to $\mathbf{s}'$. Note that, the value function is the expected discounted reward over all primary channels. When the SUs do not have perfect knowledge of the states of the primary channels, the resultant problem is a Partially Observable Markov Decision Process (POMDP) for which the effective state of the system can be taken as the belief vector. An algorithm to obtain optimal decisions for a POMDP problem was derived in [21]. However, unless the number of primary channels is very small, the algorithm leads to very high computational complexity rendering it impractical [23]. As an alternative, an optimal channel sensing decision within the class of *myopic* policies can be obtained by maximizing the total secondary transmission rate/reward over all primary channels at each time step: i.e. making the channel sensing decisions to obtain the instantaneous highest reward, rather than attempting to optimize the average reward accrued over all times. This *optimal myopic* sensing decision $\mathbf{A}_k^*$ can be expressed as:

$$\mathbf{A}_k^* = \underset{\sum_{m=1}^{M}\mathbf{A}_k(m,n)=1}{\arg\max} \sum_{m=1}^{M} \mathbb{E}\left\{r_m(k, \hat{\mathbf{S}}(k), \mathbf{A}_k, \mathbf{H}'_k)\right\}. \tag{2.35}$$

This optimal sensing decision is designed to jointly maximize the expected secondary system throughput taking into account the impact from the access assigning decision-making. Note that this problem can be cast as a *constrained nonlinear 0-1 programming* problem [59]. Since the objective function in (2.35) is non-separable, the

solution is generally hard to find. The direct search solution has an exponential complexity of M^N.

On the other hand, in order to perform this joint optimization at the SSDC, it is required that the SSDC has perfect knowledge of the channel coefficients $h'_{m,n}(k)$'s between the secondary transmitters and receivers. However, unlike the channel coefficients from the primary radios to the SUs, it might not be realistic to assume that the SSDC has the knowledge of these secondary sender-receiver channel coefficients, since it is assumed that the SUs are sensing primary signals, but not SU signals. This makes it reasonable to instead focus on finding an optimal myopic sensing policy in the sense of maximizing the secondary system transmission opportunities on the primary channels, other than the transmission throughput, similar to [26]. The optimal myopic sensing decisions in terms of maximizing the secondary transmission opportunities can be found as

$$\begin{aligned} \mathbf{A}_k^* &= \underset{\sum_{m=1}^{M} \mathbf{A}_k(m,n)=1}{\arg\max} \sum_{m=1}^{M} \mathbb{E}\{r_m(k, \mathbf{A}_k)\} \\ &= \underset{\sum_{m=1}^{M} \mathbf{A}_k(m,n)=1}{\arg\max} \sum_{m=1}^{M} B_m b_0(m,k) P_{D,m}(k, \mathbf{A}_k). \end{aligned} \tag{2.36}$$

In Section 2.5 we will show that the maximization in (2.35) gives only a marginal performance improvement compared to the performance obtained with the objective function in (2.36), especially when the number of SUs is large compared to the number of primary channels.

As an alternative with much lower computational complexity, we propose a suboptimal algorithm for solving (2.36) based on an iterative Hungarian algorithm [60]. For simplicity, we drop the time indices from the algorithm description and let $B_m = 1$. We assume that the crossover probabilities of the BAC are known. We define the $M \times N$ matrix $\Delta^{(m,n)}$ such that $\Delta^{(m,n)}(m', n') = 1$ if $(m', n') = (m, n)$, and $\Delta^{(m,n)}(m', n') = 0$ otherwise. We use Algorithm 1 below to find the channel sensing

assignment $\mathbf{A}$, which provides a sub-optimal solution to (2.36). In contrast with the Hungarian algorithm solution which forms the optimal one-to-one matching between two bipartite sets, our sensing policy allows multiple SUs to sense a single channel at a time. Thus, an intuitive solution would be to apply the Hungarian algorithm repeatedly among the primary channels with the available SUs that have not yet been assigned. In this algorithm, we set a weighting matrix $\Delta\mathbf{P}$ between the set of SUs and the primary channels. Each weight or element $\Delta\mathbf{P}(m,n)$ of this matrix is defined as the increase in the detection probability on a particular channel m if an additional SU n senses that channel. This is reflected in:

$$\Delta\mathbf{P}(m,n) = \left[P_{D,m}(\mathbf{A}+\Delta^{(m,n)}) - P_{D,m}(\mathbf{A})\right] b_0(m), \tag{2.37}$$

where $\mathbf{A}+\Delta^{(m,n)}$ is the new sensing assignment if an available SU n is assigned to sense the m-th channel, given the current sensing assignment $\mathbf{A}$. Therefore, if there are more than $M-1$ unassigned SUs at an iteration, the proposed algorithm assigns exactly M SUs to sense the primary channels. At each iteration, the Hungarian algorithm assigns the SUs such that it maximizes the sum of $\Delta\mathbf{P}(m,n)$ over all $m = 1, \cdots, M$. Note that, at each iteration, the SUs are assigned in a one-to-one mapping. Note that the above sensing decision making procedure applies to both optimization problems in (2.35) and (2.36), except when using (2.35), the extra term in (2.32) needs to be computed firstly.

The complexity of the Hungarian algorithm is $(\max\{M,N\})^3$ for an $M \times N$ bipartite graph, whereas the complexity of the proposed iterative Hungarian algorithm is in the order of $\lceil \frac{N}{M} \rceil (\max\{M,N\})^3$ since the Hungarian algorithm is used iteratively $\lceil \frac{N}{M} \rceil$ times. In brief, the proposed algorithm solves the channel sensing assignment problem with roughly an order 4 polynomial complexity. Note that, in particular, if $N \leq M$, Algorithm 1 is equivalent to the Hungarian algorithm. Next, we propose a heuristic algorithm that reduces the above complexity to be linear in number of secondary users N. This algorithm, as detailed in Algorithm 4, picks randomly a

Algorithm 1 Iterative Hungarian Algorithm

$\mathbf{A} = 0_{M\times N}$ and $\bar{\mathcal{N}} = \{1, \cdots, N\}$

while $\bar{\mathcal{N}} \neq \emptyset$ **do**

$\Delta\mathbf{P} = 0_{M\times N}$

for $m \in \{1, \cdots, M\}$ and $n \in \bar{\mathcal{N}}$ **do**

$\Delta\mathbf{P}(m,n) = \left[P_{D,m}\left(\mathbf{A} + \Delta^{(m,n)}\right) - P_{D,m}\left(\mathbf{A}\right)\right] b_0(m)$

end for

Run the *Hungarian algorithm* for the $M \times N$ bipartite graph whose edge weights are given in $\Delta\mathbf{P}$ to obtain the maximum sum matching.

Remove the assigned vertices from the set $\bar{\mathcal{N}}$.

Append the new assignments to matrix $\mathbf{A}$.

end while

secondary user n and assigns it to the m-th channel for which it has the highest detection probability. Also, we allow at most $\lceil \frac{N}{M} \rceil$ SUs to sense each channel so that the SUs sense evenly all channels and keep information about the belief of the state of every channel.

Algorithm 2 Heuristic Sensing Assignment

$\mathbf{A} = 0_{M\times N}$ and $\bar{\mathcal{N}} = \{1, \cdots, N\}$.

while $\bar{\mathcal{N}} \neq \emptyset$ **do**

Pick randomly $n \in \bar{\mathcal{N}}$.

$m^* = \arg\max_{m\in\{1,\cdots,M\}} B_m b_0(m) P_{D,m}(\Delta^{(m,n)})$

s.t. $\sum_{n\in\{1,\cdots,N\}} \mathbf{A}(m,n) \leq \lceil \frac{N}{M} \rceil$

$\mathbf{A} \leftarrow \mathbf{A} + \Delta^{(m^*,n)}$

$\bar{\mathcal{N}} \leftarrow \bar{\mathcal{N}} \backslash n$

end while

2.4 Primary channel Markov model parameter estimation

The classical algorithm used to estimate the Markov model parameters was provided in [61], which deals with the case of fixed number of observations, but not the case when the number of observations increases with time as in our problem. This classical algorithm has a linear computational complexity in $M \times T$, i.e. the product of the number of channels and the time length. This leads to a high computational complexity as T increases, since all the variables have to be re-initialized and flushed every time for new observations. As a result, in this section, we propose an algorithm to estimate the primary channel Markov model dynamically as time evolves, with a linear computational complexity only in M.

We firstly familiarize the readers with the following concepts introduced in [61]. We denote $\hat{\mathbf{P}}(m,t) = \begin{pmatrix} \hat{p}_{00}(m,t) & \hat{p}_{01}(m,t) \\ \hat{p}_{10}(m,t) & \hat{p}_{11}(m,t) \end{pmatrix}$ as the estimated Markov model transition matrix of the m-th primary channel at time t. The estimated stationary state distribution vector is denoted by $\hat{\pi}(m,t) = [\hat{\pi_0}(m,t)\, \hat{\pi_1}(m,t)]^T$ with $\hat{\pi}(m,t) = \hat{\mathbf{P}}(m,t)\hat{\pi}(m,t)$. For convenience, we use the compact notation

$$\hat{\lambda}(m,t) = (\hat{\mathbf{P}}(m,t), \hat{\pi}(m,t)), \tag{2.38}$$

to indicate the estimated parameter set. We denote $p_{m,n}(j,i,k) = \Pr\{y_{m,n}(k) = j | S_m(k) = i\}, \forall i,j \in \{0,1\}$ as the n-th SU observation symbol probability distributions of the m-th channel at time k. Note that $p_{m,n}(j,i,k) = \lambda^i_{m,n}(k)$, $\forall j \neq i$. At each time t, for the m-th channel, consider the forward variable $\alpha_{m,i}(k,t)$ and the

backward variable $\beta_{m,i}(k,t)$ defined as

$$\begin{aligned}\alpha_{m,i}(k,t) &= \Pr\{\mathbf{y}_{0:k}(m,:), S_m(k)=i \mid \hat{\lambda}(m,t-1)\}, \forall k \in \{1,\cdots,t\}, \quad (2.39)\\ \beta_{m,i}(k,t) &= \Pr\{\mathbf{y}_{k+1:t}(m,:) \mid S_m(k)=i, \hat{\lambda}(m,t-1)\},\\ &\quad \forall k \in \{1,\cdots,t-1\}. \quad (2.40)\end{aligned}$$

The forward variable $\alpha_{m,i}(k,t)$, $\forall\, m \in \{1,...,M\}$ is evaluated inductively, as follows [61]: 1) Initialization: $\alpha_{m,i}(0,t) = \hat{\pi}_i(t-1)p_m(\mathbf{y}_0(m,:),i,0), \forall i \in \{0,1\}$; 2) Induction:

$$\alpha_{m,j}(k,t) = \left[\sum_{i\in\{0,1\}} \alpha_{m,i}(k-1,t)\hat{p}_{ij}(m,t-1)\right] p_m(\mathbf{y}_k(m,:),j,k),$$
$$\forall k \in \{1,\cdots,t\},\ j \in \{0,1\},$$

where $p_m(\mathbf{y}_k(m,:),j,k)$ is defined as $p_m(\mathbf{y}_k(m,:),j,k) = \Pr\{\mathbf{y}_k(m,:) \mid S_m(k)=j\}$. The backward variable $\beta_{m,i}(k,t)$,$\forall\, m \in \{1,...,M\}$ is also evaluated inductively, as follows [61]: 1) Initialization: $\beta_{m,i}(t,t)=1$; 2) Induction: $\beta_{m,i}(k,t) = \sum_{j\in\{0,1\}} \hat{p}_{ij}(m,t-1)p_m(\mathbf{y}_{k+1}(m,:),j,k+1)\beta_{m,j}(k+1,t)$, $\forall k \in \{1,\cdots,t-1\}$, $i \in \{0,1\}$.

After the SSDC gets the observation $\mathbf{y}_t(m,:)$ of channel m at time $t \geq 1$, we define $\xi_{m,i,j}(k,t)$, $\forall k \in \{0,...,t-1\}$ as the probability of channel m being in state i at time k, and in state j at time $k+1$ given the estimated model $\hat{\lambda}(m,t-1)$ and the observation sequence $\mathbf{y}_{0:t}(m,:)$, i.e.: $\xi_{m,i,j}(k,t) = \Pr\{S_m(k)=i, S_m(k+1)=j \mid \mathbf{y}_{0:t}(m,:), \hat{\lambda}(m,t-1)\}$. Thus, $\xi_{m,i,j}(k,t) = \frac{\alpha_{m,i}(k,t)\hat{p}_{ij}(t-1)p_m(\mathbf{y}_{k+1}(m,:),j,k+1)\beta_{m,j}(k+1,t)}{\Pr\{\mathbf{y}_{0:t}(m,:)|\hat{\lambda}(m,t-1)\}}$, where $\Pr\{\mathbf{y}_{0:t}(m,:) \mid \hat{\lambda}(m,t-1)\} = \sum_{i\in\{0,1\}}\sum_{j\in\{0,1\}} \alpha_{m,i}(k,t)\hat{p}_{ij}(t-1)p_m(\mathbf{y}_{k+1}(m,:),j,k+1)\beta_{m,j}(k+1,t)$. The summation of $\xi_{m,i,j}(k,t)$ over k can be interpreted as an estimate (at time t) of the expected number of transitions from state i to state j: $\sum_{k=0}^{t-1}\xi_{m,i,j}(k,t) = \mathbb{E}\{\text{number of transitions from } i \text{ to } j\}$. Let $\gamma_{m,i}(k,t)$ denote the probability of channel in state i at time k given the model $\hat{\lambda}(m,t-1)$ and the

observation sequence $\mathbf{y}_{0:t}(m,:)$, for $k \in \{0,...,t-1\}$:

$$\begin{aligned} \gamma_{m,i}(k,t) &= \Pr\{S_m(k) = i \mid \mathbf{y}_{0:t}(m,:), \hat{\lambda}(m,t-1)\} \\ &= \frac{\alpha_{m,i}(k,t)\beta_{m,i}(k,t)}{\sum_{i\in\{0,1\}} \alpha_{m,i}(k,t)\beta_{m,i}(k,t)}. \end{aligned} \tag{2.41}$$

The summation of $\gamma_{m,i}(k,t)$ over $k \in \{0,...,t-1\}$ can be interpreted as an estimate (at time t) of the expected number of times that state i was visited, or equivalently, the expected number of transitions made from state i, so that $\sum_{k=0}^{t-1} \gamma_{m,i}(k,t) = \mathbb{E}\{\text{number of transitions from } i\}$. Thus, a set of re-estimated transition probabilities $\hat{p}_{ij}(m,t) = \frac{\sum_{k=0}^{t-1} \xi_{m,i,j}(k,t)}{\sum_{k=0}^{t-1} \gamma_{m,i}(k,t)}, \forall i,j$ and the stationary state distribution vector $\hat{\pi}(m,t)$ are obtained, resulting in the new parameter set $\hat{\lambda}(m,t) = (\hat{\mathbf{P}}(m,t), \hat{\pi}(m,t))$. For each time t, it has been proven in [62], [63] that either 1) the model $\hat{\lambda}(m,t-1)$ defines a critical point of the likelihood function, in which case $\hat{\lambda}(m,t) = \hat{\lambda}(m,t-1)$; or 2) model $\hat{\lambda}(m,t)$ is more likely than model $\hat{\lambda}(m,t-1)$ in the sense that $\Pr\{\mathbf{y}_{0:t}(m,:) \mid \hat{\lambda}(m,t)\} > \Pr\{\mathbf{y}_{0:t}(m,:) \mid \hat{\lambda}(m,t-1)\}$. Thus, at every time step t, if we iteratively use $\hat{\lambda}(m,t)$ in place of $\hat{\lambda}(m,t-1)$ and repeat the estimation process, then we improve the probability of $\mathbf{y}_{0:t}(m,:)$ being observed from the model until a limiting point is reached [61]. Due to the high complexity of the method (linear in $M \times T$), we propose Algorithm 3 that has a linear complexity only in M. Algorithm 3 drops the backward variable and does not re-initialize $\alpha_{m,i}(0,t)$ at each time $t > 0$ and use $\alpha_{m,i}(t-1,t) = \alpha_{m,i}(t-1,t-1)$ for further induction of the forward variable. The variables $\xi_{m,i,j}$ and $\gamma_{m,i}$ are then computed only for the pair $(t-1,t)$ at each time t. Then the updated estimation $\hat{\lambda}(m,t) = (\hat{\mathbf{P}}(m,t), \hat{\pi}(m,t))$ is obtained as shown in Algorithm 3. The performance of this algorithm is simulated in Section V.

Algorithm 3 Estimation of primary channel Markov model

Initialization: Pick $\hat{\lambda}(m,0)$ **randomly** $\forall m = \{1, \cdots, M\}$**, compute** $\alpha_{m,i}(0,0)$ **with** $\hat{\pi}(m,0)$**.**

while $t \geq 1$ **do**

for $m = 1 : M$ **do**

$\alpha_{m,i}(t-1,t) \leftarrow \alpha_{m,i}(t-1,t-1)$, $\forall i \in \{0,1\}$

$\alpha_{m,j}(t,t) \leftarrow \left[\sum_{i\in\{0,1\}} \alpha_{m,i}(t-1,t)\hat{p}_{ij}(m,t-1)\right] p_m(\mathbf{y}_t(m,:),j,t)$, $\forall j \in \{0,1\}$

Compute $\xi_{m,i,j}(t-1,t) = \frac{\alpha_{m,i}(t-1,t)\hat{p}_{ij}(m,t-1)p_m(\mathbf{y}_t(m,:),j,t)}{\Pr\{\mathbf{y}_{0:t}(m,:)|\hat{\lambda}(m,t-1)\}}, \forall i,j \in \{0,1\}$

Compute $\gamma_{m,i}(t-1,t) = \frac{\alpha_{m,i}(t-1,t)}{\sum_{i\in\{0,1\}} \alpha_{m,i}(t-1,t)}, \forall i \in \{0,1\}$

Update $\hat{\lambda}(m,t) = (\hat{\mathbf{P}}(m,t), \hat{\pi}(m,t))$ with $\hat{p}_{ij}(m,t) = \frac{\sum_{k=1}^{t} \xi_{m,i,j}(k-1,k)}{\sum_{k=1}^{t} \gamma_{m,i}(k-1,k)}, \forall i,j \in \{0,1\}$

end for

end while

2.5 Simulation Results and Discussions

In this section, we first show the performance of our proposed sensing/access strategies including comparison to those proposed in [26]: in each time slot, all SUs sense the *single* primary channel with the highest belief of being *idle*. Next, we show the performance of the primary channel Markov model parameter estimation when they are assumed unknown.

2.5.1 Performance of the proposed myopic spectrum sensing

In order to directly compare the performance of our proposed myopic sensing solution with the results of [26], we first simulate the discounted secondary system reward under the same assumptions as in [26]: 1) perfect knowledge about the primary signaling; 2) the signal-to-noise ratio (SNR) at the n-th SU when sensing the m-th channel at each time k: $SNR = \frac{1}{\sigma_w^2}$; 3) the discount factor is 0.999 for time horizon from 0 to 10000; 4) the SUs sensing reports to the SSDC are directly the observations

$r_{m,n}(k)$'s (i.e. no quantizations at local nodes); 5) all channel coefficients $h_{m,n}(k)$'s are set to 1's for all time (i.e. no fading); 6) unit bandwidth for all primary channels; 7) allowed probability of collisions with PUs is $\zeta = 0.1$; and 8) primary channels have i.i.d. Markovian evolutions with the transition matrix: $\mathbf{P} = \begin{pmatrix} 0.9 & 0.1 \\ 0.8 & 0.2 \end{pmatrix}$. In Fig. 2.5, we show the discounted reward in two cases: 1) 2 primary channels and 1 SU; 2) 2 primary channels and 2 SUs. The performance of the approach in [26] is exactly regenerated in this figure (2 primary channels, 1 SU). When there is only a single SU, the two competing strategies are equivalent and have the same results. However, when there are 2 SUs (the rest of the assumptions staying the same), we see that our proposed approach leads to a higher discounted reward. This is because when all SUs are allocated to sense a single channel, as suggested in [26], SUs lose access opportunities on the other channel.

Next, we compare the resulting *percentage of primary channel usage* of our proposed sensing/access strategy to the one proposed in [26]. We define the *percentage of primary channel usage* as:

$$U = \frac{\sum_{m=1}^{M}\sum_{k=1}^{T}(1-\hat{s}_m(k))(1-S_m(k))}{\sum_{m=1}^{M}\sum_{k=1}^{T}(1-S_m(k))}\ , \tag{2.42}$$

where T is the simulation time. The primary SNR at the n-th SU when sensing the m-th channel is: $SNR = \frac{\sigma_x^2}{\sigma_w^2}$ for the energy detection case, and $SNR = \frac{\pi_1\pi_0}{\sigma_w^2}$ matched filter detection case. Other assumptions are: 1) no discount factor (i.e. $\gamma = 1$); 2) channel coefficients are standard Gaussian distributed: $h_{m,n}(k) \sim \mathcal{N}(0,1)$ and known at each time; 3) unit bandwidth for all primary channels; 4) allowed probability of collisions with PUs is $\zeta = 0.1$; and 5) the primary channels have the same Markov model: $\mathbf{P} = \begin{pmatrix} 0.9 & 0.1 \\ 0.8 & 0.2 \end{pmatrix}$. Fig. 2.6 shows the *percentage of primary channel usage* for both cases: 1) Energy-detector based sensing; 2) matched-filter based sensing. As expected, when perfect knowledge about the primary signaling is assumed, higher *percentage of primary channel usage* is achieved. We also see that, under both cases,

our proposed myopic channel sensing strategy outperforms the strategy of [26]. In the case of perfect knowledge about the primary signaling, the two resulting *percentage of primary channel usage* deviate significantly after -5 dB. Again, this is because the strategy used in [26] constraints all the SUs on a *single* primary channel with the highest believe of being *idle* to sense and access at each time. As the received primary SNR becomes higher, fewer SUs on a single primary channel are needed to achieve an "accurate enough" estimation of the state of that primary channel. As a result, if all the SUs are allocated to a single primary channel at each time, the opportunities on the other channel are lost entirely. When a sufficient number of SUs are available, the more opportunities are lost using the strategy in [26]. In the case of no prior knowledge about the primary signaling, similar performance results are observed for higher primary SNR regions. From Fig. 2.6, we can also see that the the sub-optimal algorithms (iterative Hungarian algorithm with polynomial complexity and the heuristic algorithm with linear complexity) give sub-optimal (very close to the optimal myopic solution) performance at much lower computational complexities.

To address the problem of the performance gap of the optimal myopic sensing solution and the optimal solution to the POMDP, an upper-bound is obtained by assuming that SUs perform the proposed optimal myopic sensing, but after obtaining the sensing and access decisions in the current time slot, the current true states of all the channels are revealed to the secondary system in order to obtain the most accurate belief update for next time slot, and this procedure repeats. Note that the true state information in any time slot is not used to make the sensing and assess decision in that time slot, but only for the purpose of belief update for the next time slot. This process yields an upper-bound for the optimal POMDP solution because the optimal myopic policy guarantees the maximum possible reward in each current time slot given the information obtained from the past, whereas revealing the current true states of all channels gives the most accurate belief update, such that no other sensing policy gives better performance than this combined procedure. Fig. 2.8

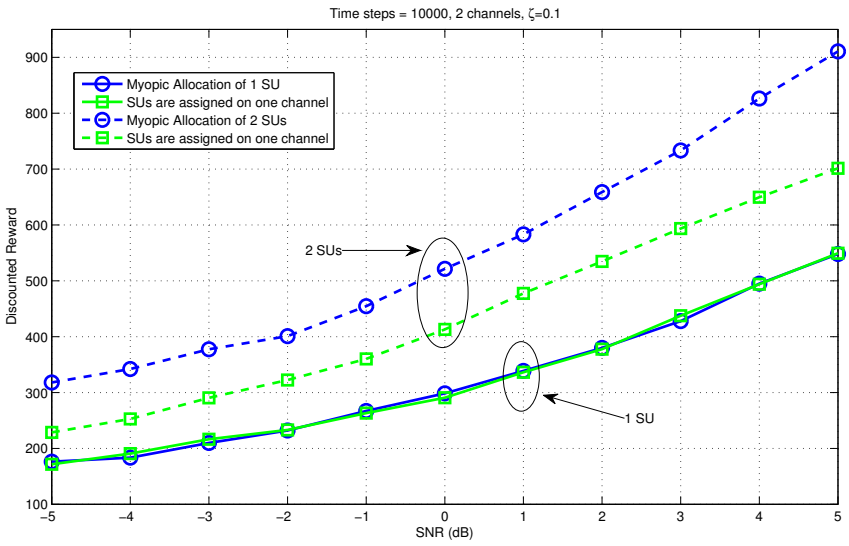

Figure 2.5: Discounted reward comparison.

and 2.9 show the performance comparison between the optimal myopic solution and the obtained upper-bound (both using the energy based detection): 1) in the first simulation set, as shown in Fig. 2.8, we set $p_{00} = 0.1$, $p_{01} = 0.9$, $p_{10} = 0.2$, $p_{11} = 0.8$ and simulated 4 channels with 1, 2, 3, and 4 SUs respectively. We see that the performance gap is quite tight. We also plotted the ratio of the myopic performance to the upper bound, which increases with SNR and is bounded below by roughly 0.88; 2) in the second simulation set, as shown in Fig. 2.9, we set $p_{00} = 0.9$, $p_{01} = 0.1$, $p_{10} = 0.02$, $p_{11} = 0.98$, and the gap is larger compared to the first simulation set, this is due to the *extreme* choices of the state transition probabilities. Note that the transition probabilities indicate that it is highly probable that channel will stay in either idle or busy for a long period of time and it is not likely to change either from busy to idle or from idle to busy, such that the assumption on the true state revealing at the end of each time slot is significantly more critical than the previous case. Due to this reason, we observe a larger performance gap. We also plotted the ratio of

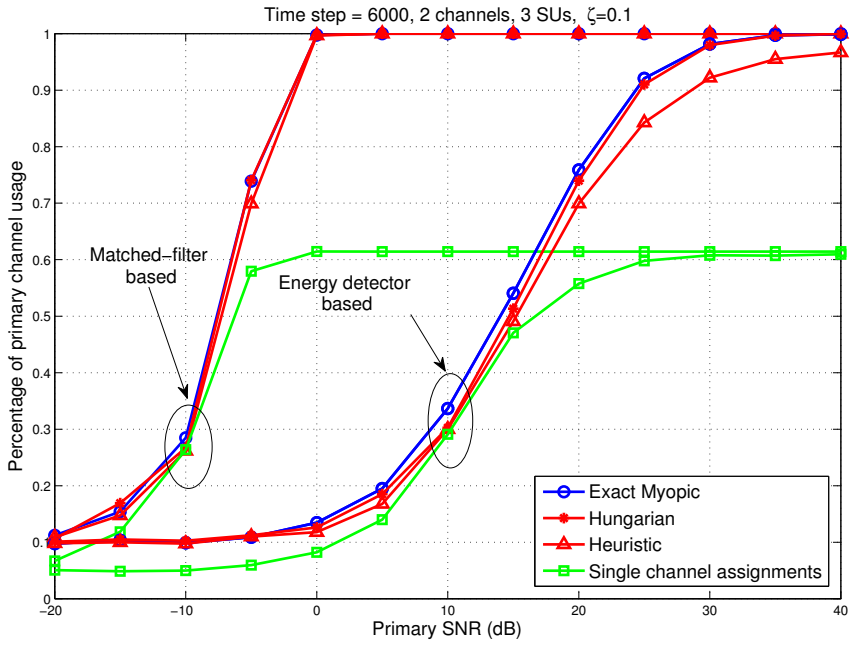

Figure 2.6: Comparisons of percentage of primary channel usage with 2 primary channels and 3 SUs.

the myopic performance to the upper-bound and found out that the ratio behaves similarly to the previous case and is bounded below by roughly 0.35. Although the performance gap is large at the low SNR when there are only few SUs, we can see that the ratio increases as the number of SUs increases. When there are 4 SUs, the ratio is bounded from below by roughly 0.7. In practical cases, the number of SUs is usually much larger than the number of primary channels, as a result, we conclude that the myopic solution is not far from the upper-bound. These results suggest that the proposed optimal myopic solution and its sub-optimal algorithms are practical and efficient.

Fig. 2.10 justifies the simplification of the objective function in (2.35) to the one in (2.36). The secondary system throughput obtained from the objective function in

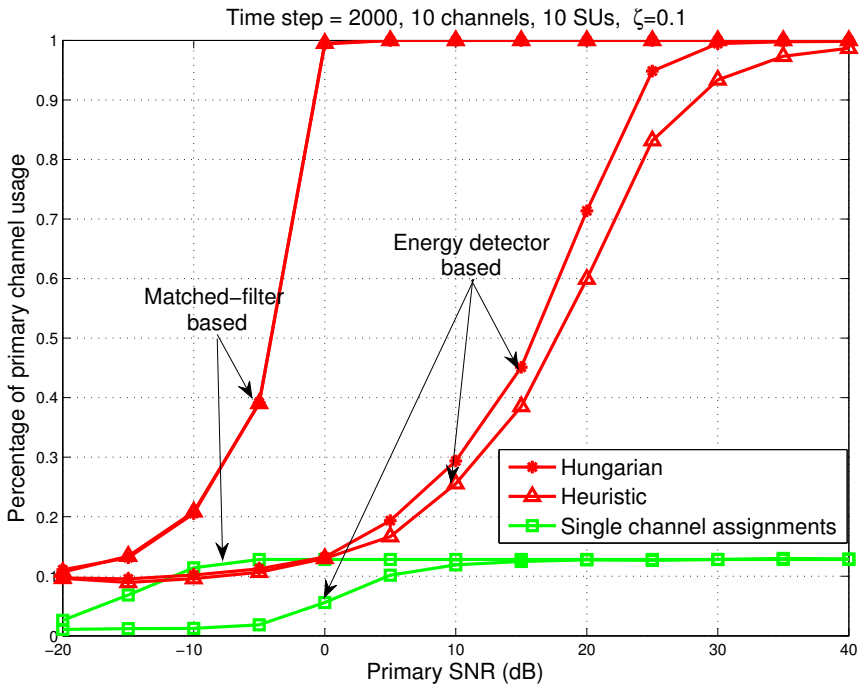

Figure 2.7: Comparisons of percentage of primary channel usage with 10 primary channels and 10 SUs.

(2.35) provides only a marginal performance improvement and as the number of SUs increases, the performance gap becomes negligible. Note that practice, the number of SUs is indeed likely to be larger than the number of primary channels which may justify the use of the objective function provided in (2.36).

2.5.2 Estimation of primary channel Markov model parameters

As shown in Fig. 2.11, we performed Algorithm 3 for the case of one primary channel, one SU and compared it to the algorithm presented in [61] which we denote as method I. We denote Algorithm 3 as method II. In this simulation we assumed

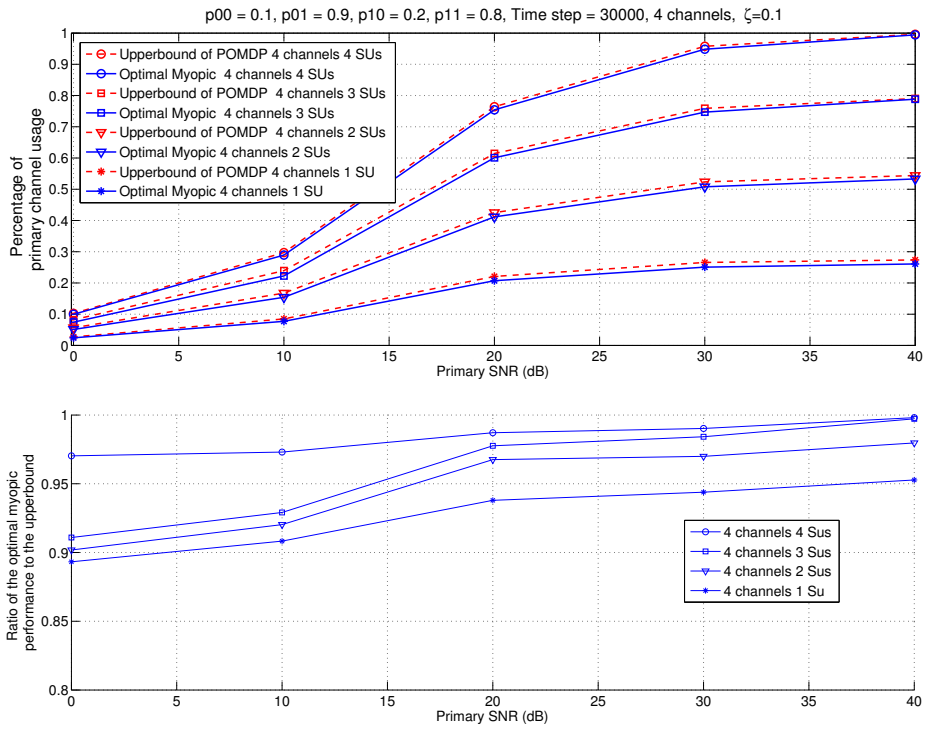

Figure 2.8: Comparisons of performance gap between the proposed optimal myopic sensing policy and the upper-bound of the optimal POMDP sensing policy, for the case of the following transition probabilities: $p_{00} = 0.1$, $p_{01} = 0.9$, $p_{10} = 0.2$, and $p_{11} = 0.8$. To illustrate clearly in the plot, this simulation is based on the energy based detection. Other sensing techniques give similar results.

the following: 1) the crossover probabilities of the observation BAC channel are: $\lambda^1_{1,1}(k) = \lambda^0_{1,1}(k) = 0.1$; 2) the true values of the channel state transition probabilities are: $p_{00} = 0.9$, $p_{01} = 0.1$, $p_{10} = 0.2$, $p_{11} = 0.8$. From Fig. 2.11 we see that there is no significant difference between the convergence times of these two methods (method I gives comparatively smoother convergence performance though). Also, both methods converge very close to the correct true values but Method II has a linear complexity only with M (method I has a linear complexity with $M \times T$).

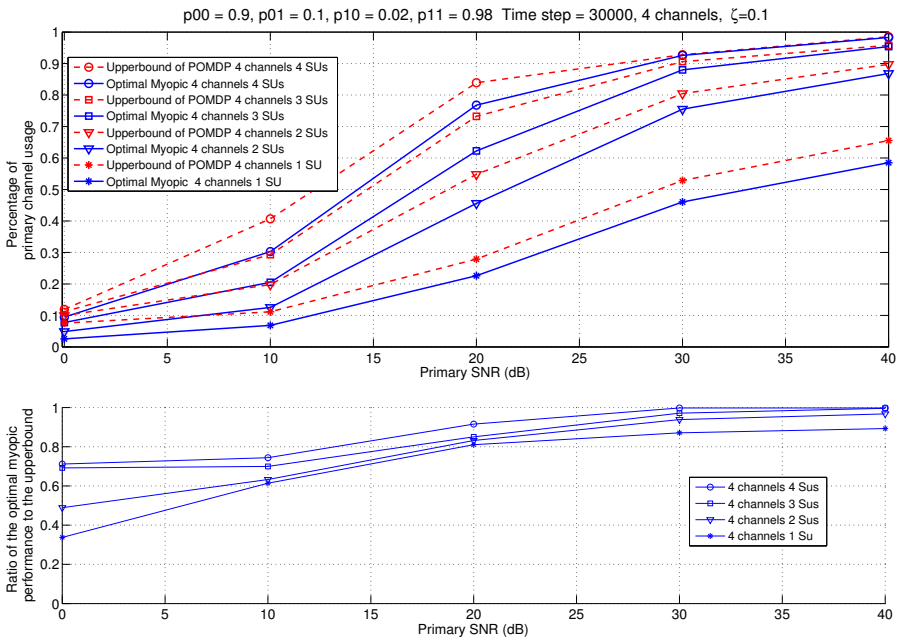

Figure 2.9: Comparisons of performance gap between the proposed optimal myopic sensing policy and the upper-bound of the optimal POMDP sensing policy, for the case of the following transition probabilities: $p_{00} = 0.9$, $p_{01} = 0.1$, $p_{10} = 0.02$, and $p_{11} = 0.98$. To illustrate clearly in the plot, this simulation is based on the energy based detection. Other sensing techniques give similar results.

2.6 Chapter Summary

In this chapter, we have presented a *universal myopic* channel sensing and access policy for a centralized CR communication system in which the channel sensing and access decisions are made at a central unit. By using the word *universal*, we mean that our proposed myopic policy is applicable to any number of primary channels, any number of SUs, and any primary channel Markov model parameters, such as the state transition probabilities and stationary distributions. Unlike other existing

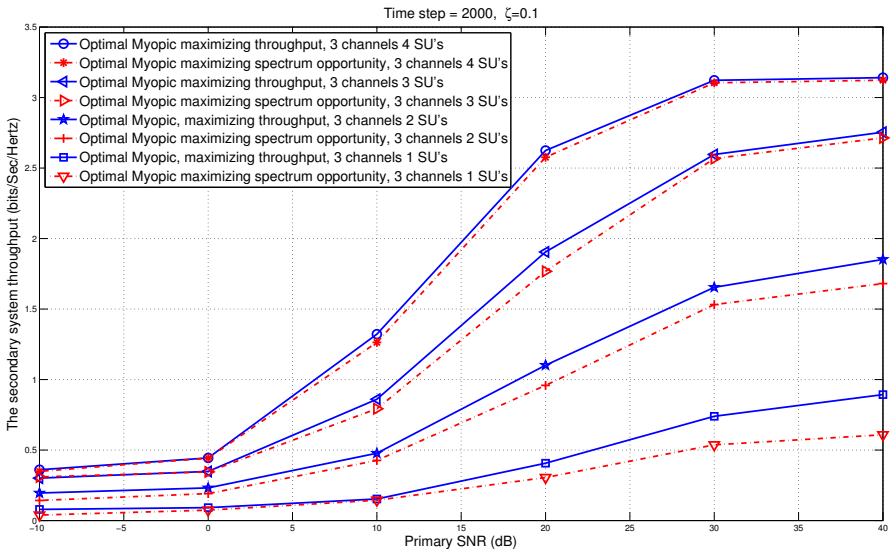

Figure 2.10: Acheived secondary system throughput comparison of the energy based detector at the SSDC with two different objective functions: 1) maximizing the secondary sysstem throughput jointly with sensing decision and the access assigning decision, assuming the channel coefficients of the secondary sender-receiver channels are known at the SSDC; 2) maximizing the spectrum opportunities without considering the access assigning decision-making.

approaches proposed in literature, our universal *myopic* channel sensing policy is more realistic because our policy explicitly assigns SUs to sense specific primary channels by taking into account the spatial and temporal variations of channel fading coefficients on different primary channels. As alternatives to the high complexity *optimal myopic* channel sensing policy, we proposed two algorithms to obtain sub-optimal policies with low complexities: The first is based on the iterative Hungarian algorithm and it has fourth-order complexity while the second algorithm is based on a heuristic method with a linear complexity. The simulation results showed that the two proposed low-complexity algorithms achieve performance very close to the optimal myopic solution, but with much smaller computational efforts. We also showed that under realistic conditions our approach outperforms previously proposed

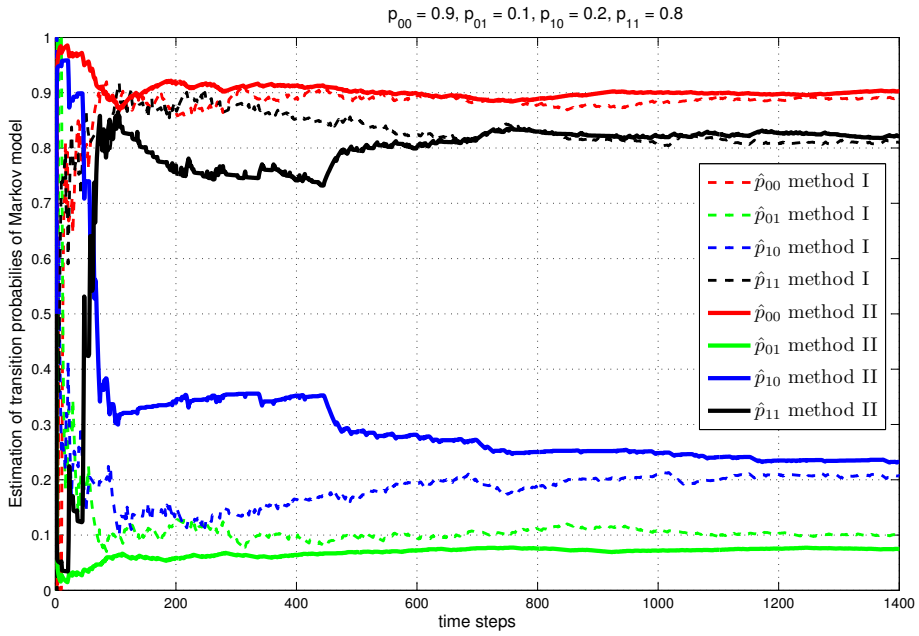

Figure 2.11: Estimations of channel Markov model state transition probabilities (Methods I and II).

approaches. To support our *myopic* sensing policy, we also proposed an effective algorithm with linear complexity to estimate unknown channel Markov model.

Chapter 3

Cyclostationarity-based Feature Extraction and Practical Concerns

3.1 Cyclostationarity-based Feature Extraction

In order to detect active RF signals, we propose to identify their carrier frequencies and the associated cyclic frequencies that are induced by the underlying periodicities of those signals. Note that, it is well-known that almost all man-made signals exhibit such underlying periodicities due to, for example, their symbol rates, coding schemes, packet/frame header structures and training symbol sequences, etc. [64]. In the following discussion, however, we will explicitly focus on the cyclic properties induced by the symbol and coding rates[1]. Using the discrete-frequency smoothing method [64] described below, we compute an estimate of the Spectral Correlation Function (SCF) $S_x^\alpha(t, f)$ for a general discrete signal $\{x(t-kT_s)\}_{k=0}^{M-1}$, where T_s is the sampling period, and M is the number of samples.

[1]It is fairly straightforward to generalize the method to include other periodicities that might be present in any given signal.

The fast Fourier transform (FFT) $\tilde{X}(t,f)$ of the sequence $\{x(t-kT_s)\}_{k=0}^{M-1}$ is defined in (3.1) over the set of frequencies $\{-\frac{f_s}{2}, -\frac{f_s}{2}+F_s, \cdots, \frac{f_s}{2}-F_s, \frac{f_s}{2}\}$, where $f_s = \frac{1}{T_s}$ is the sampling rate and $F_s = \frac{1}{MT_s}$ is the frequency increment and $a(t)$ is a triangular data tapering window [64].

$$\tilde{X}(t,f) = \sum_{k=0}^{M-1} a(t-kT_s)x(t-kT_s)e^{-j2\pi f(t-kT_s)}. \tag{3.1}$$

An estimate of the SCF can then be obtained based on the discrete-frequency smoothing method [64]:

$$\tilde{S}_x^{\alpha}(t,f) = \frac{1}{LT}\sum_{\nu=-(L-1)/2}^{(L-1)/2} \tilde{X}(t, f+\frac{\alpha}{2}+\nu F_s)\tilde{X}^*(t, f-\frac{\alpha}{2}+\nu F_s),$$

where $T = MT_s$ is the time length of the data segment, α is the cyclic frequency and L (an odd number) is the spectral smoothing window length. By setting $\alpha = 0$, we first obtain an estimation of the power spectral density (PSD) of the discrete signal $\{x(t-kT_s)\}_{k=0}^{M-1}$:

$$\tilde{S}_x^{0}(t,f) = \frac{1}{LT}\sum_{\nu=-(L-1)/2}^{(L-1)/2} \left|\tilde{X}(t, f+\nu F_s)\right|^2. \tag{3.2}$$

The active carrier frequencies in the spectrum sub-band of interest is determined by setting a threshold on the above PSD. According to [65], the threshold η_{PSD} shown below can be derived based on the Neyman-Pearson test:

$$\eta_{PSD} = \frac{\gamma^{-1}\left(L; (1-\alpha_F)\,\Gamma(L)\right) P_n}{T_s L}\,, \tag{3.3}$$

where α_F is the false alarm probability, γ^{-1} is the inverse lower incomplete gamma function (where $\gamma(k,x) = \int_0^x t^{k-1}e^{-t}dt$ and the inverse is w.r.t. the second argument), $\Gamma(k) = \int_0^\infty t^{k-1}e^{-t}dt$ is the gamma function and P_n is the noise power that can be estimated as $\hat{P}_n = T_s \sum_{f=-f_s/2}^{f_s/2} \tilde{S}_x^0(t,f)$, similar to the method discussed in [66]. The impact of noise power uncertainty was discussed and analyzed in [67, 68] where

the deterioration of the detector performance was upper-bounded by an expression involving the peak-to-peak range of noise uncertainty [67]. The carrier frequencies are estimated as the midpoints of the segments formed by the intersection between the PSD curve and the threshold line η_{PSD}, as shown in Fig. 3.1. We denote by $\mathcal{A}$ the set of all detected carrier frequencies in the sub-band of interest.

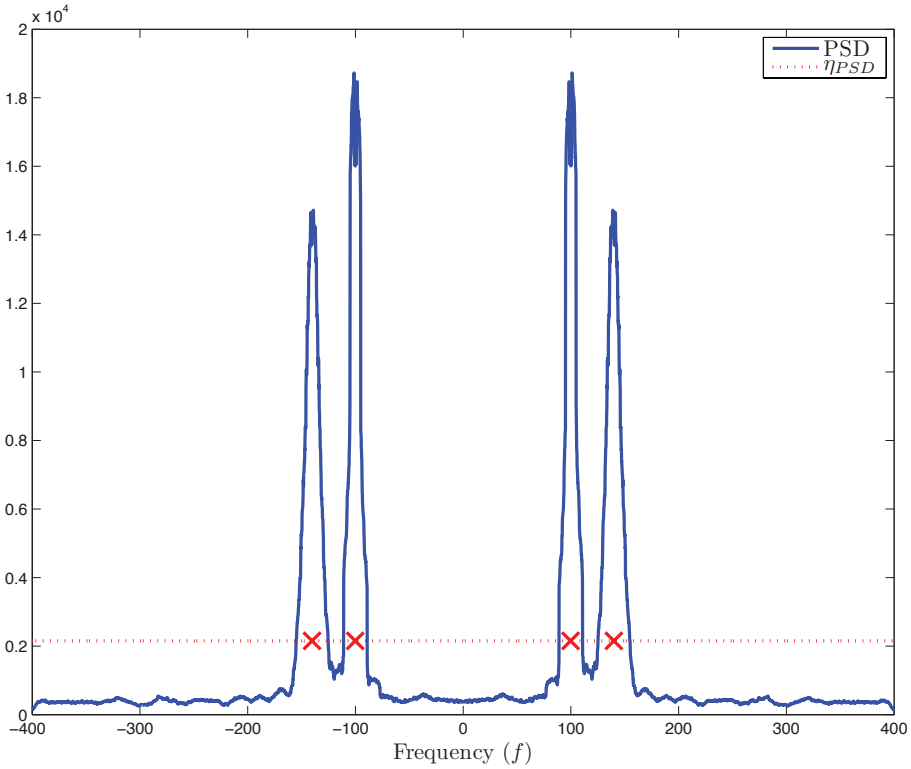

Figure 3.1: Carrier frequencies are estimated as the midpoints of the intersections between the PSD curve and the threshold line.

Next, an estimate of the spectral autocoherence function magnitude [64] is computed as:

$$|\tilde{C}_x^{\alpha}(t,f)| = \frac{|\tilde{S}_x^{\alpha}(t,f)|}{\sqrt{\tilde{S}_x^{0}(t,f+\alpha/2)\tilde{S}_x^{0}(t,f-\alpha/2)}}\,. \tag{3.4}$$

Note that $|\tilde{C}_x^{\alpha}(t,f)|$ is normalized to be between 0 and 1. Due to the fact that for

each carrier, the associated cyclic components show up peaks in a close range of the carrier, we define the *cyclic sub-domain* profile of carrier $f_c \in \mathcal{A}$ as:

$$\tilde{I}_x(t, \alpha, f_c) \;=\; \max_{f \in [f_c - \Delta f_L(f_c), f_c + \Delta f_U(f_c)]} |\tilde{C}_x^{\alpha}(t, f)| \;, \tag{3.5}$$

where the lines $f = f_c - \Delta f_L(f_c)$ and $f = f_c + \Delta f_U(f_c)$ $(\forall f_c \in \mathcal{A})$ partition the (f, α)-plane into Voronoi cells whose point sites [69] are located at the detected carrier frequency points $\{(f_c, 0) : f_c \in \mathcal{A}\}$.

In [70], it is shown that digital signals exhibit cyclostationarity at multiples of their baud rates. Moreover, the digital signals may exhibit other periodicities as well, for example, due to coding. We denote the RF signature of the signal centered at f_c as $\mathrm{RF}(f_c) = \{\alpha \neq 0 : \mathfrak{I}_E \tilde{I}_x(t, \alpha, f_c) \geq \zeta\}$, where $\mathfrak{I}_E$ denotes the indicator function of event $E = \{\tilde{I}_x(t, \alpha, f_c)$ is a local maximum$\}$, and $\zeta \in (0, 1)$ is a threshold for the peak detection in the cyclic sub-domain profile.

3.2 Impact of Time-varying Channel Fading on the cyclostationary features

In this section, we show that the cyclostationary features of signals can essentially be preserved even in the presence of channel fading. In other words, we show that the proposed cyclostationarity based detection method is robust against channel fading effects.

A continuous-time real-valued stochastic process $x(t)$ is said to be second-order *cyclostationary in the wide sense* if its mean $\mathbb{E}\{x(t)\}$ and autocorrelation function $R_{xx}(t, \tau) \triangleq \mathbb{E}\{x(t + \tau)x(t)\}$ are periodic with some period, say T_0:

$$\mathbb{E}\{x(t + T_0)\} = \mathbb{E}\{x(t)\},\; R_{xx}(t + T_0, \tau) = R_{xx}(t, \tau), \tag{3.6}$$

for all t and τ [71]. We consider a cyclostationary digital signal $x(t)$ and an linear time-varying (LTV) fading channel[2], having an impulse response of $h(\tau', t)$. According to the definition of cyclostationarity, we know that the autocorrelation function of $x(t)$ is a periodic function of t, such that $R_{xx}(t+T_0, \tau) = R_{xx}(t, \tau)$, for some period T_0. The received signal $y(t)$ through the LTV fading channel can be expressed as:

$$y(t) = \int_0^\infty x(t-\tau')h(\tau', t)d\tau' + w(t), \tag{3.7}$$

where $w(t)$ is an additive wide sense stationary (WSS) noise process. The autocorrelation function of the received signal $y(t)$ can then be expressed as:

$$\begin{aligned}
& R_{yy}(t,\tau) = \mathbb{E}\left\{y(t+\tau)y(t)\right\} \\
= \;& \mathbb{E}\left\{\left[\int_0^\infty x(t+\tau-\tau_1')h(\tau_1', t+\tau)d\tau_1' + w(t+\tau)\right]\times\right. \\
& \left.\times\left[\int_0^\infty x(t+\tau-\tau_2')h(\tau_2', t)d\tau_2' + w(t)\right]\right\} \\
= \;& \mathbb{E}\left\{\int_0^\infty\int_0^\infty x(t+\tau-\tau_1')x(t+\tau-\tau_2')h(\tau_1', t+\tau)h(\tau_2', t)d\tau_1'd\tau_2'\right\} + \\
& +\mathbb{E}\left\{w(t+\tau)w(t)\right\} \\
= \;& \int_0^\infty\int_0^\infty \mathbb{E}\left\{x(t+\tau-\tau_1')x(t+\tau-\tau_2')\right\}\times\times\mathbb{E}\left\{h(\tau_1', t+\tau)h(\tau_2', t)\right\}d\tau_1'd\tau_2' + \\
& +R_{ww}(t,\tau) \\
= \;& \int_0^\infty\int_0^\infty R_{xx}(t, \tau-\tau_1'+\tau_2')R_{hh}(\tau_1', \tau_2'; t+\tau, t)d\tau_1'd\tau_2' + R_{ww}(\tau),
\end{aligned} \tag{3.8}$$

where $R_{hh}(\tau_1', \tau_2'; t_1, t_2) \triangleq \mathbb{E}\left\{h(\tau_1', t_1)h(\tau_2', t_2)\right\}$ is the autocorrelation of the channel impulse response $h(\tau', t)$, and $R_{ww}(t, \tau) = R_{ww}(\tau)$ is the autocorrelation function of the WSS noise.

According to empirical studies, the channel can be considered as WSS as long as the mobile unit (the transmitter and/or receiver) covers a distance in the dimension of

[2]Time-varying is due to motion of the transmitter and/or receiver. Note that the LTV channels are also referred to as time-frequency dispersive/selective or doubly dispersive/selective in the literature.

a few tens of the wavelength of the carrier signal in an observation period [72]. We also assume that scattering components with different propagation delays are statistically uncorrelated. These channel models are called US (uncorrelated scattering) channel models or US models [73]. The most important class of stochastic LTV channel models is represented by models belonging both to the class of WSS and to the class of US. These channel models are called WSSUS models and are almost exclusively employed in current literature for modeling frequency selective mobile radio channels [72–76].

Under this common assumption of WSSUS, the autocorrelation function of the impulse response of the LTV fading channel can be expressed as [73]:

$$R_{hh}(\tau_1', \tau_2'; t+\tau, t) = \delta(\tau_2' - \tau_1') S_{hh}(\tau_1', \tau), \tag{3.9}$$

where $S_{hh}(\tau_1', \tau)$ is called the *delay cross-power spectral density* [73]. We substitute (3.9) back into (3.8) to obtain:

$$\begin{aligned} R_{yy}(t,\tau) &= \int_0^\infty \int_0^\infty R_{xx}(t, \tau - \tau_1' + \tau_2') \delta(\tau_2' - \tau_1') S_{hh}(\tau_1', \tau) d\tau_1' d\tau_2' + R_{ww}(\tau) \\ &= \int_0^\infty R_{xx}(t,\tau) S_{hh}(\tau_1', \tau) d\tau_1' + R_{ww}(\tau) \\ &= R_{xx}(t,\tau) \int_0^\infty S_{hh}(\tau_1', \tau) d\tau_1' + R_{ww}(\tau), \end{aligned} \tag{3.10}$$

so that

$$\begin{aligned} R_{yy}(t+T_0,\tau) &= R_{xx}(t+T_0,\tau) \int_0^\infty S_{hh}(\tau_1', \tau) d\tau_1' + R_{ww}(\tau) \\ &= R_{xx}(t,\tau) \int_0^\infty S_{hh}(\tau_1', \tau) d\tau_1' + R_{ww}(\tau) \\ &= R_{yy}(t,\tau). \end{aligned} \tag{3.11}$$

This shows that the autocorrelation function of the received signal $y(t)$ is also periodic with the same period T_0 as the transmitted signal $x(t)$. As a result, the received signal $y(t)$ is also cyclostationary with the same cyclic components as $x(t)$.

A more general class of stochastic processes is obtained if the autocorrelation function $R_{xx}(t,\tau)$ is almost periodic in t for each τ [77]: A continuous-time real-valued stochastic process $x(t)$ is said to be *almost-cyclostationary (ACS) in the wide sense* if its autocorrelation function $R_{xx}(t,\tau)$ is an almost periodic function of t (with frequencies not depending on τ) [71]. When the input signal $x(t)$ is considered as ACS, the output signal $y(t)$ through the LTV fading channel is also ACS with the same cyclic components as $x(t)$, since we can see from (3.10) and (3.11) the autocorrelation function $R_{yy}(t,\tau)$ is also almost periodic with the same period as $R_{xx}(t,\tau)$.

As a result, we see that when fading channels are considered as general LTV systems (i.e., considering both channel fading and the doppler effect), the cyclostationary properties of the transmitted signals are not altered at the output of the channel, or the received signal at the Radiobot. This justifies the robustness of the cyclostationarity based detection/classification method, in the presence of channel fading. Note that, the proposed cyclostationarity based detection method introduced in Section 3.1 also applies to the ACS assumption, since the SCF is also defined under the assumption of ACS and it has been shown that an ACS signal exhibits cyclostationarity at cycle frequency α if $R^{\alpha}_{xx}(\tau) \not\equiv 0$, similarly to the cyclostationary stochastic processes [71, 77].

3.3 Impact of the Doppler Shift on the detected carrier frequencies

In this section, we analyze the impact of Doppler shift on the PSD of the received signal. The cyclic autocorrelation function $R^{\alpha}_{yy}(\tau)$ of the received signal $y(t)$ is defined as $R^{\alpha}_{yy}(\tau) \triangleq \lim_{T\to\infty} \frac{1}{T} \int_{-\frac{T}{2}}^{\frac{T}{2}} R_{yy}(t,\tau) e^{-j2\pi\alpha t} dt$ [77]. Replacing $R_{yy}(t,\tau)$ by its value in

(3.10), we obtain:

$$R_{yy}^{\alpha}(\tau) = H(\tau)R_{xx}^{\alpha}(\tau) + R_{ww}(\tau)\delta^{K}(\alpha), \tag{3.12}$$

where $H(\tau) = \int_{-\infty}^{\infty} S_{hh}(\tau_1', \tau)d\tau_1'$ and δ^K denotes the Kronecker delta function. We may compute the PSD $S_y^0(f)$ of the received signal $y(t)$ as the Fourier transform (denoted by the operator $\mathcal{F}$) of $R_y^{\alpha}(\tau)$ at $\alpha = 0$, such that:

$$\begin{aligned}
S_y^0(f) &= \mathcal{F}\left\{\int_{-\infty}^{\infty} S_{hh}(\tau_1', \tau)d\tau_1'\right\} * S_x^0(f) + S_w(f) \\
&= \int_{-\infty}^{\infty} \mathcal{F}\left\{S_{hh}(\tau_1', \tau)\right\} d\tau_1' * S_x^0(f) + S_w(f) \\
&= \int_{-\infty}^{\infty} S(\tau_1', f)d\tau_1' * S_x^0(f) + S_w(f) \quad \text{from (7.37) in [73]} \\
&= S_{\mu\mu}(f) * S_x^0(f) + S_w(f) \quad \text{from (7.42) in [73]} ,
\end{aligned}$$

where $S(\tau_1', f)$ and $S_{\mu\mu}(f)$ are, respectively, the *scattering function* and the *Doppler power spectral density*, and $S_x^0(f)$ is the PSD of the transmitted signal. The Doppler PSD is usually defined over a range $[-f_{max}, f_{max}]$, where f_{max} is the maximum Doppler frequency shift [73]. Thus, the received PSD can be expressed as:

$$S_y^0(f) = \int_{-f_{max}}^{f_{max}} S_{\mu\mu}(\nu)S_x^0(f-\nu)d\nu + S_{ww}(f) \ . \tag{3.13}$$

Based on (3.13), the convolution of $S_x^0(f)$ with a window of length $2f_{max}$ causes the PSD to spread at most by $\pm f_{max}$ at each point. If the Doppler PSD $S_{\mu\mu}(f)$ is symmetric (such as Jakes' type [73]), the carrier frequency components of the detected feature points do not shift since the main lobes of the PSD are spread evenly in both left and right directions. However, if $S_{\mu\mu}(f)$ is not symmetric (such as Rice's, Gauss I or Gauss II types [73]), the detected carrier frequencies will shift by an amount smaller than f_{max}. Therefore, due to the Doppler shift, it may not be possible to detect and distinguish signals that are separated by less than f_{max} in the spectrum. However, based on the users activity and by using appropriate

learning algorithms, the Radiobot might be able to detect each of the signals when they are the only transmitted signals. Then using this knowledge, it may be able to distinguish them when both signals are transmitted simultaneously. This again emphasizes the importance of true learning from past experience during the signal detection and classification steps.

In order to illustrate the robustness of the cyclostationarity-based feature extraction against the channel fading and doppler effect, we simulated a Bluetooth signal with a symbol duration of 1μS (i.e., a resulting symbol rate cyclic frequency feature at 1MHz). The channel is configured as a frequency-selective (multi-path) fading channel with a maximum Doppler shift of $\pm$300Hz, which corresponds to a maximum transmitter-receiver relative speed of 37.5m/s, or around 84 mph for a signal in the 2.4GHz frequency range. There are three discrete path specified with their delays 0μS, $.15\mu$S, and $.32\mu$S, respectively, and with an average path gain of 0, -10, and -10dB, respectively. Each discrete path is modeled as an independent Rayleigh fading process. The cyclic profile of the received Bluetooth signal with SNR = -5dB, before and after the linear time-varying fading channel is shown in Fig. 3.2. As shown in Fig. 3.2, the cyclic peaks for the Bluetooth signal stays exactly at 1MHz and its multiples, for both before and after the fading channel with Doppler frequency shift. We can also see that the Bluetooth signal shows a minor cyclic peak amplitude decreasing after the fading channel, this is possibly due to the random path amplitude variation and the signal distortion in the multi-path environment.

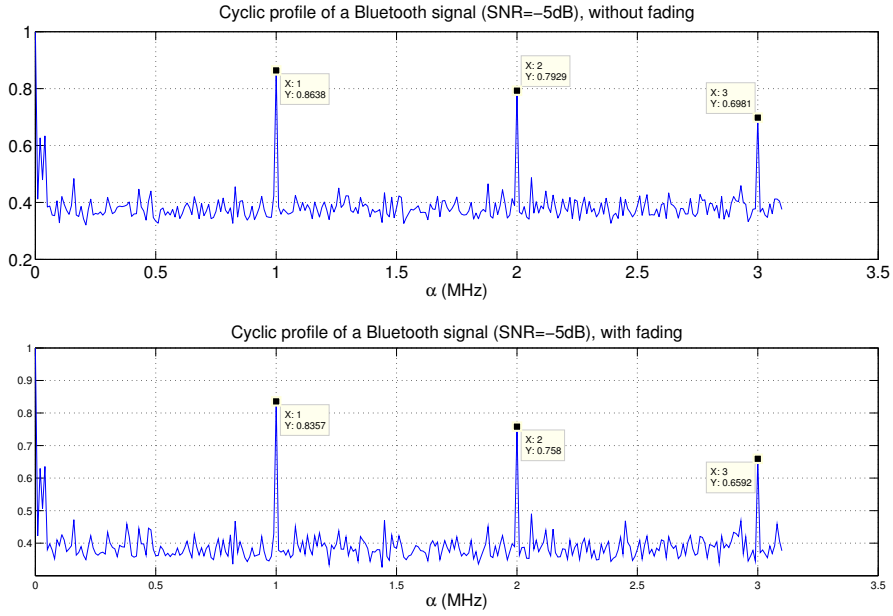

Figure 3.2: A comparison of the cyclic profile of a Bluetooth signal before and after linear time-varying channel fading.

3.4 Spectral Correlation Function of Multiple Superposed Digital Signals

In practice, the Radiobot is more likely to deal with multiple RF activities in each spectrum sub-band of interest. Thus, it needs to know the corresponding SCF properties of superposed digital signals, in order to identify the number and types of the detected signals accurately.

In order to analyze the impact of the superposition of multiple signals on the SCF of a signal $y(t)$, let us assume that $y(t) = w(t) + \sum_{m=1}^{N_s} x_m(t)$, where $\{x_m(t)\}_{m=1}^{N_s}$ are *independent zero-mean* random processes (denoting N_s superposed signals) and $w(t)$ is an independent white noise process with a double-sided PSD of $\frac{N_0}{2}$. The

autocorrelation function of $y(t)$ is $R_{yy}(t,\tau) = \frac{N_0}{2}\delta(\tau) + \sum_{m=1}^{N_s} R_{x_m x_m}(t,\tau)$, where $R_{x_m x_m}(t,\tau)$ is the autocorrelation functions of $x_m(t)$, for $m = 1, \cdots, N_s$. First, we define a Fourier transform for the cyclic autocorrelation function as [77]:

$$\begin{aligned} R^{\alpha}_{yy}(\tau) &\triangleq \lim_{T\to\infty} \frac{1}{T} \int_{T/2}^{T/2} R_{yy}(t,\tau) e^{-j2\pi\alpha t} dt \\ &= \lim_{T\to\infty} \frac{1}{T} \int_{T/2}^{T/2} \left[\frac{N_0}{2}\delta(\tau) + \sum_{m=1}^{N_s} R_{x_m x_m}(t,\tau) \right] e^{-j2\pi\alpha t} dt \\ &= \frac{N_0}{2}\delta(\tau)\delta(\alpha) + \sum_{m=1}^{N_s} R^{\alpha}_{x_m x_m}(\tau). \end{aligned} \tag{3.14}$$

The SCF of $y(t)$ can then be expressed as:

$$S^{\alpha}_{y}(f) = \int_{\mathbb{R}} R^{\alpha}_{yy}(\tau) e^{-j2\pi f\tau} d\tau = \frac{N_0}{2}\delta(\alpha) + \sum_{m=1}^{N_s} S^{\alpha}_{x_m}(f). \tag{3.15}$$

This result shows that the superposition of multiple independent signals results in a superposition of spectral peaks in the (f,α) domain. In other words, the SCF of the superposition of multiple signals has peaks at cyclic frequencies corresponding to integer multiples of, for example, the data rates of each signal.

Chapter 4

Multivariate Non-parametric Quickest detection

4.1 Introduction

In the QD problem, one observes samples sequentially. Initially, the samples are drawn from a certain distribution. At an unknown time, the distribution changes. Once this occurs, one needs to raise an alarm as quickly as possible to minimize the detection delay [78].

In non-time-slotted CR networks, the on/off radio activities at unknown times will change the distribution of the received signal by a CR. In general, QD schemes can be classified into parametric and non-parametric schemes. Parametric QD schemes rely on the knowledge of the pre-change and post-change distributions of the observations. However, in a variety of applications, including detecting radio activities in an unknown RF environment, such prior knowledge may be hard to obtain due to uncertainties induced by channel fading, channel shadowing, the distance to the primary radios, and Doppler effects, among others. In comparison, a non-parametric

QD scheme does not require any knowledge of the pre-change and post-change distributions.

In [79], QD methods were proposed for CRs. Both parametric and non-parametric based algorithms were discussed and analyzed. However, the discussed methods were only based on energy features. Note that the detection reliability can be compromised by using energy features alone under channel shadowing, since variation of the received signal power level may trigger excessive false alarms. Moreover, the non-parametric approach proposed in [79] uses the individual sample power as the test statistics instead of the average sample power over a certain duration. This, however, significantly increases the number of detection/observation steps leading to a high computational complexity compared to using a time window to obtain the average sample power. In this chapter, we show that the choice of the time window length plays a critical role in determining the achieved detection delay, false alarm rate, as well as the percentage of idle channel utilization. Setting the time window length down to one sample is evidently not the best choice.

In [7], the authors developed a blind energy and cyclostationarity-based signal identification and classification procedure that does not rely on any prior knowledge of the radio environment. It is also shown in Chapter 3 that the cyclostationarity-based signal features are robust against channel fading, and Doppler effects. As a result, in this chapter, we propose to utilize the cyclostationarity feature to overcome the aforementioned reliability issue of the traditional energy-based QD approach in complex channel conditions, and to exploit diversity to improve the detection performance. To the best of our knowledge, such an average sample power and cyclostationarity-based multivariate non-parametric QD has not been previously considered in literature. Moreover, the performance of the proposed QD algorithms is evaluated in more realistic multi-path frequency-selective fading channels with Doppler effects.

The remainder of this chapter is organized as follows. In Section 4.2 we describe our system model. The uni-variate non-parametric QD scheme is then briefly described to prepare the reader for subsequent sections. In Section 4.3, we propose the non-parametric average sample power-based and the cyclostationarity-based QD schemes. We then propose the average sample power and cyclostationarity-based multivariate non-parametric QD, followed by the novel parallel on-line QD/off-line change-point detection scheme. In Section 4.4 we present performance evaluation of the proposed QD schemes through simulations. In Section 4.5 we conclude by summarizing our results and identifying possible future directions.

4.2 System Model and Non-parametric Quickest Detection

Due to the focus of this chapter on the QD algorithm, we consider the spectrum sensing for a particular communication channel and omit the decision-making problem for scheduling of which channel to sense at any given time. Note that the proposed methods in this chapter work for detecting the state transitions from either idle to busy or from busy to idle. Without loss of generality, first we may consider the case of detecting a change from idle to busy. The detection of changes from busy to idle is further explained in later sections. We assume that after a state change is detected, observations corresponding to the past are discarded. Thus, a new observation vector is obtained by re-initializing the starting point as the previous detection point. As a result, by applying the proposed method iteratively, we may detect each state change-point in a sequence of multiple alternating state change cycles, as long as those changes are sufficiently far apart in order to obtain enough observation data to make a decision. Hence, for the proposed QD schemes to work properly, we assume that the sampling rate is set at a higher rate compared to the rate of state changes.

For example, in the simulation section, we assume that the minimum sojourn times of idle and busy channel states are 600μS (a reasonable assumption according to [80]), while sensing sampling rate is 100MHz. For a certain communication channel of interest, we denote by vector $\mathbf{Z}_1^n = [Z_1, Z_2, \cdots, Z_n]^T$ the sequence of observations or test statistics from time step 1 up to n, depending on the adopted particular sensing technique, including for example, energy detection and cyclostationarity-based detection, etc. At each time n, a CR attempts to distinguish the following two hypotheses based on $\mathbf{Z}_1^n$:

$$\begin{aligned} \mathcal{H}_0 : \quad & Z_i \sim g_0, \ \forall \ i \in \{1, \cdots, n\} \\ \mathcal{H}_1 : \quad & \exists \ \tau \in \{1, \cdots, n\}, \\ & \text{s.t.} \ \begin{cases} Z_i \sim g_0, \forall \ i \in \{1, \cdots, \tau - 1\} \\ Z_i \sim g_1, \forall \ i \in \{\tau, \cdots, n\} \end{cases} , \end{aligned} \tag{4.1}$$

where we denote by g_0 and g_1, respectively, the distribution of Z_i under channel idle and busy hypotheses and τ denotes the time of the state change from idle to busy. We denote by Γ the strategy adopted for the hypothesis testing and denote by t_a the time when the strategy raises an alarm of a state change. If $t_a \geq \tau$, the detection delay is defined as $\tau_d = t_a - \tau$. On the other hand, if $t_a < \tau$, we say a false alarm occurs. Due to the fact that a prior distribution for the change point is generally hard to find and the statistics of the state change pattern can easily be non-stationary, we consider the QD in a non-Bayesian framework.

Note that the channel allocation information[1] can generally be unknown to a Radiobot *a priori*. However, by following the procedure of the RF activity detection and classification introduced in [7], one may classify the RF activities according to

[1]Within the frequency range covered by each configuration of the reconfigurable antenna, there can, in general, be multiple channels belonging to possibly different systems, according to a static RF spectrum allocation scheme. The allocated channels generally may have different center frequencies as well as their bandwidths.

their center frequencies, cyclostationary features (symbol duration, coding structures, etc.), and bandwidths to obtain the knowledge of the RF spectrum usage, so that channel allocation information can be inferred and identified within the frequency range of interest.

In the framework of non-Bayesian QD, the *worst case conditional mean delay* is usually defined as [78, 81]

$$\bar{T}_d = \sup_{\tau \geq 1} \operatorname{ess\,sup} \mathbb{E}_{g_1}\{\tau_d = t_a - \tau \mid t_a \geq \tau, \mathbf{Z}_1^\tau\}, \tag{4.2}$$

where $\mathbb{E}_{g_1}\{\cdot\}$ denotes expectation under the distribution g_1, and the operator ess sup denotes the essential supremum or the smallest essential upper-bound. The conditioning within the expectation is with respect to the change point, and the worst case is taken over all possible values of the change point and all realizations of the measurements or the obtained test statistic sequence up to the change point. Note that the conditional mean delay can be defined as $\mathbb{E}_{g_1}\{\tau_d = t_a - \tau \mid t_a \geq \tau, \mathbf{Z}_1^\tau\}$ [78], which itself is random since τ and $\mathbf{Z}_1^\tau$ are random. One could assign a prior distribution to τ, and then define average delay by averaging the distribution on τ and $\mathbf{Z}_1^\tau$. However, it may be difficult to find a suitable prior distribution for τ in the application of cognitive radios. As a result, the worst case, meaning using the least favorite distributions of τ and $\mathbf{Z}_1^\tau$, is considered by taking the essential supremum over $\mathbf{Z}_1^\tau$, and taking the supremum over τ to the conditional mean delay. We may also define the average run length (ARL) to false alarm (mean value of the false alarm intervals) to be

$$\bar{T}_f = \mathbb{E}_{g_0}\{t_a\}, \tag{4.3}$$

where $\mathbb{E}_{g_0}\{\cdot\}$ denotes expectation under the distribution g_0. Note that in (4.3), the condition $t_a < \tau$ is not included since it is redundant. On the other hand, no essential supremum is taken, so the condition on $\mathbf{Z}_i$'s is also not necessary.

The optimization problem can then be defined to find the strategy Γ that minimizes $\bar{T}_d$ while satisfying a lower threshold T_{th} for the ARL to false alarm $\bar{T}_f$:

$$\begin{aligned} \min_{\Gamma} \quad & \bar{T}_d = \sup_{\tau \geq 1} \operatorname{ess\,sup} \mathbb{E}_{g_1}\{\tau_d = t_a - \tau \mid t_a \geq \tau, \mathbf{Z}_1^{\tau}\}, \\ & \text{subject to } \bar{T}_f \geq T_{th}. \end{aligned} \tag{4.4}$$

Let us denote by G_0 and G_1 respectively the cumulative distribution functions (cdfs) of Z_i corresponding to g_0 and g_1, such that $G_0(z) = \int_{-\infty}^{z} g_0(x)dx$ and $G_1(z) = \int_{-\infty}^{z} g_1(x)dx$. Note that G_1 is said to be stochastically greater [82] than G_0 when $G_0(x) \geq G_1(x)$ for all x, and we can write $G_1 \succ_{st} G_0$.

Observe that if for a particular random process Z_i, for $i = 1, 2, 3, \cdots$ such that the cdfs $G_{Z,0}$ and $G_{Z,1}$ instead satisfy $G_{Z,0} \succ_{st} G_{Z,1}$, and if we denote by $X_i = -Z_i$ another process with corresponding pre-change and post-change cdfs denoted by $G_{X,0}$ and $G_{X,1}$, then it is straightforward to show that $G_{X,1} \succ_{st} G_{X,0}$. This makes it easy to adopt the same QD algorithm explained in the following for both detecting the state changes from idle to busy and those from busy to idle. In case of detecting the state changes from busy to idle, we may simply add a negative sign in front of the obtained test statistics Z_i's such that the post-change distribution is stochastically greater then the pre-change distribution.

From the observation vector $\mathbf{Z_1^n} = [Z_1, \cdots, Z_n]$, we may define the rank for the i-th observation Z_i, as $\rho(i, n) = \sum_{j=1}^{n} I_{\{Z_i \geq Z_j\}}$, where $I_{\{E\}}$ is the indicator function of event E, defined as $I_{\{E\}} = 1$ if event E is true and $I_{\{E\}} = 0$ otherwise. Thus, a higher valued observation Z_i has a higher rank $\rho(i, n)$ in the first n observations. Then, we may take $\boldsymbol{\rho}_n = [\rho(1, n), \cdots \rho(n, n)]$ to determine a permutation of the first n integers. Its inverse permutation can be determined as $\boldsymbol{\mu}_n = [\mu(1, n), \cdots, \mu(n, n)]$, where we define $\mu(\rho(j, n), n) = j$, such that the function $\mu(\rho(j, n), n)$ returns the time sequence index j of an observation with rank $\rho(j, n)$.

With these definitions, the likelihood ratio of the change taking place at $\tau = k$, for $k \in \{1, \cdots, n\}$, and observing a particular $\boldsymbol{\rho}_n$ is given by

$$\Lambda_k^n(\boldsymbol{\rho}_n) = \frac{P\{Z_{\mu(1,n)} < \cdots < Z_{\mu(n,n)} \mid \tau = k\}}{P\{Z_{\mu(1,n)} < \cdots < Z_{\mu(n,n)} \mid \tau > n\}}. \tag{4.5}$$

Since the above rank based likelihood ratio is not too sensitive to the true underlying distributions [82], one can compute this likelihood ratio by choosing some representative (or hypothesized) pre and post-change distributions and design a corresponding algorithm based on this likelihood ratio [82]. Note that the invariance of the ranks under strictly increasing transformations causes the average run length (ARL) to false alarm to be identical for any continuous G_0.

For example, if we choose the representative/hypothesized pre and post-change pdfs as $f_0(x) = e^{-|x|}/2$ and $f_1(x) = p\alpha e^{-\alpha x} I_{\{x \geq 0\}} + q\beta e^{\beta x} I_{\{x<0\}}$, with $p \in (1/2, 1)$, $\alpha \in (0, 1)$, $\beta \in [1, +\infty)$, and $q = 1 - p$ [82], then we have the following cdfs:

$$F_0(x) = \begin{cases} \frac{1}{2}e^x, & \text{if } x < 0 \\ 1 - \frac{1}{2}e^{-x}, & \text{if } x \geq 0 \end{cases}, \tag{4.6}$$

$$F_1(x) = \begin{cases} qe^{\beta x}, & \text{if } x < 0 \\ 1 - pe^{-\alpha x}, & \text{if } x \geq 0 \end{cases}. \tag{4.7}$$

If we make $p\alpha \geq q\beta$, then we can verify that the F_1 is stochastically greater than F_0.

According to [82], the likelihood ratio function in this case can then be expressed as

$$\Lambda_k^n(\boldsymbol{\rho}_n) = \sum_{i=0}^{n} \lambda_{k,i}^n(\boldsymbol{\rho}_n), \tag{4.8}$$

where

$$\begin{aligned}\sum_{m=0}^{n}\lambda_{k,m}^{n}(\rho_n) &= \binom{n}{m}\left(\frac{1}{2}\right)^n\left(\frac{p\alpha}{q\beta}\right)^{U_k(m,n)}(2q\beta)^{n+1-k}\\ &\times\prod_{i=1}^{m}\left(1+\frac{V_k(i,n)}{i}(\beta-1)\right)^{-1}\\ &\times\prod_{i=m+1}^{n}\left(1+\frac{U_k(i-1,n)}{n+1-i}(\alpha-1)\right)^{-1},\end{aligned} \tag{4.9}$$

with $U_k(m,n)=\sum_{j=k}^{n} I_{\{\rho(j,n)>m\}}$, and $V_k(m,n)=(n+1-k)-U_k(m,n)$ [82].

The procedure for the QD provided in [82] is to compute the Shiryayev-Roberts statistic $R_n=\sum_{k=1}^{n}\Lambda_k^n(\boldsymbol{\rho}_n)$ and to stop at time t_a when R_n first achieves or exceeds the critical level A. The ARL to false alarm is shown in [82] to be lower-bounded as

$$A\leq\mathbb{E}_{g_0}\{t_a\}, \tag{4.10}$$

and the ARL to false alarm is shown to grow asymptotically linearly in A as the critical level becomes large. The detection delay is shown in [82] to be upper-bounded as

$$\limsup_{A\to\infty}\sup_{\tau\geq\tau(A)}\mathbb{E}_{g_1}\{t_a-\tau\mid t_a\geq\tau\}\leq\frac{\log(A)}{D(G_0,G_1;f_0,f_1)}, \tag{4.11}$$

where

$$D(G_0,G_1;f_0,f_1)=\mathbb{E}_1\left\{\log\left(\frac{f_1(F_0^{-1}(G_0(Z_1)))}{f_0(F_0^{-1}(G_0(Z_1)))}\right)\right\}. \tag{4.12}$$

The computational complexity of this uni-variate non-parametric QD procedure can be shown to be $\mathcal{O}(n^4)$ [82].

4.3 Multivariate Non-parametric Quickest Detection

4.3.1 Average Sample Power-based Non-parametric Quickest Detection

When there is no prior information about the signal of interest, at any time instance one may model the received signal in a particular channel as $Y = W$ under the assumption of no communication activity, where we denote by W the noise; and $Y = X + W$ when communication activities are present, where we denote by X the received signal contributed from the activity. When the distributions of Y under both activity absent and present are hard to find, or the distribution parameters are unknown, one may adopt the above introduced uni-variate non-parametric QD. The authors in [79] proposed to use the sample powers as the test statistic Z_i's in the non-parametric change-point detection method discussed above, which has a computational complexity of $\mathcal{O}(n^4)$. However, we find that this method is unsuitable when the idle/busy periods last for a length that is at least several transmission-packets long, which is normally the case. This is because the computational complexity becomes high when the size of the vector $\mathbf{Z}_1^n$ is large. Instead, we propose to use a number of consecutive samples to compute an average signal power as the test statistic. In particular, we assume that for every M number of samples, we compute $Z_i = \frac{1}{M}\sum_{j=1+(i-1)M}^{iM} |Y(j)|^2$ as the test statistic. In this case, the computational complexity of obtaining the average power at each step is $\mathcal{O}(M)$. Thus, the computational complexity of the overall uni-variate non-parametric QD scheme becomes $\mathcal{O}(Mn^4)$. It is straightforward to see that, by increasing the number of samples M in each step, the expected number of detection steps n may be significantly reduced. As a result, a lower computational complexity may be obtained by using a time window

to compute an average power, instead of using individual sample powers for the QD. In the simulations section, we also investigate the effect of the choice of M in terms of the detection delays and false alarm rates. In this case, the ARL to false alarm and the detection delay are as characterized in (4.10) and (4.11), respectively.

4.3.2 Cyclostationarity-based Non-parametric Quickest Detection

Under the assumption of the channel being wide sense stationary and uncorrelated scattering (WSSUS), it has been shown in Chapter 3 that the autocorrelation function of a received signal is also periodic with the same period T_0 as the transmitted signal, so that the received signal is also cyclostationary with the same cyclic components as the transmitted signal.

Using the same discrete-frequency smoothing method as in Chapter 3, we may compute an estimate of the Spectral Correlation Function (SCF) $S_x^\alpha(t,f)$ for a general discrete signal $\{x(t-kT_s)\}_{k=0}^{M-1}$ in a particular channel (assuming that the signal is band-limited to the frequency range from f_L to f_H), with M number of samples and a sampling period of T_s. An estimate of the spectral autocoherence function magnitude [64] can then be computed as:

$$|\tilde{C}_x^\alpha(t,f)| = \frac{|\tilde{S}_x^\alpha(t,f)|}{\sqrt{\tilde{S}_x^0(t,f+\alpha/2)\tilde{S}_x^0(t,f-\alpha/2)}}, \tag{4.13}$$

for all $f \in [f_L, f_H]$. Note that $|\tilde{C}_x^\alpha(t,f)|$ is normalized to be between 0 and 1. A *channel cyclic profile* for a channel from f_L to f_H can then be defined as

$$\tilde{I}_x(t,\alpha) \;=\; \max_{f\in[f_L,f_H]} |\tilde{C}_x^\alpha(t,f)|. \tag{4.14}$$

The authors in [7] proposed a blind cyclostationarity-based signal identification and classification strategy, which extracts the underlying cyclic components induced by their symbol rates and coding structures *without any prior information*. The cyclic components induced by signal symbol rates and coding structure can be extracted by finding local maxima of $\tilde{I}_x(t,\alpha)$. The local maxima are not hard to be determined by setting a threshold to the cyclic profile since the profile has sharp peaks at the cyclic frequencies corresponding to the symbol rate and coding rate. The same authors in [7] also developed a machine learning based algorithm for setting the threshold of the cyclic profile in order to better extract the cyclic components without any prior information in a later work in [11]. By utilizing the blind signal identification and classification method in [7], we may obtain knowledge of the channel information including channel carrier frequency, bandwidth, and cyclic components associated with each channel. On the other hand, in the context of traditional dynamic spectrum sharing, channel information and primary signal characteristics, such as carrier frequency, signal bandwidth, symbol rates etc., are generally assumed to be known beforehand. As a result, the following proposed QD schemes are applicable for the traditional CRs as well.

Assuming a particular cyclic frequency α_0 that is of interest for a particular channel from f_L to f_H, one may compute the value of $\tilde{I}_x(t,\alpha_0)$. It can be seen from (4.13) and (4.14) that, $\tilde{I}_x(t,\alpha_0)$ takes value in the interval of $(0,1)$. However, due to channel fading, shadowing effects, sensing duration, sampling frequency, unknown signal-to-noise ratio (SNR), and estimation errors etc., the distribution of $\tilde{I}_x(t,\alpha_0)$ is generally hard to find in closed-form. As a result, we propose to use the non-parametric scheme as introduced in [82] to perform the QD. We assume that for every M time samples of the received signal of interest, at a sampling rate of f_s, we may obtain a test statistic $Z_i = \tilde{I}_x(i,\alpha_0)$, in which we replaced the time index t by the sequence index i to indicate the i-th test statistic. We denote by G_0 and G_1 the cdf of Z_i under hypothesis $\mathcal{H}_0$ and $\mathcal{H}_1$, respectively. It has been shown in [7]

that when an RF signal with the cyclic component α_0 is present, the function $\tilde{I}_x(i,\alpha)$ tends to exhibit a local peak with a value close to 1 at $\alpha = \alpha_0$; and on the other hand, if the signal is absent, the function tends to have a low value close to 0 at $\alpha = \alpha_0$. Consequently, it is reasonable to assume that the distribution G_1 is stochastically greater than G_0 and we verify this by simulations in the following.

As shown in Fig. 4.1, we obtained the estimated cdfs of the averaged sample

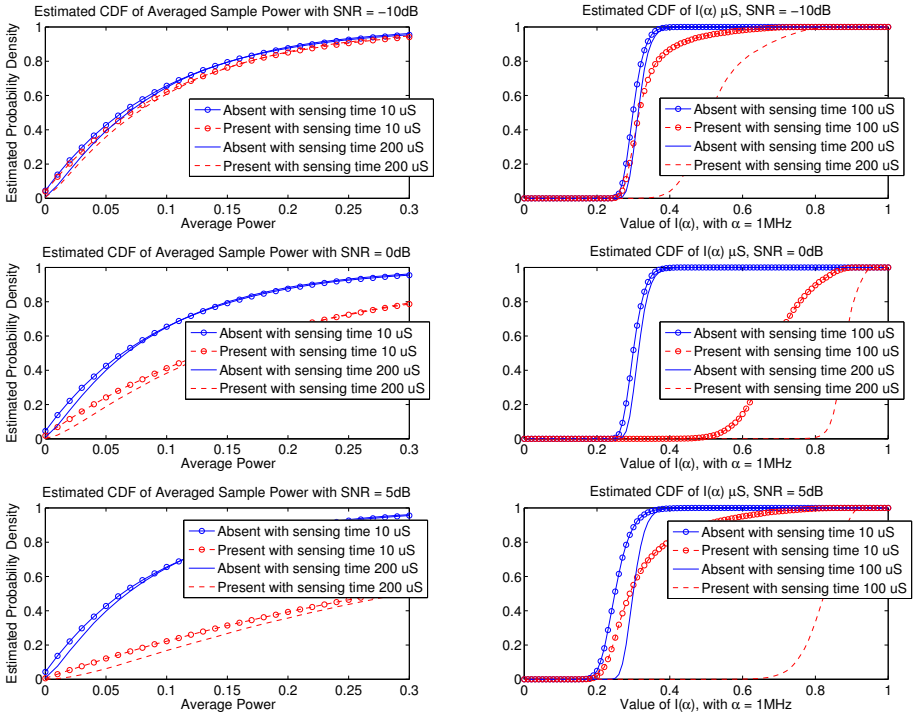

Figure 4.1: Estimated cdfs for the averaged power and $\tilde{I}_x(t,\alpha_0)$ when the signal with cyclic component α_0 is absent and present.

power and $\tilde{I}_x(i,\alpha_0)$ at $\alpha_0 = 1$MHz under both signal absent and present scenarios (we plot the cdfs of the average sample power in Fig. 4.1 in order to compare to the cyclostationarity-based case) with various sensing time window lengths and three

different SNRs: -10dB, 0dB and 5dB. The simulated signal is a Bluetooth signal with a symbol duration of 1μS (i.e., a resulting symbol rate cyclic frequency feature at 1MHz). The channel is a frequency-selective (multi-path) fading channel with a maximum Doppler shift of $\pm$300Hz, which corresponds to a maximum transmitter-receiver relative speed of 37.5m/s, or around 84 mph for a signal in the 2.4GHz frequency range. There are three discrete paths specified with their delays 0μS, $.15\mu$S, and $.32\mu$S, respectively, and with an average path gain of 0dB, -10dB, and -10dB, respectively. Each discrete path is modeled as an independent Rayleigh fading process. As is seen from Fig. 4.1, in all cases, the resulting G_1 (signal present) is stochastically greater than G_0 (signal absent), or $G_1 \succ_{st} G_0$.

We can also see from Fig. 4.1 that when the SNR is low (-10dB), the pre and post-change cdfs of the averaged sample power does not differ as much compared to the case of $\tilde{I}_x(i, \alpha_0)$, even with a long sensing time (200μS). On the contrary, the pre and post-change cdfs of $\tilde{I}_x(i, \alpha_0)$ differ from each other noticeably even when $SNR = -10$dB with a sensing time of 100μS. Intuitively, the more the pre- and post-change cdfs are distinguishable, the better detection performance can be expected in terms of the averaged detection delay and ARL to false alarms. This suggests that when the SNR is low, the cyclostationarity-based scheme can be more effective with longer sensing time window length. On the other hand, as we can see from Fig. 1, with a short sensing time of 10μS at $SNR = 5$dB, the difference between the pre- and post-change cdfs is greater in the case of the averaged sample power, compared to the difference of those of $\tilde{I}_x(i, \alpha_0)$. This suggests that, when SNR is high, the average sample power-based QD scheme may be more efficient. This is because a short sensing time for the cyclostationarity-based case is not adequate for obtaining distinguishable pre- and post-change cdfs as in the average sample power-based case. It is then straightforward to see that the sensing time length can be a critical factor of the efficiency and the effectiveness of the QD. In particular, by using a longer sensing time length in both cases, more distinguishable pre- and post-change distributions

are obtained for the metrics. However, note that the detection delay is expressed in terms of the observation steps in [82] as discussed in Section II. Thus, the detection delay of the proposed non-parametric QD method is given by the product of the number of observation steps and the sensing time length at each step. As a result, a longer sensing time length setting for each observation step may also increase the overall detection delay.

From the above observations, it is reasonable to exploit the diversity and consider combining the energy-based and the cyclostationarity-based QD schemes, since each offers distinct advantages and disadvantages under different conditions. In particular, one may consider a vector test statistic based on the observations of the averaged sample power and the value of $\tilde{I}_x(i, \alpha_0)$ for each operation step, and perform the QD. In the next sub-section, we discuss such a multivariate QD scheme.

4.3.3 Combined Multivariate Non-parametric Quickest Detection

Combining the average sample power-based and the cyclostationarity-based test statistics at each time step, we may generate a multivariate observation at each step by stacking the obtained average sample power and $\tilde{I}_x(i, \alpha)$ into a 2×1 column vector at each time, i.e. at time n, with a slight abuse of the notation, we obtain the matrix

$$\mathbf{Z}_1^n = [\mathbf{Z}_1 \mathbf{Z}_2, \cdots, \mathbf{Z}_n], \tag{4.15}$$

where we denote by $\mathbf{Z}_i$'s 2×1 column vectors, for all $1 \leq i \leq n$. In [83], a class of multivariate rank-like quantities is defined and used to develop multivariate tests to mimic traditional one-dimensional rank tests. We may adopt the algorithm developed

in [50] to define the centered directional rank vector [50] of $\mathbf{Z}_i$ for all $1 \leq i \leq n$ as

$$\mathbf{R}_n(\mathbf{Z}_i) = \sum_{j=1}^{n} \mathbf{D}_{ij}, \tag{4.16}$$

where we let

$$\mathbf{D}_{ij} = \frac{\mathbf{Z}_i - \mathbf{Z}_j}{||\mathbf{Z}_i - \mathbf{Z}_j||}. \tag{4.17}$$

The interpretation is that $\mathbf{D}_{ij}$ is a unit vector pointing from $\mathbf{Z}_j$ to $\mathbf{Z}_i$, or the normalized difference between $\mathbf{Z}_i$ and $\mathbf{Z}_j$. The centered directional rank vector $\mathbf{R}_n(\mathbf{Z}_i)$ may be considered as the accumulated difference between the point $\mathbf{Z}_i$ and the rest of data points, similar to the idea of ranking in the traditional one-dimensional case. We may then define the test statistic $R_{k,n}$ as

$$R_{k,n} = \bar{\mathbf{R}}_n^{(k)^T} \hat{\mathbf{\Sigma}}_{R_{k,n}}^{-1} \bar{\mathbf{R}}_n^{(k)}, \tag{4.18}$$

where

$$\bar{\mathbf{R}}_n^{(k)} = \frac{1}{k} \sum_{i=1}^{k} \mathbf{R}_n(\mathbf{Z}_i), \tag{4.19}$$

and

$$\hat{\mathbf{\Sigma}}_{R_{k,n}} = \frac{n-k}{(n-1)nk} \sum_{i=1}^{n} \mathbf{R}_n(\mathbf{Z}_i)\mathbf{R}_n(\mathbf{Z}_i)^T, \tag{4.20}$$

for $k = 1, \cdots, n$. Note that $\bar{\mathbf{R}}_n^{(k)}$ may be interpreted as the average of the first k ranking values. If $\{\mathbf{Z}_1 \cdots \mathbf{Z}_k\}$ are from the same distribution, then these data points are located more closely compared to the case in which there exists a distribution change before the k-th point. As a result, comparatively, a shorter vector $\bar{\mathbf{R}}_n^{(k)}$ is obtained for the case of no distribution change, and a longer vector $\bar{\mathbf{R}}_n^{(k)}$ is obtained for the case with a distribution change before the k-th point. Then, the quadratic term $R_{k,n}$ of $\bar{\mathbf{R}}_n^{(k)}$ may be used as the test statistic to detect a distribution change

point, since $R_{k,n}$ reflects the length of the vector $\bar{\mathbf{R}}_n^{(k)}$, which is affected by the existence/absence of a change point. The QD may then proceed as follows: 1) obtain $R_{max,n} = \max_{1<k\leq n} R_{k,n}$; 2) If $R_{max,n} > h_{n,p_f}$, raise an alarm for state change, otherwise collect another multivariate vector observation and repeat steps 1) and 2). The threshold h_{n,p_f} is chosen such that the conditional probability of a false alarm when observation n is added is equal to p_f, given that no previous false alarm has occurred, or

$$\Pr\{R_{max,n} > h_{n,p_f} \mid R_{max,j} \leq h_{j,p_f}; j < n\} = p_f. \tag{4.21}$$

Note that again this detection method works for both detecting the state changes from idle to busy as well as for detecting those from busy to idle. However, as also noted in [50], finding an analytical solution for the sequence of control thresholds h_{n,p_f} is generally difficult due to the unknown distributions of the observations in the first place. As a result, we resort to simulations in Section 4.4 to illustrate the performance of this combined QD scheme. In practice, we suggest to combine this approach with a suitable machine learning (adaptive) technique [84] to obtain the appropriate control thresholds. However, this is out of the scope of this dissertation and left as a future research task.

The computational complexity of the proposed multivariate non-parametric QD algorithm can be shown to be linear in n^3, i.e. $\mathcal{O}(n^3)$, where n denotes the number of time steps before a state-change detection. However, the author in [50] has developed a recursive algorithm to make the computational complexity of the multivariate QD algorithm linear in n, or $\mathcal{O}(n)$. This is accomplished by deriving an expression to compute the test statistics $R_{k,n+1}$ from $R_{k,n}$. Note that the computational complexity of obtaining average sample power in each step is $\mathcal{O}(M)$, where M denotes the number of samples in each step. Whereas, the computational complexity of obtaining the cyclostationary feature for a particular cyclic frequency in each step is dominated by the FFT, which is $\mathcal{O}(M \log M)$. The overall computational complexity of the

proposed multivariate QD procedure is then $\mathcal{O}(nM \log M)$. On the other hand, the computational complexity of the energy-based uni-variate QD algorithm has a complexity of $\mathcal{O}(Mn^4)$. Thus, when $\log M < n^3$, the complexity of multivariate case may be expected to be even less than the uni-variate case, due to the recursive algorithm proposed in [50]. In case when M is large and $M \gg n$, the complexities of these two cases should still be comparable.

In our case, since we are dealing with alternating idle and busy state changes, we propose that whenever a state change has been detected, we use new observations after each detection point for the QD of subsequent state changes. In this way, we may control the computation complexity of the proposed multivariate QD to be manageable. In case of either an idle or a busy state lasts for a long time of period, we may adopt a moving time window to discard older observations and make use of only the recent observations to perform the QD and effectively keep the computation complexity low.

To provide the self-awareness of false alarms and the achieved detection delays in the QD procedure, in the following we propose a novel approach to combine the above QD procedure with an offline change-point detection algorithm.

Whenever a false alarm is encountered, either an alarm of state changing from busy to idle is raised before its actual change, or an alarm of state changing from idle to busy is raised while the state is still idle. In the first case, if the CR (or the Radiobot) further decides to start transmitting data on the monitored channel, collisions with other radio activities may occur. In the second case, though there may not be collisions, valuable spectrum opportunities are lost. In either case, any false alarm can certainly affect the performance of the subsequent QDs, causing detection delays and possibly more subsequent false alarms, since the observations from different distributions (pre-change and post-change) are treated as from the same distribution. Note that, detection delays may also affect the detection performance

of subsequent detections in a similar way since a detection delay may omit one or more state alternating cycles (a state change from busy to idle followed by a change back to busy is referred as an alternating cycle and vice versa). In order to provide the self-awareness of false alarms and detection delays to improve subsequent detections, we propose to incorporate a parallel offline change-point detection algorithm with our proposed multivariate QD algorithm. Although the method of the offline change-point detection has already been discussed in [50], the concept of the combination of QD and the offline change-point detection has not been considered in the literature.

The exact off-line change-point detection procedure can be explained as follows. For a given sequence of observations with a length of N, one may obtain the test statistics

$$R_{k,N} = \bar{\mathbf{R}}_N^{(k)^T} \hat{\mathbf{\Sigma}}_{R_{k,N}}^{-1} \bar{\mathbf{R}}_N^{(k)}, \text{ for all } k = 1, \cdots, N, \tag{4.22}$$

similarly to the QD procedure described above. Then an estimate of the change point can be obtained as [50]

$$\hat{\tau}_C = \underset{1 \le k \le N}{\arg\max}\ R_{k,N}. \tag{4.23}$$

The parallel on-line QD/off-line change-point detection algorithm can be explained as follows: The off-line change-point detection procedure is invoked whenever a state change alarm is raised from the on-line QD procedure. The QD outcome is trusted for the time being, so that the QD may drop previous observations, re-initialize and take new observations for a subsequent detection of state change. However, the dropped observations from the previous QD procedure are kept for the off-line change-point detection procedure. As the on-line QD procedure continues, newly obtained observations are also fed into the off-line change-point detection procedure. For a short period of time, the off-line change-point detection algorithm may then re-estimate the past state change-point based on both the newly obtained

observations and the kept observation history. If the re-estimated change-point were to be different from the initial result declared by the on-line QD procedure, then the re-estimated change-point from the off-line detector is used to re-initialize the starting point for the current on-line QD procedure. In this way, detection delays are made known to CR by comparing the results from the on-line QD procedure and that from the off-line change-point detection procedure.

On the other hand, in order to detect false alarms, we propose to use an off-line threshold h_{off} on the test statistics: if $\max R_{k,N} \geq h_{off}$, then $\hat{\tau}_C = \underset{1\leq k\leq N}{\arg\max}\ R_{k,N}$ is used to update the change-point as introduced above; if $\max R_{k,N} < h_{off}$, cancel the state-change alarm and re-initialize the current on-line QD procedure from the previous confirmed state change-point. Note that false alarm rates can be reduced by directly setting a higher threshold in the on-line QD procedure. However, this causes longer detection delays. As an alternative, by having a higher threshold h_{off} for the off-line change-point detection procedure (compared to that of the on-line QD procedure), false alarms can be corrected to some extent without compromising the detection delay performance. Note that since the off-line change-point detection procedure relies on more observations, it can provide more accurate/reliable results on average compared to those obtained in the on-line QD procedure. The detailed procedure of the parallel on-line QD/offline change-point detection is presented in Algorithm 4.

4.4 Simulations and Results

In this section, we show representative simulation results to illustrate the advantages of the proposed methods for the channel state QD in CRs such as Radiobots. Note that all the following simulations are based on the same multi-path frequency-

Algorithm 4 Parallel Quickest detection and Offline Change-point detection

Initialization: Alarm flag $f \leftarrow 0$, set offline window wait length c, set threshold h and h_{off}, set $n_p = n_0 = 1$
for $n = 1, 2, 3, \cdots$ **do**
  Obtain observations $\mathbf{Z}_{n_0}^n$
  $R_{k,n} \leftarrow \bar{\mathbf{R}}_n^{(k)^T} \hat{\mathbf{\Sigma}}_{R_{k,n}}^{-1} \bar{\mathbf{R}}_n^{(k)}$, for all $k = n_0, \cdots, n$
  if $\max\limits_{n_0 \le k \le n} R_{k,n} \ge h$ **then**
    Set the alarm flag to current step: $f \leftarrow n$
    Keep track of the previous state change-point: $n_p \leftarrow n_0$
    Set current state change point: $n_0 \leftarrow n$
  end if
  if $n = f + c$ and $n \neq c$ **then**
    if $\max\limits_{n_p \le k \le n} R_{k,n} \ge h_{off}$ **then**
      $\hat{\tau}_C \leftarrow \arg\max\limits_{n_p \le k \le n} R_{k,n}$
      Re-initialize starting point as $n_0 \leftarrow \hat{\tau}_C$
    else
      Re-initialize starting point as $n_0 \leftarrow n_p$
    end if
  end if
end for

selective channel with Doppler effect as used in Section 4.3.2.

In Fig. 4.2, a typical situation of the non-parametric cyclostationarity-based (univariate, without using the average sample power) QD procedure introduced in Section 4.3.2 is shown. In the top panel, we show the values of $Z_i = \tilde{I}_x(i, \alpha_0)$ up to roughly 15000μS. In the middle panel, the sequentially obtained Shiryayev-Roberts statistic is shown. The QD threshold A for the Shiryayev-Roberts statistic is set to 500. Other parameters are shown in the panel itself. In the bottom panel, the true state change history and the detection results are superposed to show detection delays. The procedure for the average sample power based QD introduced in Section 4.3.1 is similar.

Fig. 4.3 shows a typical scenario of the proposed parallel QD/offline change-point

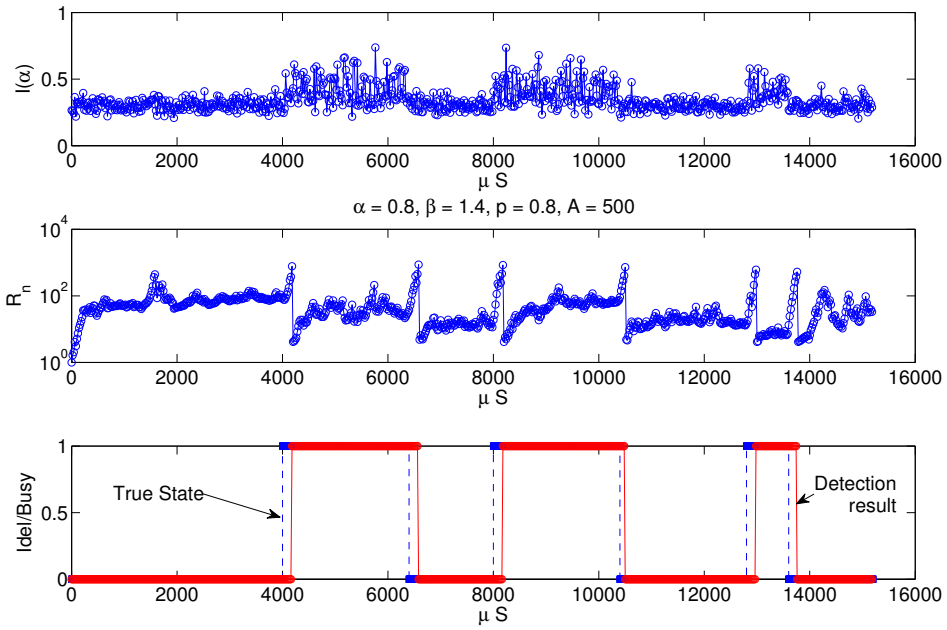

Figure 4.2: A typical scenario of the QD procedure at $SNR = 0$dB, with a sampling rate at 100MHz and the sensing time interval of 20μS.

detection procedure. We set the threshold $h_{n,p_f} = 11$ for all n of the on-line QD and $h_{off} = 15$ for the off-line change-point detection. We show the state change history and the QD results in the top panel. In the middle panel, we show the plot of test sequence $R_{k,n}$ for each time an alarm is raised, i.e. when $R_{max,n} > h_{n,p_f}$ where $R_{max,n} = \max R_{k,n}$. In the bottom panel, we show the plot of $R_{k,n}$ for each time the off-line change-point detection is engaged. Note that the off-line change-point detection detects the false alarm ($R_{max,n} < h_{off}$) at stage 1 and detects detection delays from stage 2 to stage 5. The estimated chant-points are re-adjusted for all stages. As shown in the middle panel, the re-adjusted change-point of each stage is the first data point of $R_{k,n}$ sequence of the next stage, which is the same as the maximum point of $R_{k,n}$ of the corresponding stage in the bottom panel. However,

the on-line QD point of each stage is the last data point of of $R_{k,n}$ sequence of that stage, as shown in the middle panel. The off-line re-adjusted change-points are closer to the real change-points compared to the on-line estimates.

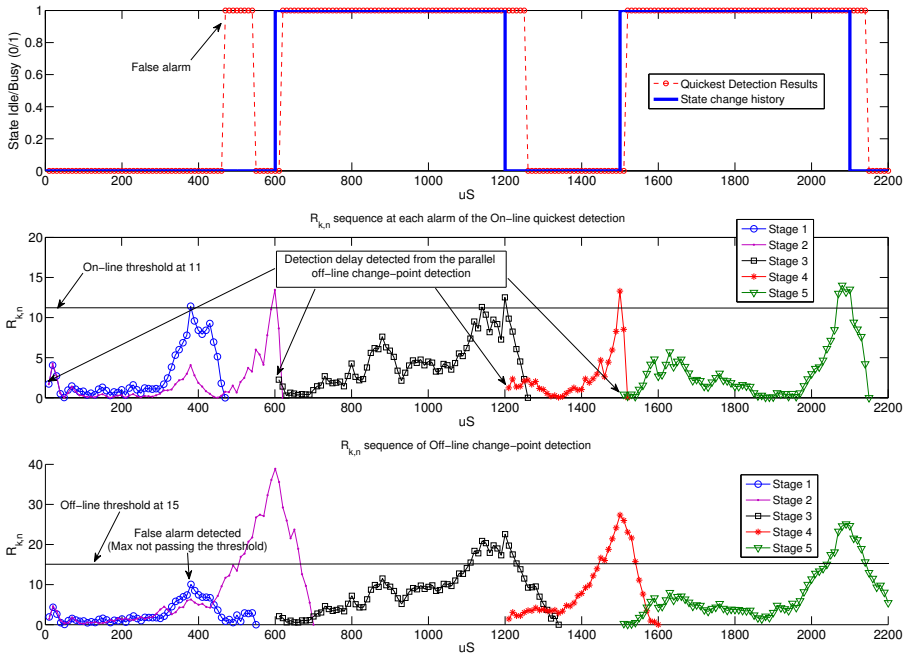

Figure 4.3: A typical scenario of the multivariate parallel on-line QD/offline change-point detection procedure at SNR= -5dB, with a sampling rate of 100MHz and sensing interval of 10μS.

Fig. 4.4 shows performance comparisons of the average sample power-based, the cyclostationarity-based, and the multivariate parallel QD strategies. The comparison of average detection delay is shown in Fig. 4.4(a), the probability of change-point detection and the false alarm probability are shown in Fig. 4.4(b), and the resulting percentage of idle state usage is shown in Fig. 4.4(c). In the two uni-variate QD cases, the threshold for the Shiryayev-Roberts statistic R_n was set to $A = 830$. In

the multivariate parallel QD case, the detection thresholds are set to be $h_{n,p_f} = 17$ and $h_{off} = 20$ in order to make the false alarm probabilities lower than the other two cases for a fair performance comparison. Note that higher threshold setting in all cases may result in lower false alarm probability but at the expense of less change-point detection and longer detection delays. The minimum idle/busy state sojourn time is set to 600μS in all three cases. For fair comparison, we assume that whenever a false alarm is raised prior to a state change from busy to idle, the following idle period is not used by the CR. However, in practice a CR may still make use of some portion of the idle period using the multivariate parallel detection scheme. As we can see, slightly shorter detection delays are achieved by using the average sample power based QD, compared to that using the cyclostationarity-based features. However, by exploiting the power/cyclostationarity diversity, the multivariate parallel QD scheme yields superior performance, in terms of both lower detection delays and lower false alarm probabilities for each sensing duration compared to the other two schemes. Although similar probabilities of change-point detections are achieved for all three schemes, the multivariate parallel scheme yields much higher average percentage of idle channel usage in the SNR region from -10 to 10dB. It is also shown in Fig. 4.4(c) that the average sample power based scheme with sensing duration of 5uS achieves the highest average percentage of idle channel usage in SNR region from -16 to -12dB. This suggests that the average sample power based scheme may be more efficient in the extreme low SNR region compared to the other schemes.

From the performance comparisons shown in Fig. 4.4, we can also see the tradeoff between the length of sensing duration and the resulting percentage of usage of the idle state in all three cases. In particular, the highest percentage of usage is not necessarily always achieved by using the shortest sensing duration of 5μS, although it may achieve lower detection delays. This is due to its limited probability of change-point detection and comparatively high false alarm probability. Note that the false alarm probability is related to the ARL to false alarm. In particular, a shorter ARL

to false alarm results in a higher false alarm probability. Moreover, the lower-bound of ARL to false alarm in (4.10) is given in terms of number of steps, but not in terms of the absolute time length. As a result, when using a shorter sensing duration for each step (with the same threshold value), false alarms are raised more frequently since there are more sensing steps prior to any change-point compared to that using a longer sensing duration for each step. This also points out the disadvantage of performing QD using individual samples (for example, the traditional individual sample power-based QD scheme proposed in [79]), which can be considered as the extreme case of using a short sensing duration.

The optimal setting of the sensing duration and the test threshold may not be easy to be derived analytically (since they depends on the pre and post-change distributions of the observations, which are assumed unknown in the first place). However, suitable machine learning (adaptive) techniques [84] may help in practice to find the optimal or a near-optimal solution. In particular, by using the proposed parallel on-line QD/off-line change-point detection scheme, performance feedback of detection delay and false alarm probability may help to estimate/predict the idle channel usage for any particular setting. Then, an appropriately chosen machine learning algorithm may be used to find the optimal/near optimal solution.

4.5 Chapter Summary

In this chapter, we have proposed non-parametric quickest detection schemes to keep track of the state changes (idle/busy) of communication channels. This capability can be useful for future cognitive radios, since prior information on the statistics of channel usage is generally hard to obtain in practice. We also proposed a novel average sample power and cyclostationarity-based multivariate parallel quickest de-

tection/offline change-point detection scheme to improve detection performance compared to the traditional energy-based methods. The performance of the proposed detection schemes is evaluated through simulations. Compared to traditional energy-based quickest detection schemes, smaller detection delays and higher percentage of spectrum usage are obtained using the proposed schemes. The incorporation of the decision-making for wideband spectrum sensing scheduling, and the evaluation of communication throughput are left as future work.

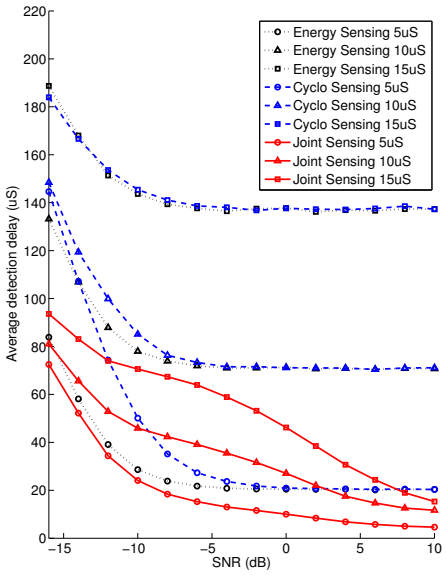

(a) Average detection delays.

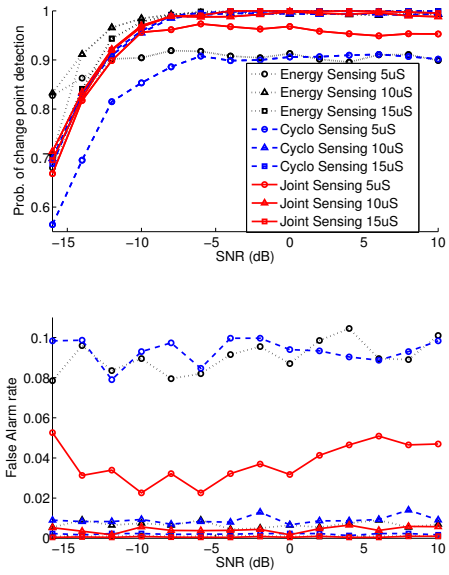

(b) Probability of change-point detection and false alarm rate.

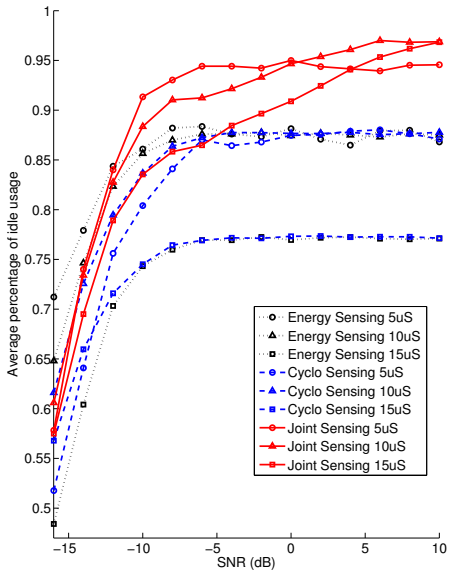

(c) Percentage of idle chanel usage.

Figure 4.4: Performance comparisons of the average sample power-based, the cyclo-stationarity based, and the multivariate parallel QD strategies. With a sampling rate of 100MHz, the sensing time durations are set to 5μS, 10μS, and 15μS, respectively in all cases.

Chapter 5

Wideband PHY/MAC Bandwidth Aggregation Optimization For CRs

5.1 Introduction

The simultaneous transmission over multiple radio interfaces by a single mobile terminal has been previously discussed in the literature under the term of the bandwidth aggregation (BAG) [32–37] (also known as channel aggregation), which aims at performing simultaneous use of multiple interfaces (including Bluetooth, WiFi, satellite communications etc.) to improve transmission quality or throughput depending on specific architectural designs. A similar idea called Carrier aggregation (CA) can also be found in recent literature on the Third Generation Partnership Project Long Term Evolution-Advanced (3GPP LTE-A) [38–41]. CA is one of the key features assumed in the LTE-A, in which mobile users can access a much wider transmission bandwidth

up to 100 MHz compared with LTE Release 8 standard (up to 20 MHz) [38]. This is achieved by aggregating two or more individual component carriers (CCs) belonging to contiguous or non-contiguous frequency bands [38], essentially scheduling a mobile user on multiple CCs simultaneously.

In this chapter, we provide a general formulation for the bandwidth aggregation (BAG) problem in a wideband spectrum access setup, taking into account the essential practical issues and derive an optimal BAG strategy as the solution to a multi-objective optimization problem: one objective is the communication throughput of the mobile Radiobot device and the other one is the power consumption of the device. Note that, by self-adjusting coefficients used to give different priorities for each of the objectives, the Radiobot can achieved autonomous operations as envisioned in [6]. The proposed multi-objective optimization problem takes the following essential practical issues into account: imperfect spectrum sensing, time varying channel coefficients (caused by fading and shadowing), hardware reconfiguration time delay, hardware reconfiguration power consumption, and communication power consumptions.

5.2 Problem Formulation

We assume that the spectrum range of interest is divided into N sub-bands, with labels $1, 2, \cdots, N$. We denote by f_n, B_n and T_n, respectively, the center-frequency, the bandwidth, and the sensing time length of the n-th sub-band. We assume that the maximum number of simultaneous transmissions that can be supported by the Radiobot is L.

We assume that spectrum sensing is performed in each sub-band in an arbitrary order. Let time sequence index $k = 0, 1, 2, \cdots$ denote the time instance at the end of

the k-th spectrum sensing. We denote by i_k and j_k, respectively, for $1 \leq i_k, j_k \leq N$, the sub-band the Radiobot has just finished sensing on and the sub-band that is about to be sensed immediately at time k. We denote by $M_n(k)$ the number of

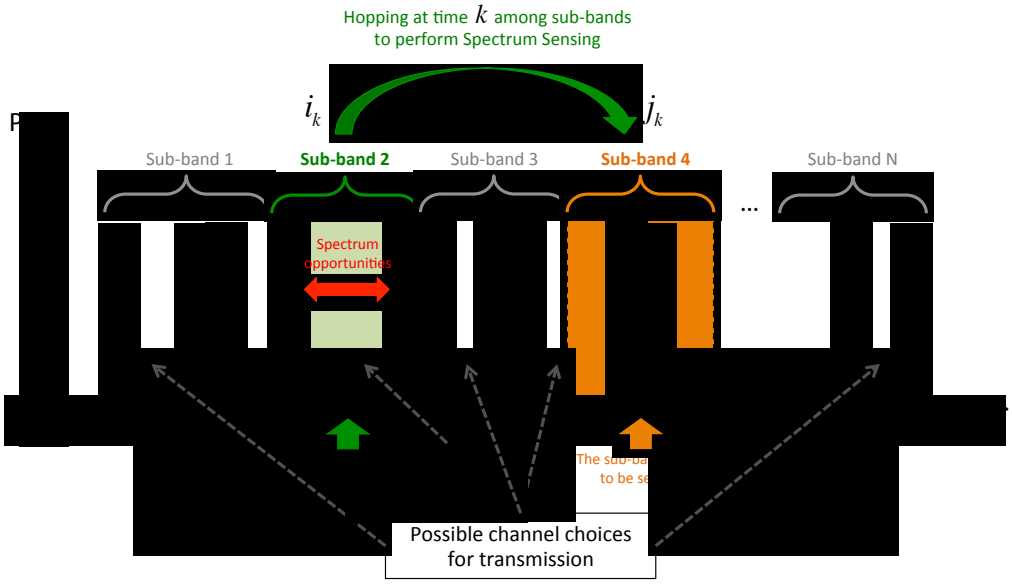

Figure 5.1: A diagram of the system operation with N number of sub-bands.

detected idle channels in the n-th sub-band at time k. We index the m-th idle channel in the n-th sub-band by (n, m), where $1 \leq n \leq N$ and $1 \leq m \leq M_n(k)$. We assume that the Radiobot is free to choose to transmit on all the detected idle channels including the ones in the sub-band that is immediately going to be sensed by itself. This assumption is made based on the recent advances of the full duplex radio capability [85], which is based on RF interference cancellation algorithms. A diagram of the system operation is illustrated in Fig. 5.1.

In [86], a semi-Markov model was proposed to describe the channel state switching based on measurements of a WLAN in the $2.4 - 2.475$ GHz ISM band, in which the sojourn time of idle periods was shown to fit a generalized Pareto distribution

(GDP) [87] having a probability density function (pdf)

$$f(t \mid s,\sigma,\theta) = \begin{cases} \frac{1}{\sigma}\left(1+s\frac{(t-\theta)}{\sigma}\right)^{-1-1/s} & \text{, for } s \neq 0 \\ \frac{1}{\sigma}\exp\left(-\frac{(t-\theta)}{\sigma}\right) & \text{, for } s = 0 \end{cases} \tag{5.1}$$

with the domain $\theta \leq t < +\infty$ for $s \geq 0$ and $\theta \leq t \leq \theta - \sigma/s$ for $s < 0$, where s is the shape parameter, $\sigma > 0$ is the scale parameter, and θ is the location parameter [87]. Note that when $s = 0$, (5.1) reduces to an exponential distribution. In [88], an Maximum Likelihood (ML) estimator for the sojourn time (both idle and busy) distribution was proposed. The estimation of the sojourn times with time-varying distributions was also discussed in [88]. In this work, the details of the estimation of the sojourn time distributions are not addressed, but left as a future work in this dissertation. We denote by $F^I_{n,m}(t)$ and $F^B_{n,m}(t)$, in general, the cdfs of the idle period and busy period respectively, of channel (n,m), with

$$F^I_{n,m}(t) = \int_0^t f^I_{n,m}(\tau)d\tau, \quad \text{and } F^B_{n,m}(t) = \int_0^t f^B_{n,m}(\tau)d\tau$$

where $f^I_{n,m}(t)$ and $f^B_{n,m}(t)$ are the probability density functions (pdf's) of the idle period and busy period respectively.

The transmission rate on an idle channel (n,m) at time instance k can be defined as

$$r_{n,m,k} = B_{n,m,k}\log_2\left(1+\frac{h^2_{n,m,k}P_{n,m,k}}{B_{n,m,k}N_0}\right) \text{ bits/s}, \tag{5.2}$$

where $B_{n,m,k}$ is the bandwidth of the channel (n,m) at time k, with $1 \leq m \leq M_n(k)$. We denote by $h_{n,m,k}$ and $P_{n,m,k}$, respectively, the channel coefficient and the transmit power with the constraint $0 \leq P_{n,m,k} \leq \bar{P}$, and N_0 is the single-sided noise power spectral density level. Note that, one can obtain the knowledge of the channel coefficients by performing the pilot-assisted transmission (PAT) training periodically or before each transmission [89, 90]. In this work, we assume that only the distributions of the channel coefficients are known *a priori*.

Recall that the allowed maximum number of simultaneous transmission is L, and we use the notation $(n_{l,k}, m_{l,k})$, for $l = \{1, \cdots, L\}$ to denote the channel being selected at time k for the l-th transmission. We may use the $L \times 3$ matrix $\mathbf{A}_k$ to denote the action of the Radiobot at time k:

$$\mathbf{A}_k = \begin{bmatrix} n_{1,k} & m_{1,k} & P_{1,k} \\ \vdots & \vdots & \vdots \\ n_{L,k} & m_{L,k} & P_{L,k} \end{bmatrix}. \tag{5.3}$$

When $(n_{l,k-1}, m_{l,k-1}) \neq (n_{l,k}, m_{l,k})$, we say that the l-th transmission performed a frequency hopping. When $n_{l,k-1} \neq n_{l,k}$, we denote by the constants Δ_t and Δ_p the incurred time delay and power consumption for the hardware reconfiguration, respectively, and denote by the constants δ_t and δ_p the incurred time delay and power consumption respectively when $n_{l,k-1} = n_{l,k}$ but $m_{l,k-1} \neq m_{l,k}$. We assume that $\Delta_t > \delta_t$ and $\Delta_p > \delta_p$, since switching channels from one sub-band to another may generally involve much more complicated RF hardware reconfigurations compared to the case of switching within a sub-band.

Thus, given $(n_{l,k-1}, m_{l,k-1})$ and $(n_{l,k}, m_{l,k})$, the time delay incurred on the l-th transmission can be expressed as

$$\tau_{l,k}(\mathbf{A}_k, \mathbf{A}_{k-1}) = \Delta_t \mathcal{I}_{\left\{n_{l,k-1} \neq n_{l,k}\right\}} + \delta_t \mathcal{I}_{\left\{n_{l,k-1} = n_{l,k}, m_{l,k-1} \neq m_{l,k}\right\}}, \tag{5.4}$$

and the power consumption overhead incurred on the l-th communication hardware can be expressed as

$$p_{l,k}(\mathbf{A}_k, \mathbf{A}_{k-1}) = \Delta_p \mathcal{I}_{\left\{n_{l,k-1} \neq n_{l,k}\right\}} + \delta_p \mathcal{I}_{\left\{n_{l,k-1} = n_{l,k}, m_{l,k-1} \neq m_{l,k}\right\}}, \tag{5.5}$$

where $\mathcal{I}_{\{E\}}$ is the indicator function of event E such that

$$\mathcal{I}_{\{E\}} = \begin{cases} 1\,, & \text{if } E \text{ is true} \\ 0\,, & \text{if } E \text{ is not true} \end{cases}. \tag{5.6}$$

We assume that there are always data to be transmitted and the Radiobot assumes that a primary user is interfering its communication if several packets are sent wihtout receiving any ACK, and therefore, stops its transmission on a channel. Let us denote by τ_s the amount of time needed before it stops transmission. We define a multi-objective problem: high communication throughput, and low transmission energy consumption. The throughput $G_{l,k}(\mathbf{A}_k, \mathbf{A}_{k-1})$ on the channel $(n_{l,k}, m_{l,k})$ from time k to $k+1$ is given by

$$\begin{aligned}
& G_{l,k}(\mathbf{A}_k, \mathbf{A}_{k-1}) \\
= & \left[\left(T^I_{n_{l,k},m_{l,k},k} - t_{k,n_{l,k}} - \tau_{l,k}(\mathbf{A}_k, \mathbf{A}_{k-1})\right) r_{n_{l,k},m_{l,k},k} \mathcal{I}_{\{C\}} + \right. \\
& \qquad \left. + \left(T_{j_k} - \tau_{l,k}(\mathbf{A}_k, \mathbf{A}_{k-1})\right) r_{n_{l,k},m_{l,k},k} \mathcal{I}_{\{D\}}\right] \mathcal{I}_{\{E\}} \\
= & \; r_{n_{l,k},m_{l,k},k} \left[\left(T^I_{n_{l,k},m_{l,k},k} - t_{k,n_{l,k}} - \tau_{l,k}(\mathbf{A}_k, \mathbf{A}_{k-1})\right) \mathcal{I}_{\{C\}} + \right. \\
& \qquad \left. + \left(T_{j_k} - \tau_{l,k}(\mathbf{A}_k, \mathbf{A}_{k-1})\right) \mathcal{I}_{\{D\}}\right] \mathcal{I}_{\{E\}}, \qquad (5.7)
\end{aligned}$$

where $t_{k,n}$ denotes the amount of time that has passed since the end of the last sensing on the n-th sub-band at time instance k, $T^I_{n,m,k}$ denotes the random variable of the idle sojourn time of the channel (n, m), and T_{j_k} denotes the sensing time duration for the j_k-th sub-band. The events C, D, and E are defined as:

$$\begin{aligned}
C &= \left\{0 < \left(T^I_{n_{l,k},m_{l,k},k} - t_{k,n_{l,k}} - \tau_{l,k}(\mathbf{A}_k, \mathbf{A}_{k-1})\right) < \left(T_{j_k} - \tau_{l,k}(\mathbf{A}_k, \mathbf{A}_{k-1})\right)\right\} \\
&= \left\{t_{k,n_{l,k}} + \tau_{l,k}(\mathbf{A}_k, \mathbf{A}_{k-1}) < T^I_{n_{l,k},m_{l,k},k} < t_{k,n_{l,k}} + T_{j_k}\right\}, \qquad (5.8) \\
D &= \left\{T^I_{n_{l,k},m_{l,k},k} \geq t_{k,n_{l,k}} + T_{j_k}\right\}, \qquad (5.9) \\
E &= \left\{\text{channel } (n_{l,k}, m_{l,k}) \text{ is indeed idle, given it is detected idle}\right\}. \qquad (5.10)
\end{aligned}$$

The total expected throughput of the Radiobot from time k to $k+1$ can be given

as:

$$\begin{aligned}
&\mathbb{E}\left\{G_k(\mathbf{A}_k,\mathbf{A}_{k-1})\right\} = \sum_{l=1}^{L}\mathbb{E}\left\{G_{l,k}(\mathbf{A}_k,\mathbf{A}_{k-1})\right\} \\
= &\sum_{l=1}^{L}\mathbb{E}_H\{r_{n_{l,k},m_{l,k},k}\}p_I^{(n_{l,k},m_{l,k})}\left[\int_{t_{k,n_{l,k}}+\tau_{l,k}(\mathbf{A}_k,\mathbf{A}_{k-1})}^{t_{k,n_{l,k}}+T_{j_k}}\tau f^I_{n_{l,k},m_{l,k}}(\tau)d\tau + \right. \\
&+\left(T_{j_k}-\tau_{l,k}(\mathbf{A}_k,\mathbf{A}_{k-1})\right)\int_{t_{k,n_{l,k}}+T_{j_k}}^{\infty} f^I_{n_{l,k},m_{l,k}}(\tau)d\tau + \\
&\left.-\left(t_{k,n_{l,k}}+\tau_{l,k}(\mathbf{A}_k,\mathbf{A}_{k-1})\right)\int_{t_{k,n_{l,k}}+\tau_{l,k}(\mathbf{A}_k,\mathbf{A}_{k-1})}^{t_{k,n_{l,k}}+T_{j_k}} f^I_{n_{l,k},m_{l,k}}(\tau)d\tau\right], \qquad (5.11)
\end{aligned}$$

where

$$\begin{aligned}
p_I^{(n_{l,k},m_{l,k})} &= \mathbb{E}\{\mathfrak{I}_{\{E\}}\} \\
&= \Pr\left\{\text{channel } (n_{l,k},m_{l,k}) \text{ is idle, given it is detected idle}\right\}, \qquad (5.12)
\end{aligned}$$

denotes the posteriori probability of channel $(n_{l,k},m_{l,k})$ being idle, and $\mathbb{E}_H\{r_{n_{l,k},m_{l,k},k}\}$ can be given as:

$$\begin{aligned}
&\mathbb{E}_H\{r_{n_{l,k},m_{l,k},k}\} \\
= &\int_{-\infty}^{\infty} B_{n_{l,k},m_{l,k},k}\log_2\left(1+\frac{h^2P_{n_{l,k},m_{l,k},k}}{B_{n_{l,k},m_{l,k},k}N_0}\right)f_{H_{n_{l,k},m_{l,k},k}}(h)dh. \qquad (5.13)
\end{aligned}$$

The energy consumption $E_{l,k}(\mathbf{A}_k,\mathbf{A}_{k-1})$ on the channel $(n_{l,k},m_{l,k})$ from time k to $k+1$ can be given as,

$$\begin{aligned}
&E_{l,k}(\mathbf{A}_k,\mathbf{A}_{k-1}) \\
&= \Big\{P_{l,k}\Big[\Big(T^I_{n_{l,k},m_{l,k},k}-t_{k,n_{l,k}}-\tau_{l,k}(\mathbf{A}_k,\mathbf{A}_{k-1})\Big)\mathfrak{I}_{\{C\}}+ \\
&+\left(T_{j_k}-\tau_{l,k}(\mathbf{A}_k,\mathbf{A}_{k-1})\right)\mathfrak{I}_{\{D\}}\Big]+p_{l,k}\left(\mathbf{A}_k,\mathbf{A}_{k-1}\right)\tau_{l,k}(\mathbf{A}_k,\mathbf{A}_{k-1})\Big\}\mathfrak{I}_{\{E\}}+P_{l,k}\tau_s\mathfrak{I}_{\{F\}}, \\
&\qquad (5.14)
\end{aligned}$$

where event $F = E^C$ is the complement of event E.

The total expected energy consumption of the Radiobot from time k to $k+1$ is then given by

$$\begin{aligned}
&\mathbb{E}\left\{E_k(\mathbf{A}_k, \mathbf{A}_{k-1})\right\} = \sum_{l=1}^{L} \mathbb{E}\left\{E_{l,k}(\mathbf{A}_k, \mathbf{A}_{k-1})\right\} \\
= &\sum_{l=1}^{L} p_I^{(n_{l,k}, m_{l,k})} \left\{ P_{l,k} \left[\int_{t_{k,n_{l,k}}+\tau_{l,k}(\mathbf{A}_k,\mathbf{A}_{k-1})}^{t_{k,n_{l,k}}+T_{j_k}} \tau f^I_{n_{l,k},m_{l,k}}(\tau) d\tau \; + \right.\right. \\
- &\left(t_{k,n_{l,k}} + \tau_{l,k}(\mathbf{A}_k, \mathbf{A}_{k-1})\right) \int_{t_{k,n_{l,k}}+\tau_{l,k}(\mathbf{A}_k,\mathbf{A}_{k-1})}^{t_{k,n_{l,k}}+T_{j_k}} f^I_{n_{l,k},m_{l,k}}(\tau) d\tau + \\
+ &\left.\left. (T_{j_k} - \tau_{l,k}(\mathbf{A}_k, \mathbf{A}_{k-1})) \int_{t_{k,n_{l,k}}+T_{j_k}}^{\infty} f^I_{n_{l,k},m_{l,k}}(\tau) d\tau \right] + \right. \\
+ &\left. p_{l,k}\left(\mathbf{A}_k, \mathbf{A}_{k-1}\right) \tau_{l,k}(\mathbf{A}_k, \mathbf{A}_{k-1}) \right\} + \\
+ &(1 - p_I^{(n_{l,k}, m_{l,k})}) P_{l,k} \tau_s. \qquad (5.15)
\end{aligned}$$

The optimization problem of achieving transmission throughput and low energy consumption can then be expressed as follows:

$$\begin{aligned}
\text{maximize} \quad & \alpha_1 \mathbb{E}\left\{G_k(\mathbf{A}_k, \mathbf{A}_{k-1})\right\} - \alpha_2 \mathbb{E}\left\{E_k(\mathbf{A}_k, \mathbf{A}_{k-1})\right\} \\
\text{subject to} \quad & (n_{l,k}, m_{l,k}) \neq (n_{l',k}, m_{l',k}) \; \forall \; l, l' \in \{1, \cdots, L\}, \\
& \text{and } 0 \leq P_{l,k} \leq \bar{P}, \; \forall \; l \in \{1, \cdots, L\},
\end{aligned}$$

where $\alpha_1 \geq 0$ and $\alpha_2 \geq 0$ are the priority coefficients for the transmission throughput and the energy consumption respectively. The optimization problem can equivalently be expressed as follows:

$$\mathbf{A}_k^* = \arg\max_{\mathbf{A}_k} \sum_{l=1}^{L} R_{l,k}\left(\mathbf{A}_k, \mathbf{A}_{k-1}\right) \qquad (5.16)$$

$$\text{subject to} \quad (n_{l,k}, m_{l,k}) \neq (n_{l',k}, m_{l',k}) \; \forall \; l, l' \in \{1, \cdots, L\},$$
$$\text{and } 0 \leq P_{l,k} \leq \bar{P}, \; \forall \; l \in \{1, \cdots, L\},$$

where $R_{l,k}\left(\mathbf{A}_k, \mathbf{A}_{k-1}\right)$ in (5.16) denotes the reward function of l-th transmission and is given as:

$$\begin{aligned} & R_{l,k}\left(\mathbf{A}_k, \mathbf{A}_{k-1}\right) \\ = \; & p_I^{(n_{l,k}, m_{l,k})} \left[\left(\alpha_1 \mathbb{E}_H\{r_{n_{l,k}, m_{l,k}, k}\} - \alpha_2 P_{l,k}\right) J_{l,k}\left(\mathbf{A}_k, \mathbf{A}_{k-1}\right)\right. \\ - \; & \left. \alpha_2 p_{l,k}\left(\mathbf{A}_k, \mathbf{A}_{k-1}\right) \tau_{l,k}(\mathbf{A}_k, \mathbf{A}_{k-1})\right] - (1 - p_I^{(n_{l,k}, m_{l,k})}) \alpha_2 P_{l,k} \tau_s \; . \end{aligned} \tag{5.17}$$

The quantity $J_{l,k}\left(\mathbf{A}_k, \mathbf{A}_{k-1}\right)$ in (5.17) is defined as

$$\begin{aligned} J_{l,k}\left(\mathbf{A}_k, \mathbf{A}_{k-1}\right) = \Bigg[& \int_{t_{k,n_{l,k}} + \tau_{l,k}(\mathbf{A}_k, \mathbf{A}_{k-1})}^{t_{k,n_{l,k}} + T_{j_k}} \tau f^I_{n_{l,k}, m_{l,k}}(\tau) d\tau \; + \\ & - \left(t_{k,n_{l,k}} + \tau_{l,k}(\mathbf{A}_k, \mathbf{A}_{k-1})\right) \int_{t_{k,n_{l,k}} + \tau_{l,k}(\mathbf{A}_k, \mathbf{A}_{k-1})}^{t_{k,n_{l,k}} + T_{j_k}} f^I_{n_{l,k}, m_{l,k}}(\tau) d\tau \; + \\ & + \left(T_{j_k} - \tau_{l,k}(\mathbf{A}_k, \mathbf{A}_{k-1})\right) \int_{t_{k,n_{l,k}} + T_{j_k}}^{\infty} f^I_{n_{l,k}, m_{l,k}}(\tau) d\tau \Bigg] . \end{aligned} \tag{5.18}$$

The optimal solution of $\mathbf{A}_k^*$ in (5.16) can be solved using a combination of the *Hungarian* algorithm [91] and a convex optimization procedure, by separating the problem of channel selection and the problem of power allocation in each transmission. The separation is valid since the objective function in (5.16) is in the form of a summation of rewards on each transmission link and the power constraints on each transmission link are decoupled, i.e. not a joint total constraint, such that a choice of transmission power for any transmission link does not affect the choice of any other transmission links.

First, for a given channel allocation $(n_{l,k}, m_{l,k})$ of the l-th transmission, the optimal transmission power $P^*_{l,k}|_{(n_{l,k},m_{l,k})}$ can be found as

$$P^*_{l,k}|_{(n_{l,k},m_{l,k})} = \arg\max_{P_{l,k}} R_{l,k}\left(\mathbf{A}_k, \mathbf{A}_{k-1}\right). \tag{5.19}$$

Since it can be shown that $R_{l,k}\left(\mathbf{A}_k, \mathbf{A}_{k-1}\right)$ is a concave function, we have

$$P^*_{l,k}|_{(n_{l,k},m_{l,k})} = P^{\triangle}_{l,k}\ , \tag{5.20}$$

if $P^{\triangle}_{l,k}$ is the solution of

$$\frac{dR_{l,k}\left(\mathbf{A}_k, \mathbf{A}_{k-1}\right)}{dP_{l,k}} = 0, \tag{5.21}$$

such that $0 < P^{\triangle}_{l,k} < \bar{P}$. Otherwise, if such a solution can not be found, we have

$$P^*_{l,k}|_{(n_{l,k},m_{l,k})} = \arg\max_{P_{l,k}\in\{0,\bar{P}\}} R_{l,k}\left(\mathbf{A}_k, \mathbf{A}_{k-1}\right). \tag{5.22}$$

Note that the solution $P_{l,k}$ to (5.21) can be shown to equivalently satisfy

$$\int_{-\infty}^{\infty} \frac{h^2 f_{H_{n_{l,k},m_{l,k},k}}(h)}{B_{n_{l,k},m_{l,k},k}N_0 + h^2 P_{l,k}} dh - \frac{\alpha_2(\tau_s/p_I^{(n_{l,k},m_{l,k})} + J_{l,k}\left(\mathbf{A}_k, \mathbf{A}_{k-1}\right) - \tau_s)}{\alpha_1 J_{l,k}\left(\mathbf{A}_k, \mathbf{A}_{k-1}\right) B_{n_{l,k},m_{l,k},k}\log_2(e)} = 0. \tag{5.23}$$

Second, the channel assignment problem can be represented by a weighted bipartite graph[1], where the detected idle channels and the L number of transmissions constitute the two disjoint sets of vertices, and the edge weight between the channel $(n_{l,k}, m_{l,k})$ and l-th transmission is $R_{l,k}\left(\mathbf{A}_k, \mathbf{A}_{k-1}\right)|_{P_{l,k}=P^*_{l,k}|_{(n_{l,k},m_{l,k})}}$.

The problem of assigning the channels to the L transmissions is a special case of the Hitchcock problem [92], and it can be solved by the Hungarian algorithm [91]. The Hungarian algorithm solves the weighted matching problem for a complete

[1]A bipartite graph is a graph whose vertices belong to two disjoint sets, such that every vertex is connected to at most one vertex from the other set.

bipartite graph. A complete bipartite graph has the same number of elements in both sets, but according to [92], we can always assume that a bipartite graph is complete by setting the weights of the missing edges to be equal to 0, and still get the optimal solution for the bipartite graph by applying this modification [93]. The goal is to find the optimal matching between the elements of the two sets so that we maximize the sum of the weights of the matching edges.

The bipartite graph illustrating the channel assignment problem with M number of detected channels and $L \leq M$ transmissions is shown in Fig. 5.2

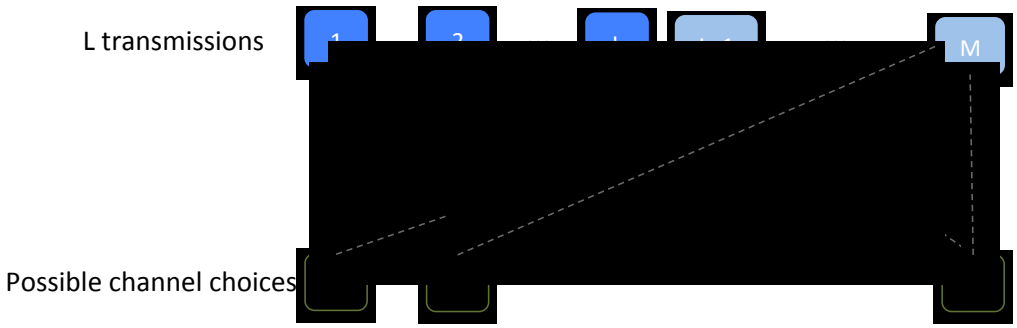

Figure 5.2: An illustration of the bipartite graph representation of the channel assignment problem with M number of channels and L number of transmissions. The dashed edges have weight of 0.

5.3 Simulation results

To illustrate the performance of the proposed wideband BAG solution, a simulation was first carried out under the following conditions: 1) maximum number of simultaneous transmissions of the Radiobot is $L = 2$; 2) number of sub-bands $N = 3$; 3) number of channels in each sub-band are 2, 3, and 3, respectively, and each of these channels have bandwidths 22, 22, 40, 40, 40, 36, 36, and 36MHz respectively;

4) the sojourn time of idle and busy periods are all exponentially distributed with a common idle sojourn time mean of 0.3ms and a common busy sojourn time mean of 0.6ms [86]; 5) $\bar{P} = 1$ Watt, and $\tau_s = 0.2$ms. The transmission throughput of the Radiobot as a function of the probability of idle state detection, in a time period of 100ms is shown in Fig. 5.3. As shown in Fig. 5.3, we see that the first case with $\alpha_1 = 1$ and $\alpha_2 = 0.2$ results in more transmission throughput compared to the second case with $\alpha_1 = 1$ and $\alpha_2 = 5$, as expected. This is due to the fact that the power consumption was considered more critical in the second case by setting a higher value for α_2.

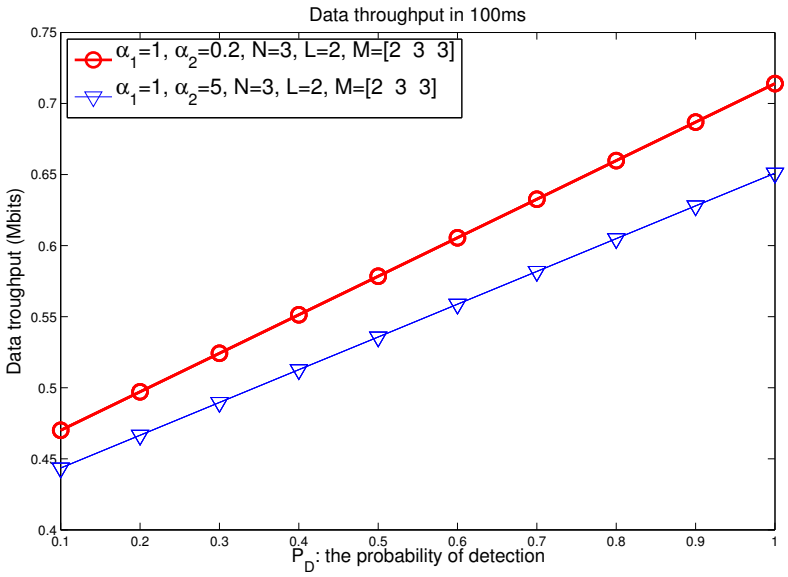

Figure 5.3: Achieved throughput as a function of the probability of detection of idle channels in two cases: 1) $\alpha_1 = 1$, $\alpha_2 = 0.2$; and 2) $\alpha_1 = 1$, $\alpha_2 = 5$.

With the same radio environment setup, in Fig. 5.4, we show the performance comparison for the following two cases: 1) $L = 2$ and $\alpha_1 = 1$; 2) $L = 1$ and $\alpha_1 = 1$, in terms of the data throughput as a function of α_2, in a time period of 1000ms. The probability of idle state detection was set to be 0.8. We observe that

in the first case, the Radiobot is able to perform $L = 2$ number of simultaneous transmissions, resulting in a higher data throughput compared to the second case with only one supported transmission. We can also see that as the α_2 increases, the data throughput drops to conserve energy as expected.

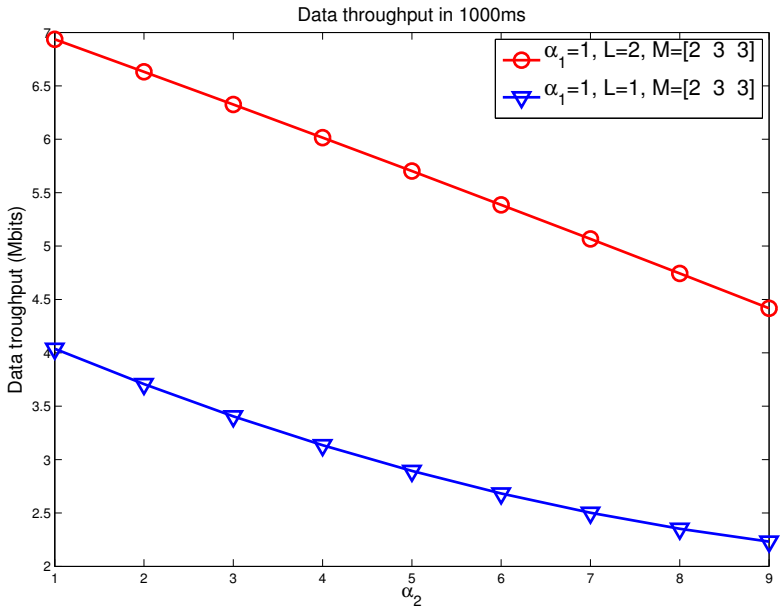

Figure 5.4: Achieved throughput as a function of the α_2 in two cases: 1) $L = 2$, $\alpha_1 = 1$; and 2) $L = 1$, $\alpha_1 = 1$.

5.4 Chapter Summary

We proposed an optimal wideband bandwidth aggregation strategy as the solution to a multi-objective optimization problem: one objective is the communication throughput of the mobile cognitive radio device and the other one is power consumption of the device. The optimal bandwidth aggregation strategy was derived taking into

account practical issues including imperfect spectrum sensing, channel fading, hardware reconfiguration time delay and power consumption, and communication power consumptions. Moreover, we analyzed and verified the performance of the proposed strategy through simulations.

Chapter 6

Learning-aided Sub-band Selection for Wideband CRs

6.1 Introduction

Spectrum sensing has been identified as a fundamental task for CRs to detect spectrum opportunities and achieve awareness of the surrounding RF environment [3, 13, 94–96]. Several sensing techniques have been proposed for sensing primary signals[1] in either narrow or wide frequency bands [13, 96–99]. In narrowband applications, a CR senses a particular channel (or a particular set of channels) to identify the existence of primary signals. In this case, the decision-making reduces to a binary hypothesis testing problem to determine whether a particular channel is idle or

[1] A primary signal refers to a signal that is licensed to a certain frequency range by the regulations of static RF spectrum allocation.

busy [27, 100–102]. In a wideband CR application, however, in order to maximize its communication throughput, a CR not only has to determine the existence of primary signals, but it also has to determine the spectrum range to sense in the first place, since the limitations of the RF hardware and the signal processing capabilities often prohibit a wideband CR from sensing the whole spectrum range of interest at the same time and the spectrum usage patterns are in general non-homogeneous across the wide spectrum range of interest [103].

In this chapter, we propose a dynamic spectrum sensing scheduling framework for wideband CRs. The considered wideband CR is assumed to be equipped with a reconfigurable RF front-end (reconfigurable antennas and reconfigurable RF circuitry) that may operate over several wide frequency bands, with each configuration corresponding to one of the wide frequency bands. We assume that the CR can only be configured to operate in one of the frequency bands at a time and that the CR may determine to reconfigure at any time. Each of the wide frequency bands is assumed to be further segmented into several non-overlapping sub-bands and each of the segmented sub-bands is assumed to contain multiple communication channels. Without loss of generality, we assume that the CR can only operate in one of the sub-bands at a time due to hardware and signal processing limitations. Note that we also assume that the wideband CR is capable of simultaneous transmissions of multiple signals on multiple channels within a single sub-band. Note that there may exist multiple distinguishable radio interfaces or communication protocols within any particular sub-band. The simultaneous transmission over multiple radio interfaces by a single mobile terminal is discussed in Chapter 5. In this chapter, we focus on the sub-band selection problem that arise in wideband spectrum sensing instead of the optimization of the BAG problem.

Note that although the wideband spectrum sensing scheduling problem may be

formulated as a POMDP problem[2] when the RF environment exhibit Markov state transition properties, the optimal solution to the POMDP is *computationally prohibitive* because of the continuum of the state space, as also noted in [25–27]. As a result, three myopic sub-band selection policies are proposed to maximize the probability of finding spectrum opportunities and communication throughput. The proposed policies take into account realistic reconfiguration energy consumptions and time delays. The first sub-band selection policy rely on the knowledge of the channel Markov parameters. Note that, however, it may require a tremendous amount of efforts to obtain the Markov parameters of each and every channel through learning when the channels are not independent and identically distributed (non-i.i.d.) and the number of channels is large. Hence, the second sub-band selection policy is proposed to rely on only the Markov properties of the sub-bands to avoid the necessity of obtaining the Markov knowledge of each and every channel. Note that, although both of these two policies may achieve good results, they rely on the knowledge of the Markov parameters of the RF environment and thus may become computationally infeasible when the knowledge of the Markov models are unavailable. As a result, the third sensing policy based on the Q-learning [104] technique is proposed to avoid the necessity of any knowledge of the Markov properties.

The Q-learning algorithm is one of the most important *temporal difference* (TD) reinforcement learning (RL) methods and it has been shown to converge to the optimal policy when applied to single agent Markov decision process (MDP) models [104,105]. The Q-learning has also been recently applied to CRs [106,107]. Although the sub-band selection problem is a POMDP problem, we may still use the Q-learning technique to achieve reasonable performance results since it has been shown that the application of Q-learning in POMDP problems may achieve near-optimal solutions

[2]The wideband spectrum sensing scheduling problem can be formulated as a POMDP problem since at each time step, only the state of the sensed sub-band is revealed and the complete state of the RF environment is not fully observable.

[100, 108, 109]. Performance of the three policies are compared and discussed against a performance upper-bound of the optimal solution to the POMDP formulation. We validate the suitability of the Q-learning technique for this type of wideband spectrum sensing problems by showing that it achieves good performance in both simulated and real measured RF environments.

The remainder of the paper is organized as follows: In Section 6.2 we introduce the system model and problem formulation. In Section 6.3, the sub-band selection policies for spectrum sensing are developed. In Section 6.4, the alternative Q-learning based solution is proposed. In Section 6.5 we show the simulation results. In Section 6.6 we conclude by summarizing our results.

6.2 System Model and Problem Formulation

6.2.1 Spectrum Segmentation Model for Wideband Sensing

The proposed CR architecture consists of a tunable RF front-end with wideband capabilities and a cognitive engine (CE), as shown in Fig. 6.1. The CE is equipped with signal processing, learning and decision-making capabilities, as proposed in the Radiobot architecture in [6]. The CE controls the RF front-end to perform spectrum sensing and communication functionalities. The concept of CE is also aligned with the original vision of CRs in [3].

We assume that a reconfigurable antenna is adopted to cover R number of different frequency bands $\mathcal{W}_1, \cdots, \mathcal{W}_R$ spanning a wide range of frequency spectrum. Note that the frequency bands $\mathcal{W}_1, \cdots, \mathcal{W}_R$ are determined by the capabilities of each configuration of the reconfigurable antenna. We denote by $W_l = |\mathcal{W}_l| > 0$ the

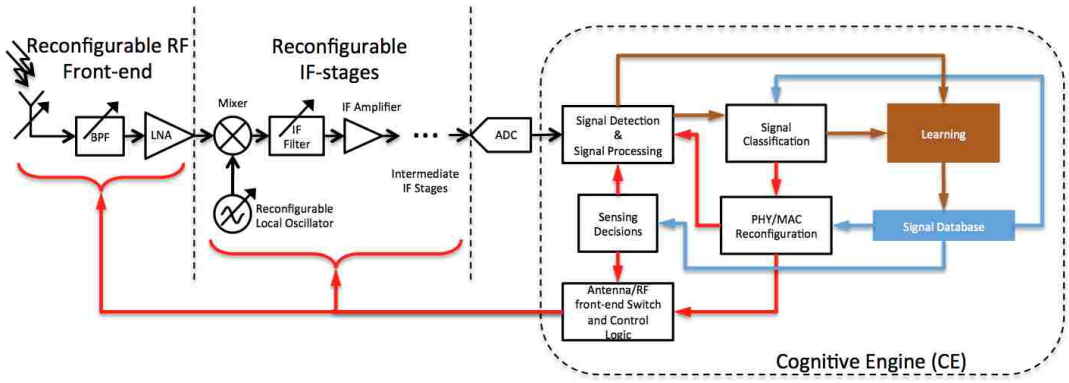

Figure 6.1: System architecture for the proposed wideband CR.

bandwidth of the frequency band $\mathcal{W}_l$, for $l \in \{1, \cdots, R\}$. Since the bandwidths $W_1, \cdots, W_R$ are considered to be still wide, the processing cost of the corresponding signals may be high, which requires further segmenting those frequency bands into smaller sub-bands prior to processing. Therefore, the sensing reconfigurable antenna will be connected to a reconfigurable band-pass filter or a filter bank of reconfigurable band-pass filters allowing proper segmentation of each of the frequency bands $\mathcal{W}_1, \cdots, \mathcal{W}_R$. We also assume that spectrum sensing can only be performed on a single sub-band at a time due to software and hardware limitations. There are several characteristics that need to be specified in order to determine the optimal number of sub-bands in each frequency band, such as the maximum sampling rate of the analog-to-digital converter (ADC), the required quantization accuracy, and the power consumptions to name a few. However, we omit the problem of finding the optimal number of sub-bands in each frequency band due to the focus of this work. Without loss of generality, we may assume that there are N_l number of sub-bands in the l-th RF configuration mode (corresponding to the frequency band $\mathcal{W}_l$) and denote by $\mathcal{N}_l$ the set of sub-bands contained in the l-th RF configuration mode, such that $|\mathcal{N}_l| = N_l$. An illustration of the frequency bands and the further segmented sub-bands in each frequency band is shown in Fig. 6.2. Note that the collection

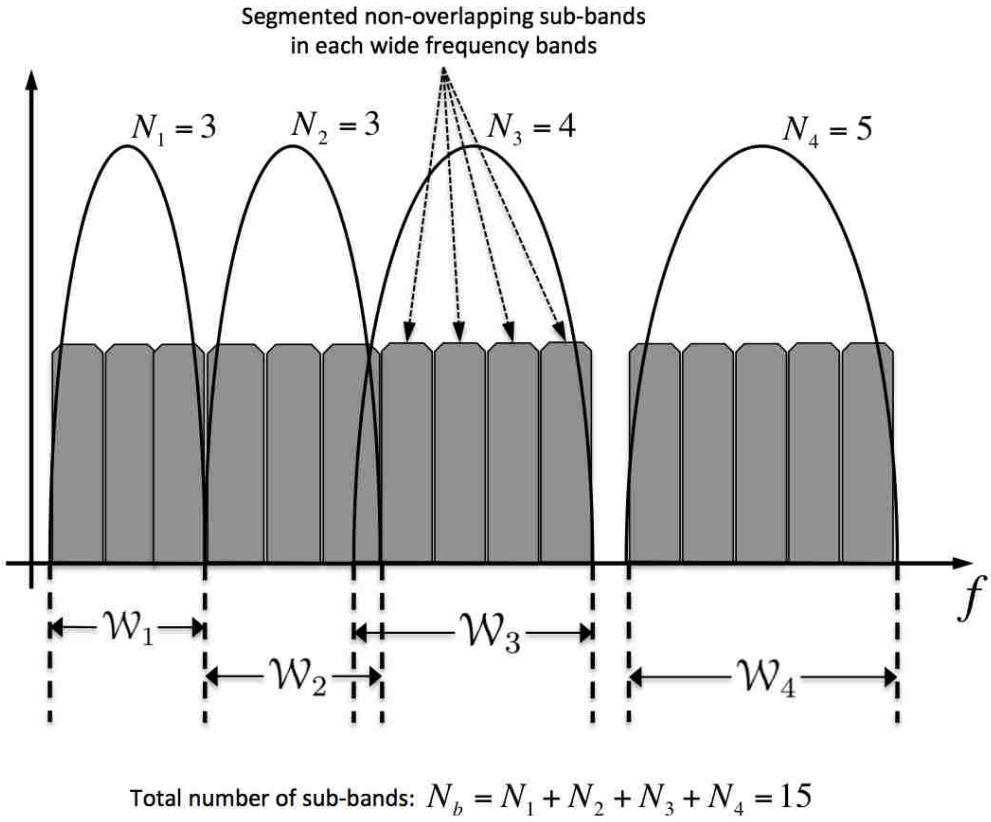

Figure 6.2: An illustration of wide frequency bands and further segmented sub-bands in each wide frequency band.

of the operable wide frequency bands may not perfectly cover the whole spectrum range due to antenna imperfections. The operable wide frequency bands may also overlap and/or be non-contiguous. Such reconfigurable antenna designs can be found in [46–49].

Since the RF spectrum environment is in general non-homogeneous [103], a spectrum sensing scheduling policy can be designed to dynamically change the RF front-end configurations to aim at suitable sub-bands to perform spectrum sensing. This sensing scheduling policy chooses a sub-band according to the real-time variations of the RF environment in order to maximize potential communication opportunities.

We propose such a sensing selection policy for the CR to perform spectrum sensing. We assume that the total bandwidth of interest is divided into $N_b = \sum_{l=1}^{R} N_l$ sub-bands and there are $M_1, \cdots, M_{N_b}$ number of identified communication channels in each of the N_b sub-bands respectively. In order to develop the proposed sub-band selection policies in Section 6.3, we introduce the channel and sub-band Markov models in the rest of this section.

6.2.2 Channel Markov Model

We assume a semi-infinite slotted time horizon with each time slot having an equal time length of T sec. We denote by $k = \{0, 1, 2, \cdots\}$ the time indices of the time slots. For simplicity, we assume that the state of any communication channel does not change within a single time slot, so that the CR may spend a short period of time at the beginning of each time slot to determine the corresponding state. We denote by $S_{i,j}(k) \in \{0, 1\}$ the true state of the (i, j)-th channel (the j-th channel in the i-th sub-band) at time k, for $j \in \{1, \cdots, M_i\}$ and $i \in \{1, \cdots, N_b\}$. As shown in Fig. 6.3, for a single channel, we may assume that the state *busy* (state 0) indicates the channel is occupied by other radio activities, and the state *idle* (state 1) indicates no radio activities over that channel and it is available for a CR to access. As a result, the state dynamics of each communication channel may be modeled as a two-state Markov chain. This Markov model, also known as the Gilbert-Elliot model [51], has been commonly used to abstract physical primary channels with memory (see, for example [22,26,27,52]). Note that it is worth mentioning that the choice of the value T may play a critical role in terms of the validity of the channel Markov models. In other words, the channel Markov property may not hold for some choices of T, or the channel dynamics may be better represented by higher-order Markov models as opposed to the first order Markov model considered in this chapter. However,

due to the focus of this work, the problem of finding the appropriate value of T is not investigated. Detailed discussions on this topic can be found in [110] and the references therein.

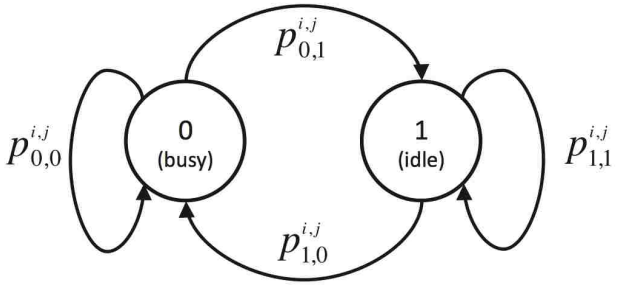

Figure 6.3: The Markov model for a single communication channel (Gilbert-Elliot model).

Since different channels may exhibit non-identical statistical behaviors [103], the assigned Markov chain models are, in general, non-identical, i.e. the state transition probabilities and the stationary distributions are different. Moreover, for those channels belonging to the same communication system, some level of channel access control may be present [111] for a centralized setup. As a result, communication traffics in those channels may be correlated. As a result, we assume that the Markov models can be correlated in general. The time-invariant transition probability of the (i,j)-th channel Markov model from state x to state y is defined as $p_{x,y}^{i,j} = \Pr\{S_{i,j}(k+1) = y \mid S_{i,j}(k) = x\}$, $\forall x, y \in \{0,1\}$. The *transition probability matrix* of the (i,j)-th channel Markov model is denoted by $\mathbf{P}^{i,j} = \begin{pmatrix} p_{0,0}^{i,j} & p_{0,1}^{i,j} \\ p_{1,0}^{i,j} & p_{1,1}^{i,j} \end{pmatrix}$. We denote by vector $\boldsymbol{\pi}^{i,j} = \left[\pi_0^{i,j}, \pi_1^{i,j}\right]$ the stationary distribution vector, such that $\boldsymbol{\pi}^{i,j} = \boldsymbol{\pi}^{i,j}\mathbf{P}^{i,j}$, with $\pi_0^{i,j}$ and $\pi_1^{i,j}$ being the stationary probabilities of busy and idle, respectively.

6.2.3 Sub-band Markov Models

We may further define the random variable $N_i^{idle}(k)$ as the number of idle channels in the i-th sub-band at time k. Note that, due to the Markov property of the communication channels, the dynamics of $N_i^{idle}(k)$ also forms a Markov chain as shown in Fig. 6.4. Since there are M_i number of channels in the i-th sub-band, we

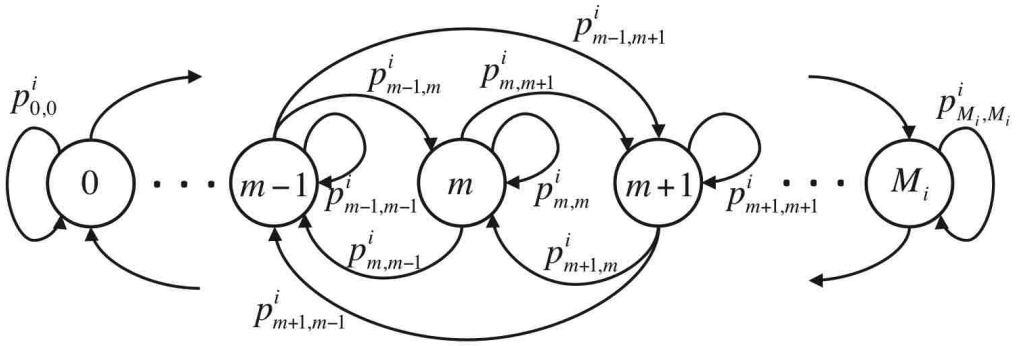

Figure 6.4: The Markov model of the i-th sub-band. The state of the Markov model is defined as the number of idle channels in the i-th sub-band.

obtain a $(M_i + 1)$-state Markov chain for the i-th sub-band, with a state space of $\{0, 1, \cdots, M_i\}$. As shown in Fig. 6.4, the time-invariant transition probability of the Markov model from state m to state n is defined as

$$p^i_{m,n} = \Pr\{N_i^{idle}(k+1) = n \mid N_i^{idle}(k) = m\}, \forall m, n \in \{0, 1, \cdots, M_i\}. \tag{6.1}$$

The $(M_i+1)\times(M_i+1)$ *transition probability matrix* of the Markov model of the i-th sub-band is then denoted by $\mathbf{P}_i = \begin{pmatrix} p^i_{0,0} & p^i_{0,1} & \cdots & p^i_{0,M_i} \\ p^i_{1,0} & p^i_{1,1} & \cdots & p^i_{1,M_i} \\ \vdots & \vdots & \ddots & \vdots \\ p^i_{M_i,0} & p^i_{M_i,1} & \cdots & p^i_{M_i,M_i} \end{pmatrix}$. We denote by vector $\boldsymbol{\pi}_i = \left[\pi^i_0, \cdots, \pi^i_{M_i}\right]$ the stationary distribution vector, such that $\boldsymbol{\pi}_i = \boldsymbol{\pi}_i \mathbf{P}_i$ with $\pi^i_0, \cdots, \pi^i_{M_i}$ being the stationary probabilities of the states $0, 1, \cdots, M_i$, respectively.

6.3 Sub-band Selection For Wideband Spectrum Sensing

In this section, we propose two sub-band selection policies for the wideband spectrum sensing scheduling problem. The first policy solely relies on the knowledge on the channel Markov models; whereas the second policy mainly relies on the knowledge on the sub-band Markov models. The performance comparison of the two policies are provided in Section 6.5.

6.3.1 Channel Markov Model based Sub-band Selection

In order to derive the sensing sub-band selection policy, let us first denote by $BW_{i,j}$ the identified channel bandwidth of the j-th channel in the i-th sub-band, for $i \in \{1, \cdots, N_b\}$ and $j \in \{1, \cdots, M_i\}$. Note that the instantaneous transmission rate of a channel with a bandwidth of B is $r = B \log_2 \left(1 + \frac{h^2 P}{B N_0}\right)$ bits/sec, where we denote by h, P, and N_0 the channel coefficient between the receiver and the transmitter, the transmission power, and the single-sided noise power spectrum density (PSD) level, respectively. We assume that the distributions of the channel coefficients are either known or can be obtained through learning and we denote by $f_{H_{i,j}}$ the corresponding distribution function of the channel coefficient of the (i,j)-th channel.

For simplicity, we may assume that whenever the i-th sub-band is sensed (or visited) at time k, the information of $N_i^{idle}(k)$ and the states of the channels in the i-th sub-band are revealed exactly by sophisticated sensing algorithms, and they cannot be revealed otherwise. Since only one sub-band can be sensed at a time, it is impossible to consecutively obtain the information of $N_i^{idle}(k)$ as well as the channel states for every sub-band. At time k, we denote by $\mathbf{t}(k) = [t_1(k), t_2(k), \cdots, t_{N_b}(k)]$

the sub-band visiting history, where we denote by $t_i(k)$ the time index of the last visit of the i-th sub-band. Note that $t_i(k) \leq k$ and $N_i^{idle}(t_i(k))$ is known. However, $N_i^{idle}(t)$ is unknown for all $t \in \{t_i(k)+1, \cdots, k\}$. An illustration of the sensing history is shown in Fig. 6.5. Note that, in the case when the i-th sub-band has not yet been visited, we may assign a negative integer value, say -1, to $t_i(k)$ in order to distinguish from others. Also, we may initialize $N_i^{idle}(t_i(k))$ accordingly based on the prior knowledge of the Markov properties, whenever $t_i(k) = -1$.

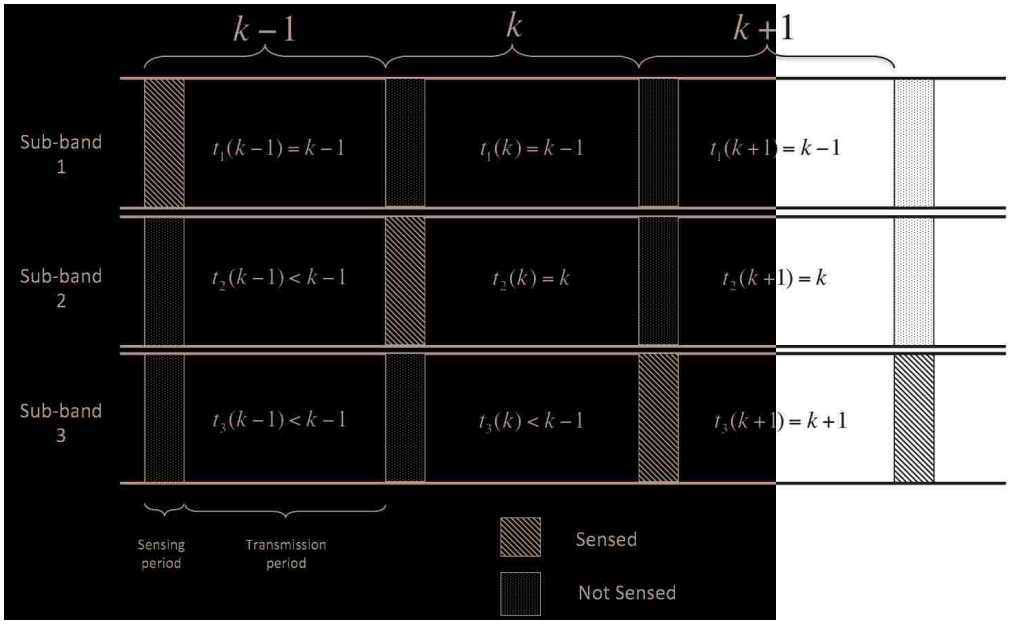

Figure 6.5: An illustration of the sensing history $t_i(k)$ for three sub-bands.

Note that, in practice, imperfect sensing is indeed one of the most critical impact factors for CRs. In particular, when a CR may mistake an idle channel as a busy one and vice versa, performance can be degraded due to the missed channel opportunities and the constraint on the interference to other radios. The imperfect sensing issue has been addressed in our previous work [27] and many other works [25, 42] for narrow-band spectrum sensing scenarios. One may incorporate the imperfect sensing

by using a *believe vector*. The belief vector is used to maintain the distribution (belief) of future states of the RF environment based on the observation history, the observation emission probabilities, and the Markov state transition probabilities. Note that this is as opposed to using only the Markov state transition probabilities as in this chapter under perfect sensing assumption. On the other hand, sensing errors may be substantially limited by the state-of-the-art spectrum sensing techniques by involving multivariate detection (e.g., energy and cyclostationary features [112]) and network sensing cooperations [27]. As a result, the imperfect sensing problem is not considered here due to the space limitation and the focus of this work.

We denote by $T_{i,j}(k)$ the discrete-valued random variable of the idle sojourn time[3] of the (i,j)-th channel starting from time k given the observation history, with $T_{i,j}(k) \in \{0, T, 2T, \cdots\}$, where T is the length of a time slot. Note that the probability mass function (pmf) of $T_{i,j}(k)$ can be found using the Markov properties:

$$\begin{aligned} f_{T_{i,j},k}(nT) &= \Pr\{T_{i,j}(k) = nT \mid S_{i,j}(t_i(k))\} \\ &= \begin{cases} p^{i,j,(k-t_i(k))}_{S_{i,j}(t_i(k)),0}, & \text{if } n = 0 \\ p^{i,j,(k-t_i(k))}_{S_{i,j}(t_i(k)),1} \cdot (p^{i,j}_{1,1})^{n-1} \cdot p^{i,j}_{1,0}, & \text{if } n \in \{1, 2, 3, \cdots\} \end{cases}, \end{aligned} \tag{6.2}$$

where we denote by $p^{i,j,(k-t_i(k))}_{S_{i,j}(t_i(k)),m}$ the $(k - t_i(k))$-step transition probability from state $S_{i,j}(t_i(k))$ to m of the (i,j)-th channel, for $m \in \{0, 1\}$, which can be found as the $(S_{i,j}(t_i(k)) + 1, m + 1)$-th element in $(\mathbf{P}^{i,j})^{(k-t_i(k))}$, the $(k - t_i(k))$-th power of $\mathbf{P}^{i,j}$. Whereas, $(p^{i,j}_{1,1})^{n-1}$ is the $(n-1)$-th power of $p^{i,j}_{1,1}$. The expected value of $T_{i,j}(k)$ can then be found as

$$\mathbb{E}\{T_{i,j}(k)\} = \sum_{n=0}^{\infty} f_{T_{i,j},k}(nT) \cdot nT. \tag{6.3}$$

[3]The idle sojourn time refers to the time duration of the channel being consecutively idle. Since we assumed that the state of any communication channel does not change within a single time slot, the sojourn time of a channel is discrete-valued.

Note that since sensing errors indeed exist in practice, different frequency bands may have different spectrum sensing requirements. For instance, in some licensed frequency bands, there can be a more stringent regulation of collisions with licensed users such that the upper bound on the probability of collision is low. This requires a CR to spend more time on spectrum sensing in order to achieve the required level of probability of detecting licensed signals (if any) thereby lowering the chances of colliding with them. On the other hand, in an unlicensed frequency band, such as the Industrial, Scientific and Medical (ISM) band, the collision is not often strictly controlled. Hence, a CR may spend less time to detect a transmission opportunity at the expense of a possible higher collision probability. Since we are considering perfect sensing for simplicity, we may assume that the CR spends T_0^i sec for sensing the i-th sub-band. If the sensing result for the channel is idle, it can then access that channel. Note that, when formulating the problem under imperfect sensing, the required sensing time T_0^i can be easily modeled as a function of the characteristics of the sensing detector and the constrained collision probability.

Note that a CR may achieve a high communication throughput by frequently jumping among the frequency sub-bands, at the expense of a high rate of hardware reconfigurations. This, however, generally require a certain amount of energy consumption and time delay. In order to take into account the practical RF front-end reconfigurable energy consumptions in the sub-band selection decision-making, we may denote by $c_s(i', i)$ the switching energy cost from the i'-th sub-band to the i-th sub-band, such that

$$c_s(i', i) = \begin{cases} c_1 + c(T_0^i), & \text{if } i' \in \mathcal{N}_{l'},\ i \in \mathcal{N}_l, \text{ and } l' \neq l \\ c_2 + c(T_0^i), & \text{if } i' \in \mathcal{N}_{l'},\ i \in \mathcal{N}_{l'}, \text{ and } i' \neq i \\ c(T_0^i), & \text{if } i' = i \end{cases}, \tag{6.4}$$

where c_1 denotes the energy cost when switching between different RF configuration

modes, and c_2 denotes the energy cost when switching between different sub-bands within the same RF configuration mode. The quantity $c(T_0^i)$ denotes the energy cost required for spectrum sensing in the i-th sub-band, as a function of the required sensing time T_0^i. Since hardware reconfiguration may require more energy consumption, we assume that $c_1 > c_2$. Note that in practice c_1 and c_2 may not necessarily be constant. In such cases, we may easily re-adjust them depending on the specific adopted RF front-end.

We may also define $t_s(i', i)$ the switching time delay incurred when the CR switches from the i-th sub-band to the i'-th sub-band, such that

$$t_s(i', i) = \begin{cases} t_1, & \text{if } i' \in \mathcal{N}_{l'},\ i \in \mathcal{N}_l, \text{ and } l' \neq l \\ t_2, & \text{if } i' \in \mathcal{N}_{l'},\ i \in \mathcal{N}_{l'}, \text{ and } i' \neq i \\ t_3, & \text{if } i' = i \end{cases}, \tag{6.5}$$

where t_1, t_2 and t_3 include the computation time of decision-making at each time step, the circuit switching time, software reconfiguration time, and settling time for the RF front-end (especially the settling time for the phase-locked loop (PLL) in the frequency synthesizer [113]).

In order to consider possible bandwidth aggregation [10, 32, 33] capability, we may assume that the CR is capable of utilizing up to a maximum of L idle channels simultaneously, all from a single sub-band. When the CR has the knowledge of channel Markov models but not the Markov models of the sub-bands, we may define the total expected communication throughput by switching from the i'-th sub-band to the i-th sub-band in time slot k as

$$R_{i'}(i, k) = \sum_{j \in \mathcal{M}_{i,L}^*} \mathbb{E}_{H_{i,j}}\{r_{i,j}\} \min\left\{ \left[\mathbb{E}\{T_{i,j}(k)\} \left(1 - \frac{T_0^i}{T}\right) - t_s(i', i) \right],\ T_{max} \right\}, \tag{6.6}$$

where function $\min\{x, y\} = x$, if $x \leq y$ and $\min(x, y) = y$ otherwise. Note that the

expectation of transmission rate $\mathbb{E}_{H_{i,j}}\{r_{i,j}\}$ on the (i,j)-th channel in (6.6) is with respect to the channel coefficient and is defined as

$$\mathbb{E}_{H_{i,j}}\{r_{i,j}\} = \int BW_{i,j}\log_2\left(1+\frac{h^2P}{BW_{i,j}N_0}\right)\times f_{H_{i,j}}(h)dh. \tag{6.7}$$

The expression $\left[\mathbb{E}\{T_{i,j}(k)\}\left(1-\frac{T_0^i}{T}\right)-t_s(i',i)\right]$ in (6.6) gives the expected transmission time on the (i,j)-th channel. We denote by T_{max} the maximum considered staying time for any sub-band. The T_{max} is introduced to prevent the CR from selecting a sub-band when the achievable transmission rate in a sub-band is extremely low, but the expected channel idle sojourn time is extremely large. In this case, although the expected throughput may be large, the extremely low transmission rate may not be desirable. We denote by $\mathcal{M}_{i,L}^*$ in (6.6) the set of L channels in the i-th sub-band that have top L highest expected transmission throughput. As a result, the following inequality is satisfied:

$$\begin{aligned}&\sum_{j\in\mathcal{M}_{i,L}^*}\mathbb{E}_{H_{i,j}}\{r_{i,j}\}\min\left\{\left[\mathbb{E}\{T_{i,j}(k)\}\left(1-\frac{T_0^i}{T}\right)-t_s(i',i)\right],\ T_{max}\right\}\geq\\ &\sum_{j\in\mathcal{M}_{i,L}}\mathbb{E}_{H_{i,j}}\{r_{i,j}\}\min\left\{\left[\mathbb{E}\{T_{i,j}(k)\}\left(1-\frac{T_0^i}{T}\right)-t_s(i',i)\right],\ T_{max}\right\},\end{aligned} \tag{6.8}$$

where we denote by $\mathcal{M}_{i,L}$ any set of L channels in the i-th sub-band.

When the CR has only the knowledge of channel Markov models, by taking the switching energy and time delays into account, we may then define the quality of the i-th sub-band (switching from the i'-th sub-band) at time k as

$$Q_{i'}(i,k) = R_{i'}(i,k) - \beta c_s(i',i), \tag{6.9}$$

where the coefficient β (bits/Joule) is used to convert the units and to help weighting the energy consumption priority. The sub-band selection policy $a(i',k,\mathbf{t}(k))$ (in the

i'-th sub-band and time slot k) may then be defined as

$$a(i', k, \mathbf{t}(k)) = \underset{i \in \{1, \cdots, N_b\}}{\arg\max} \quad Q_{i'}(i, k). \tag{6.10}$$

6.3.2 Sub-band Markov Model based Sub-band Selection

In the case when the knowledge of both the sub-band Markov models and the channel Models are available, we may define the total expected communication throughput by switching from the i'-th sub-band to the i-th sub-band in time slot k as

$$\begin{aligned} & R_{i'}(i, k, N_i^{idle}(t_i(k))) \\ = \; & \frac{1}{M_i} \left(\sum_{j=1}^{M_i} \mathbb{E}_{H_{i,j}}\{r_{i,j}\} \min \left\{ \left[\mathbb{E}\{T_{i,j}(k)\}(1 - \frac{T_0^i}{T}) - t_s(i', i) \right], T_{max} \right\} \right) \times \\ \times \; & \min \left\{ \hat{N}_i^{idle}(k, N_i^{idle}(t_i(k))), L \right\}, \end{aligned} \tag{6.11}$$

where $N_i^{idle}(t_i(k))$ is the visiting history of the i-th sub-band and M_i is the number of channels in the i-th sub-band. Note that, the average expected per channel throughput within the i-th sub-band, or

$$\frac{1}{M_i} \left(\sum_{j=1}^{M_i} \mathbb{E}_{H_{i,j}}\{r_{i,j}\} \min \left\{ \left[\mathbb{E}\{T_{i,j}(k)\} \left(1 - \frac{T_0^i}{T} \right) - t_s(i', i) \right], T_{max} \right\} \right), \tag{6.12}$$

in (6.11), requires the knowledge of the individual channel Markov models in order to obtain $\mathbb{E}\{T_{i,j}(k)\}$. This, of course, is not possible when the channel Markov parameters are unavailable. However, when only the sub-band Markov model is assumed to be known, we may replace the average expected channel throughput term by $\bar{r}_i \min \left\{ \left[\bar{T}_i \left(1 - \frac{T_0^i}{T} \right) - t_s(i', i) \right], T_{max} \right\}$, where we denote by $\bar{r}_i$ and $\bar{T}_i$ the average achievable individual channel throughput and the average idle sojourn time of the

channels in the i-th sub-band. Note that the average individual channel throughput and the average channel idle sojourn time may be easily summarized from past channel access history. However, due to the space limitation, we do not go into details of estimation methods for $\bar{r}_i$ and $\bar{T}_i$. Note that the function $\min\{x, y\} = x$, if $x \leq y$, and $\min\{x, y\} = y$ otherwise. The term $\min\left\{\hat{N}_i^{idle}(k, N_i^{idle}(t_i(k))), L\right\}$ in (6.11) is the estimated number of accessible and usable channels at time k, where we denote by $\hat{N}_i^{idle}(k, N_i^{idle}(t_i(k)))$ the estimated number of idle channels in the i-th sub-band in time slot k, given the visiting history $N_i^{idle}(t_i(k))$. The estimate of $\hat{N}_i^{idle}(k, N_i^{idle}(t_i(k)))$ may be obtained, for example, using the following two criteria:1) The maximum *a posteriori* (MAP) criterion: given $N_i^{idle}(k) = m$ for $m \in \{0, 1, \cdots, M_i\}$, we may predict the state $N_i^{idle}(k + k')$ for any integer $k' \geq 1$ as $\hat{N}_i^{idle}(k + k') = \underset{n \in \{0, \cdots, M_i\}}{\arg\max} \Pr\{N_i^{idle}(k + k') = n \mid N_i^{idle}(k) = m\} = \underset{n \in \{0, \cdots, M_i\}}{\arg\max} p_{m,n}^{i,(k')}$,where we denote by $p_{m,n}^{i,(k')}$ the k'-step transition probability from state m to n. Note that the k'-step transition probability can be obtained by finding the $(m + 1, n + 1)$ entry of $\mathbf{P}_i^{k'}$, the k'-th power of the transition probability matrix $\mathbf{P}_i$, where $\mathbf{P}_i^{k'} = \underbrace{\mathbf{P}_i \times \mathbf{P}_i \cdots \times \mathbf{P}_i}_{k'}$; 2) The minimum mean square error (MMSE) criterion: $\hat{N}_i^{idle}(k + k') = \mathbb{E}\{N_i^{idle}(k + k') \mid N_i^{idle}(k) = m\} = \sum_{n=0}^{M_i} n \cdot p_{m,n}^{i,(k')}$. Note that although the MMSE estimator may give a non-integer result for $\hat{N}_i^{idle}(k + k')$, it would still make sense when we use $\hat{N}_i^{idle}(k + k')$ to obtain the expected sub-band communication throughput. We verify in simulations that both methods achieve close results and thus we choose to use the MAP criterion since its computation is straightforward.

The quality of the i-th sub-band may then be defined as:

$$Q_{i'}(i, k, N_i^{idle}(t_i(k))) = R_{i'}(i, k, N_i^{idle}(t_i(k))) - \beta c_s(i', i). \tag{6.13}$$

The sub-band selection policy $a(i', k, \mathbf{t}(k))$ (in i'-th sub-band and time slot k) is

defined as

$$a(i', k, \mathbf{t}(k)) = \underset{i \in \{1, \cdots, N_b\}}{\arg\max} \quad Q_{i'}(i, k, N_i^{idle}(t_i(k))). \tag{6.14}$$

When the knowledge of the sub-band Markov models is not directly available, but the knowledge of the channel Markov models is available, one may obtain the knowledge of the sub-band Markov models from the knowledge of the channel Markov models, at least in theory (However, note that this is extremely unlikely when channels are non-i.i.d.). Note that the time-invariant transition probability $p_{m,n}^i$ of the i-th sub-band may be expressed as (for all $m \in \{0, \cdots, M_i\}$ and $n \in \{0, \cdots, M_i\}$)

$$\begin{aligned} p_{m,n}^i &= \Pr\left\{ \sum_{j=1}^{M_i} S_{i,j}(k+1) = n \mid \sum_{j=1}^{M_i} S_{i,j}(k) = m \right\} \\ &= \sum_{\mathcal{A}_{i,m}} \sum_{\sum_j^{M_i} s_{i,j} = n} \left[\left(\prod_{j \in \mathcal{A}_{i,m}} p_{1,s_{i,j}}^{i,j} \right) \left(\prod_{j \in \mathcal{A}'_{i,m}} p_{0,s_{i,j}}^{i,j} \right) \right], \end{aligned} \tag{6.15}$$

where we denote by $\mathcal{A}_{i,m}$ a subset of channels in the i-th sub-band, with cardinality m and we denote by $\mathcal{A}'_{i,m}$ the relative complement of $\mathcal{A}_{i,m}$ with respect to the set of all channels in the i-th sub-band. The summation in (6.15) is taken over all possible $\mathcal{A}_{i,m}$'s and all possible combination of states $s_{i,1}, \cdots, s_{i,M_i}$, where $s_{i,j} \in \{0, 1\}$ for all $j \in \{1, \cdots, M_i\}$, such that $\sum_j^{M_i} s_{i,j} = n$.

On the other hand, the stationary probability π_m^i, for $m \in \{0, \cdots, M_i\}$ can be expressed as

$$\pi_m^i = \Pr\left\{ \sum_{j=1}^{M_i} S_{i,j}(k) = m \right\}. \tag{6.16}$$

In case the channels are independent, the stationary distribution can be further

expressed as

$$\pi_m^i = \sum_{\mathcal{A}_{i,m}} \left(\prod_{j \in \mathcal{A}_{i,m}} \pi_1^{i,j} \right) \left(\prod_{j \in \mathcal{A}'_{i,m}} \pi_0^{i,j} \right), \tag{6.17}$$

The summation in (6.17) is taken over all possible $\mathcal{A}_{i,m}$'s. The closed-form expression of (6.17) requires a computational complexity of $\left[\binom{M_i}{m} \times M_i\right] - 1$ [103] when channels are assumed non-identical, but independent. In case the channels in a sub-band are non-identical, but statistically independent, we may also approximate the stationary distributions using the Poisson-Normal approximation method that is proposed in [103]. However, since we assume that channels may be correlated (i.e. non-independent) in general, to obtain the closed-form expression of π_m^i requires the knowledge of the joint distribution of $S_{i,j}(k)$'s, which is even harder to be obtained. We can see that the computational complexity to obtain the transition probabilities is at least $\left[\binom{M_i}{m}\binom{M_i}{n} \times M_i\right] - 1$, which is even higher than that of obtaining the stationary distributions. This observation suggests that to obtain the knowledge of the sub-band Markov models from the channel Markov models may not be advisable.

As an alternative, we may adopt the hidden Markov model (HMM)-based parameter estimation algorithm proposed in Chapter 2 to perform on-line estimation of the transition probabilities of the Markov chain model, without the computation of (6.15). The estimation algorithm has been shown to have a computation complexity linear in the number of the states of the Markov chain, or in this case, M_i, the number of channels in the i-th sub-band. However, when the number of sub-bands and the number of channels in each sub-band are both large, the overall computational complexity is still high[4]. Moreover, to obtain accurate estimates of the transition probability matrices, it may require a long period of time. As a result, in the case when the sub-band transition probabilities are unknown but the channel Markov

[4]Note that the computational complexity is also high when there are a large number of channels and the CR directly attempt to learn the channel Markov models.

models are known, we suggest to use the channel Markov models based sub-band selection policy defined in (6.10). When both the knowledge of the channel Markov models and the sub-band Markov models are available, one may choose either (6.6) or (6.11) to express the expected sub-band throughput. We compare the resulting performances between these two strategies in simulations later in Section 6.5. In the case when both channel and sub-band Markov models are unknown, we propose a Q-learning based Machine learning technique in Section 6.4 to bypass the computation complexity.

We may assume that an autonomous CR triggers to execute the above derived sub-band selection decision rule only when current transmission performance falls below a certain performance threshold, as opposed to triggering the decision rule in each time slot. This will avoid unnecessarily frequent sub-band switching when the performance objectives can be met without switching. The performance threshold may be fine tuned using a learning process. Note that a high threshold triggers more decision-making process and thus may result in more computation and reconfiguration energy consumptions. On the other hand, a lower threshold may result in lower communication throughput. An example illustration diagram of this procedure is shown in Fig. 6.6. Due to the space limitation and the focus of this chapter being on the sub-band selection algorithm design itself, we do not further investigate the use of such a performance threshold.

6.4 Machine Learning aided sub-band selection

In the case when neither the channels' nor the sub-bands' Markov models are known, we may rely on Reinforcement Learning (RL) techniques [104]. A Q-table $Q(s, a)$ is maintained that is used to summarize the value (benefit) of each action a in each

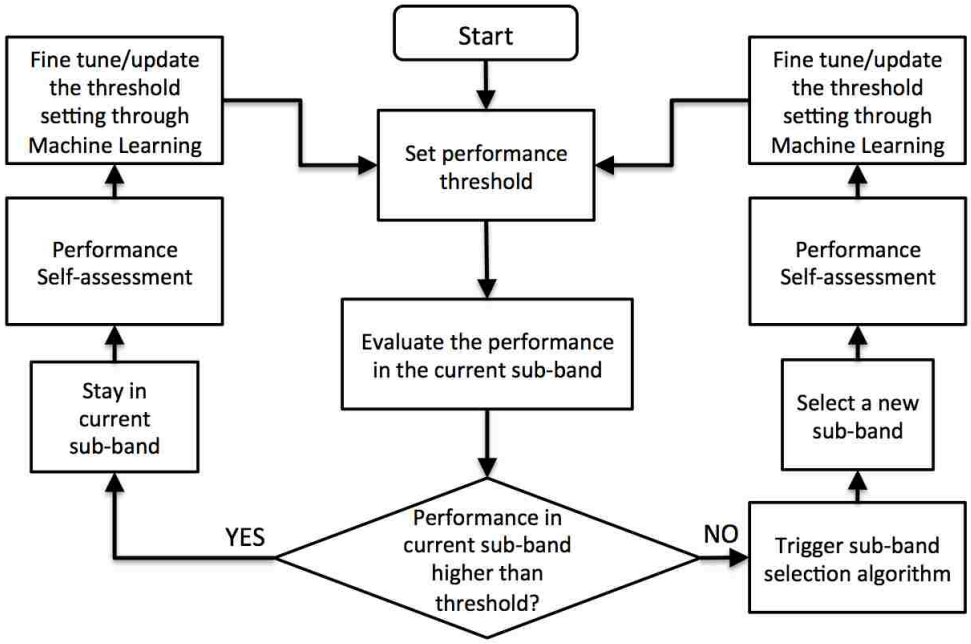

Figure 6.6: An illustration of the operation procedure of a performance threshold setting for higher level autonomous operation of the CR.

and every state s. In our case, the action a refers to the selection of a sub-band, with $a \in \mathcal{N}_1 \cup \mathcal{N}_2 \cdots \cup \mathcal{N}_R$. Each time an action is chosen in a certain state, the Q-table may be updated using the following rule:

$$Q(s_{k-1}, a_{k-1}) \leftarrow (1-\alpha)Q(s_{k-1}, a_{k-1}) + \alpha \left[r_k \left(s_{k-1}, a_{k-1} \right) + \gamma \max_a Q(s_k, a) \right], \tag{6.18}$$

where we denote by s_{k-1} and a_{k-1} the observed state and the action in time interval $k-1$, respectively. Note that the state s_k does not refer to the whole RF environment true state. This is explained in the following. Note that the action a_{k-1} denotes the index of the sub-band selected that is to be sensed at time k. We denote by $\alpha \in (0, 1)$ the learning rate. The function $r_k(s_{k-1}, a_{k-1})$ denotes the reward obtained in time interval k, as a result of the action a_{k-1} in state s_{k-1}, which can be defined as the

actual achieved performance. In the simulation, the reward is calculated as

$$r_k(s_{k-1}, a_{k-1}) = \tilde{r}(s_{k-1}, a_{k-1}) - \beta c_s(a_{k-2}, a_{k-1}), \tag{6.19}$$

where we denote by $\tilde{r}(s_{k-1}, a_{k-1})$ the actual achieved communication throughput by taking action a_{k-1} in state s_{k-1}. The term $c_s(a_{k-2}, a_{k-1})$ in (6.19) is the switching energy cost from the a_{k-2}-th sub-band to a_{k-1}-th sub-band as defined in (6.4), and β is the same coefficient as in (6.9). We denote by γ the discount factor, with $\gamma \in [0, 1)$. Note that the state at time $k-1$ may be defined as $s_{k-1} = [a(k-2),\ N^{idle}_{a(k-2)}(k-1)]$, where $a(k-2)$ denotes the index of the sensed sub-band in time interval $k-1$. Also note that, the state s_k in (6.18) is the result of taking action a_{k-1} in state s_{k-1} and the term $\gamma \max_a Q(s_k, a)$ represents the discounted delayed reward by taking action a_{k-1} in state s_{k-1}. The value of $\max_a Q(s_k, a)$ is obtained by finding the maximum value in the row of the Q-table corresponding to the state s_k. The decision-making rule for choosing an action a^* in the state s may be defined as $a^* = \arg\max_a Q(s, a)$. Since the state of the whole RF environment is not obtained at each time due to the RF hardware limitation (sensing can be done only in one sub-band at a time), the Q-learning application is for the POMDP case as discussed in the introduction section.

Note that the Q-learning is usually implemented as a balance between exploration and exploitation. Exploration refers to the effort of searching new opportunities, whereas exploitation refers to taking actions for immediate reward. Maintaining a certain level of exploration may help the agent avoid being trapped in local maxima. An exploration rate $\epsilon \in (0, 1)$ is often defined, such that the agent each time takes an action using a^* with probability $1 - \epsilon$ and uniformly choose an action out of all the possible actions with probability ϵ. Choosing a high exploration rate may help the agent to quickly *understand* the environment. However, it may also reduce the overall performance due to excessively exploring. On the other hand, a low exploration

rate may increase the required time for the algorithm to converge to the optimal solution. In the simulation section, we investigate the performance of the Q-learning technique using different parameter options. The variable parameters include the exploration rate ϵ, the learning rate α, and the discount factor γ. Since the Q-learning technique is simple to implement and it does not require any prior knowledge of the environment, we also compare its performance to the previously proposed sub-band selection policies to validate the application of Q-learning techniques in this type of problems. A temporal illustration of the Q-learning procedure on the slotted time horizon is shown in Fig. 6.7.

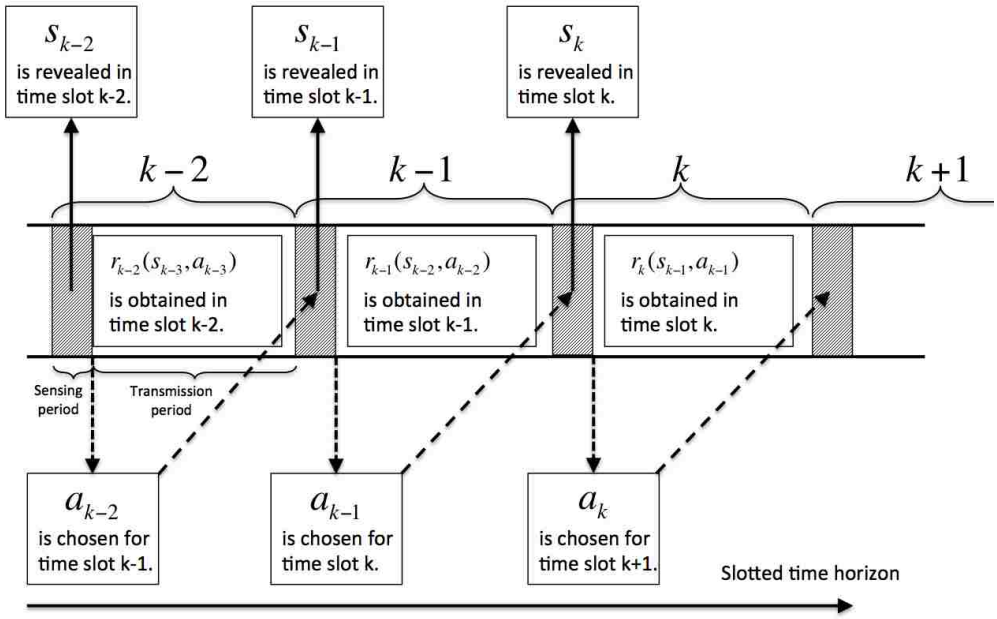

Figure 6.7: An illustration of the Q-learning procedure on the slotted time horizon.

6.5 Simulation Results and Discussions

In order to evaluate the performance of the proposed sub-band selection policies, we have conducted simulations for 3 test cases. The simulation settings for the 3 test cases are summarized in Table. 6.1. Note that the test cases 1, and 2 are based on simulated RF environments, whereas the test case 3 is based on real RF measurements for the $20-1500$MHz band, with center frequency at 770 MHz inside a modern office building at Aachen, Germany [114].

Table 6.1: Simulation settings for the considered 4 test cases.

Settings \ Test cases	Test case 1	Test case 2	Test case 3
# of configuration modes	2	2	2
# of sub-bands in each mode	[3 3]	[2 2]	[2 3]
Total # of sub-bands	6	4	5
# of channels in each sub-band	10 each	10 each	10 each
Total # of channels	60	40	50
Max # of channels can be used for each time step: L	2	2	2
Time slot duration: T (seconds)	1	1	1
# of simulation time steps	10,000	10,000	12,000
Channel Markov models	Randomly generated.		measurement data.
Required sensing time duration	The required sensing time duration in each sub-band is chosen uniformly between 0.1 sec and 1.0 sec.		
Sub-band Markov models	Obtained from channel Markov models.		
Reconfiguration coefficients	$c_1 = 1$, $c_2 = 0.8$; $t_1 = 0.1$, $t_2 = 0.05$, $t_3 = 0.01$; $\beta = 1$.		

For test cases 1, and 3, we assume that all channels have the same bandwidth, but the channel coefficients are independently Rayleigh-distributed. On the other hand, in test case 2, the individual channel throughputs are specifically assigned with non-random values for comparison purposes: in each configuration mode, one of the

sub-bands is assumed to have channels with the same individual channel throughputs, whereas the other sub-band is assumed to have 2 channels with very high channel throughput and the other 8 channels with very low individual throughputs, such that all the sub-bands have the same sum of channel throughputs.

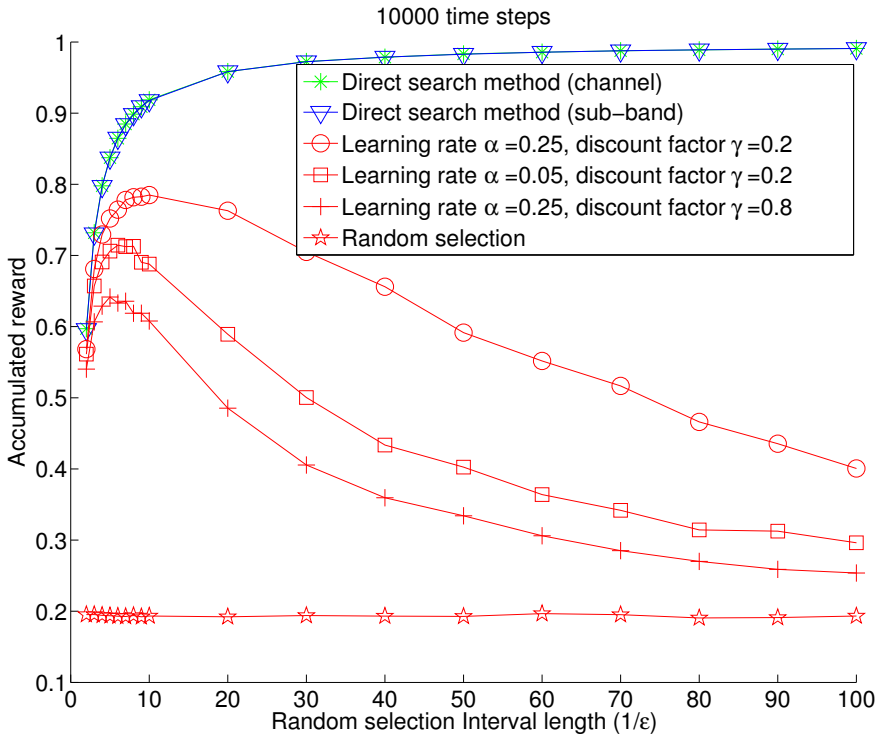

Figure 6.8: Comparison of normalized accumulated reward of sub-band selection policies in $10,000$ time steps for the first test case. The considered random selection interval length is set from 2 to 100.

In Fig. 6.8, we show the performance of the sub-band selection policies in the first test case. The simulated policies are: 1) the channel Markov models based policy using (6.10), 2) the sub-band Markov models based policy using (6.14), and 3) the Q-learning policy without any knowledge of the channel and sub-band Markov models. A trivial random policy is also included for comparison. The reward for all

policies is defined as the actual obtained throughput less the energy consumption due to hardware reconfigurations (the energy consumption is weighted by the coefficient β), similar to the way the sub-band quality is defined in (6.9) and (6.13). The accumulated reward is then normalized with respect to a performance upper-bound. The performance upper-bound is obtained by assuming that each time after a sub-band selection decision is made, not only the state of the selected sub-band is revealed, but the states of all other sub-bands are also revealed. Since each time the sub-band selection maximize the immediate reward without affecting information update for the next step, the policy achieves the performance upper-bound for the POMDP solution. Note that this performance upper-bound is commonly used for the optimal POMDP solutions [26, 27]. The normalized accumulated reward is plotted against the random selection interval length. The random selection interval length refers to the average number of steps for which the CR makes a random selection. For instance, when the random selection interval is 100, the CR makes a random selection for every 100 steps on average. In all other time steps, the sub-band selection decisions are made accordingly to the selected policy. Note that the random selection interval length is equivalent to the inverse of the exploration rate ϵ in Q-learning. The trivial random selection policy selects a sub-band randomly and stays in that sub-band until the next time step in which another sub-band is randomly selected.

As shown in Fig. 6.8, the trivial random selection policy can only achieve a 20% of the performance whereas the two direct search methods (using (6.10) and (6.14)), achieve almost 100% of performance when the random selection interval is long (low exploration rate). In this case, the channel Markov model based policy and the sub-band Markov model based policy achieve almost the same performance. This may be explained by the structure of the simulated RF environment: all channels are statistically identical such that the product of the expected average individual channel throughput and the expected number of accessible channels is rather close to the sum of the expected highest throughputs from the expected accessible channels.

As a result, the two different approaches of defining the sub-band qualities does not make a difference.

In the case of the Q-learning, the performance achieves the highest value of 78% when the random selection interval is roughly between 5 and 10, corresponding to an exploration rate in the range from 1/10 to 1/5. The highest performance of the Q-learning technique is achieved when the learning rate $\alpha = 0.25$ and the discount factor $\gamma = 0.8$. Since there is a total of 60 channels, without sufficient exploration (long random selection intervals), the performance of the Q-learning technique degrades. On the other hand, when the exploration rate is too high (very short random selection intervals), the performance degrades as well. Note that this delicate balance between the exploration and exploitation is a well-known aspect of all RL algorithms [100, 104,105]. A detailed performance of the Q-learning based policy for the first test case is shown in Fig. 6.9 for various combinations of the exploration rate ϵ, the learning rate α and the discount factor γ. For all the selected parameter combinations, the highest achieved performance is observed to be 78.03%, which is achieved when when $\epsilon = 1/7$, $\alpha = 0.05$ and $\gamma = 0.2$.

In Fig. 6.10, we show the performance of the sub-band selection policies in the second test case. The performance is normalized with respect to the performance upper-bound as introduced in the first test case. We can see that the trivial random selection method may achieve roughly 65% of the performance whereas the sub-band selection policy using the channel Markov models achieves almost 100% performance at low exploration rate (long random selection interval). The sub-band selection policy using the sub-band Markov models can only achieve roughly 50% with a high exploration rate. The performance difference between the channel Markov model based policy and the sub-band Markov model based policy can be explained as follows. Note that the expected individual channel throughputs are specifically assigned such that in each configuration mode, one of the sub-bands is assumed to have chan-

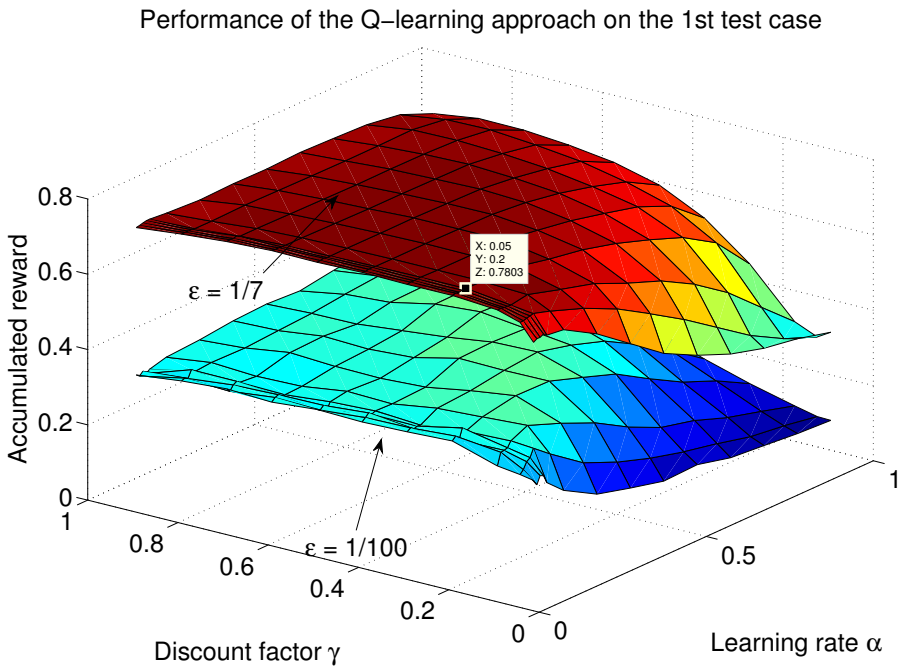

Figure 6.9: Comparison of normalized accumulated reward of the Q-learning-based sub-band selection policy in $10,000$ time steps for the first test case with different Q-learning parameter settings.

nels with the same individual channel throughputs, whereas the other sub-band is assumed to have 2 channels with very high channel throughput and the other 8 channels with very low individual throughputs but the resulting sum throughputs of all individual sub-bands are the same. Also note that the sub-band quality defined in the sub-band Markov model based policy computes the expected sub-band throughput by finding the product of the expected average individual channel throughput and the expected number of accessible channels. On the other hand, the channel Markov model based policy computes the expected sub-band throughput by finding the sum of the expected highest individual channel throughputs of the expected accessible channels. The latter gives a better estimate of the expected sub-band throughputs with the setting of $L = 2$, since the sub-band Markov model based policy sees all

the sub-bands having the same expected sub-band throughput. However, the channels are distinct and the actual communication throughput is much lower in those sub-bands with channels of the same channel throughput, compared to those sub-bands with 2 channels with very high channel throughput. As a result, the channel Markov model based policy gives much better performance compared to the sub-band Markov model based policy. Note that although the channel Markov models based sub-band selection policy may achieve better results, the unavailability of the required knowledge in practical scenarios may prohibit the application of the policy. In this case, using the Q-learning based policy may be a better choice. As shown in Fig. 6.10, the Q-learning based policy is capable of achieving the performance at 90%, when $\alpha = 0.25$, $\gamma = 0.2$, and the exploration rate ϵ between 1/8 and 1/6.

A detailed performance of the Q-learning policy in the second test case is shown in Fig. 6.11 for various combinations of the exploration rate ϵ, the learning rate α and the discount factor γ. For all the selected parameter combinations, the highest achieved performance is observed to be 92.24%, which is achieved when $\epsilon = 1/6$, $\alpha = 0.01$ and $\gamma = 0.5$.

In Fig. 6.12, we show the Q-learning policy for the third test case with real RF measurement data for the $20 - 1500$MHz band, with center frequency at 770 MHz inside a modern office building at Aachen, Germany [114]. The data is the measured values of the power spectrum density (PSD) with a resolution bandwidth of 200kHz taken each second. For simplicity, the communication channels are also considered as spaced at 200kHz and each data point corresponds to a channel [114]. We randomly selected 50 channels over a time duration of 12,000 seconds for the simulation. We assume that the wideband CR has two reconfiguration modes with the first mode contains two sub-bands and the other contains three sub-bands and that each sub-band contains 10 channels as shown in Table. 6.1. The channel occupancies (idle and busy states) are then determined by a thresholding test of the measurement

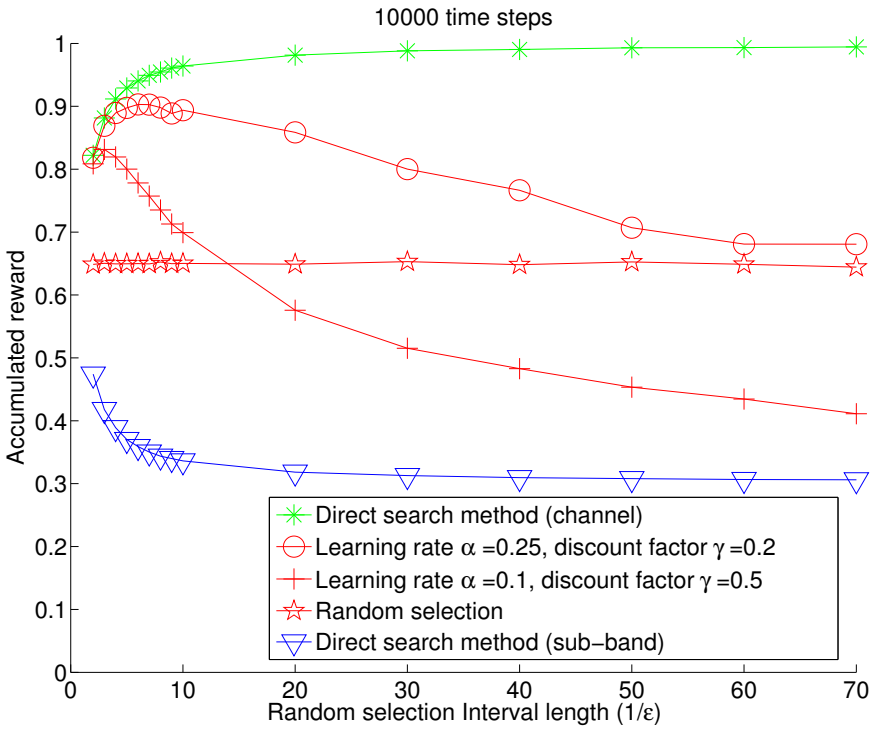

Figure 6.10: Comparison of normalized accumulated reward of sub-band selection policies in 10,000 time steps for the second test case. The considered random selection interval length is set from 2 to 70.

data of each channel, similar to [114]. In this test case, we found that the channel and sub-band state transitions do not exhibit stationary Markov properties. This is found out by performing the built-in Matlab function *hmmestimate* on the data such that different portions of the data (with each portion corresponds to 2,000 seconds of data) give significantly different estimated state transition probabilities. Note that this is similar to the observation in [115] that a simple discrete-time Markov chain model is not able to accurately capture the channel load variations[5]. In this case, in

[5]When the channel is sparsely used (low load), the length of idle periods is significantly higher than that of busy periods. On the other hand, when the channel is subject to an intensive usage (high load), the length of busy periods increases, whereas idle periods

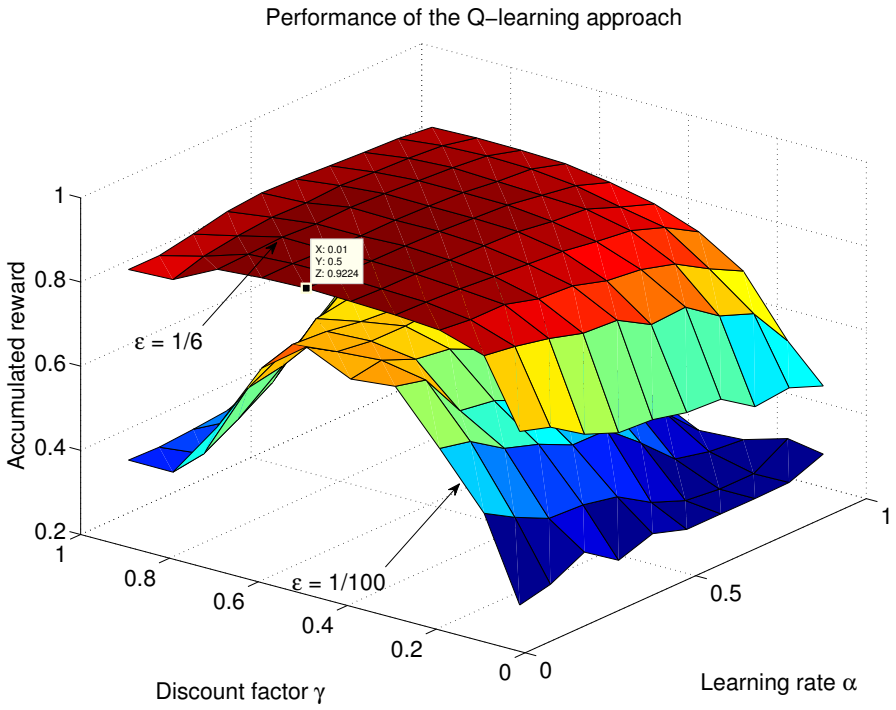

Figure 6.11: Comparison of normalized accumulated reward of the Q-learning-based sub-band selection policy in $10,000$ time steps for the second test case with different Q-learning parameter settings.

order to obtain the performance upper-bound as used in previous two test cases, we obtained the Markov model parameters for the entire data. However, we observed that the Q-learning base policy outperforms the 'upper-bound'. This is due to the non-stationarity of the state dynamics of the measured RF environment and the assumptions of the time-invariant transition probabilities of the channels and sub-bands do not *capture* the non-stationary scenario, so that the obtained performance 'upper-bound' is not a performance upper-bound. As a result, we obtained a loose performance upper-bound by assuming that before a sub-band selection decision is about made, all sub-band and channels states are exactly revealed for the next

become notably shorter.

time step. As shown in Fig. 6.12, the obtained Q-learning policy performance is normalized to the loose upper-bound. A performance of 78.9% is achieved when the exploration rate $\epsilon = 1/6$, the learning rate $\alpha = 0.01$, and the discount factor $\gamma = 0.7$. For comparison, the trivial random selection policy as introduced in the first test case can only achieve a 52% of performance. Due to the space limitation, we do not show the performance of the random selection policy.

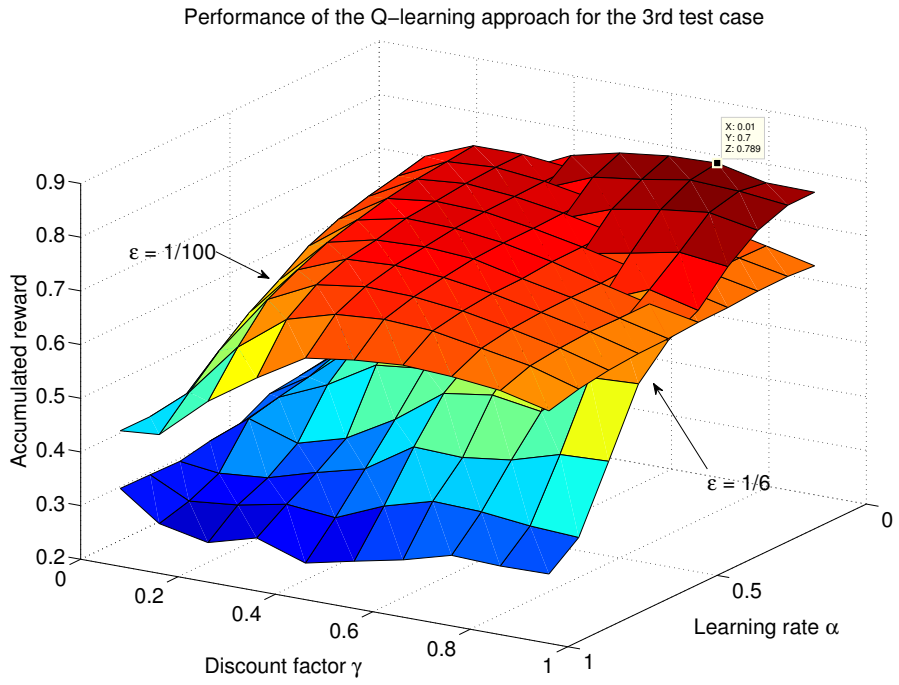

Figure 6.12: Comparison of normalized accumulated reward of the Q-learning-based sub-band selection policy in $12,000$ time steps for the third test case with different Q-learning parameter settings.

In summary, the two Markov-based sub-band selection policies may achieve good results. However, the performance may vary depending on the RF environment. The required Markov knowledge may not be easy to obtain in some cases. On the other hand, the Q-learning policy achieves reasonable results (around $80-90\%$ per-

formance) in all test cases, with a much lower computational effort without any knowledge of the channel/sub-band Markov models. As a result, we validate the application of the Q-learning technique in the wideband spectrum sensing problem. In order to achieve the autonomous operation of the CR in practical RF environments, the CR may adopt a certain Machine-learning technique to fine tune the parameters of the Q-learning method. However, due to the focus of this chapter, the higher level autonomous behavior is out of the scope of this work.

6.6 Chapter Summary

In this chapter, we have investigated a frequency spectrum sensing scheduling problem in a realistic wideband spectrum sensing setup for a CR equipped with a reconfigurable RF front-end with several operation modes to cover a wide frequency range of interest. We assume that within each operation mode, the frequency range is further divided into several frequency sub-bands and that the CR can only perform spectrum sensing in one sub-band at a time. We propose three different sub-band selection policies for the spectrum sensing scheduling problem: 1) a myopic sub-band selection policy based on the channel Markov models; 2) a myopic sub-band selection policy based on the sub-band Markov models; 3) a Q-learning policy without the knowledge of the channel and sub-band Markov models. Realistic RF front-end reconfiguration costs such as energy consumption and time delays are considered. We show that the proposed sub-band selection policies achieve good results comparing to a commonly used performance upper-bound for the POMDP solution. We also show that in both simulated and real measured RF environments, the Q-learning technique may achieve around $80-90\%$ of the performance upper-bound without any knowledge of the RF environment, which validates the Q-learning application in the wideband spectrum sensing problems.

Chapter 7

Summary of the Dissertation and Research Directions

In this dissertation, we have developed the algorithms for spectrum sensing, spectrum sharing, and spectrum decision making for the robust wideband operable autonomous cognitive radios, or the Radiobots. The target Radiobot is targeted to be able to work autonomously in alien wideband RF environments. Although the self-learning and reasoning of the Radiobot is not a major research topic in this dissertation, some machine learning techniques are still present. In the followings, we summarize the main aspects and contributions of this dissertation. We also propose possible research directions that can be addressed in the near future.

7.1 Summary of the Dissertation

In Chapter 2, we proposed the optimal myopic spectrum sensing and access policy in a centralized CR network environment. We also proposed the sub-optimal alternative spectrum sensing policies with low-complexity and performance close to the myopic policy. We also showed that our proposed myopic policies achieve close performance to the optimal solution when considered under a POMDP formulation. A Hidden Markov model based parameter estimation algorithm is also proposed to estimate the channel Markov properties with linear computation complexity. This parameter estimation algorithm is assumed to be used when the channel Markov knowledge is absent.

In Chapter 3, we proposed the non-parametric cyclostationarity-based signal feature extraction algorithm. The proposed feature extraction algorithm is able to extract multiple superposed RF signals and distinguish signal cyclostationary feature for different signals. The proposed feature extraction algorithm assumes no prior knowledge of the signals, unlike the existing similar algorithms in the literature. We also analytically evaluated the robustness of the proposed feature extraction algorithm under channel fading, and Doppler effects. The proposed algorithm is also used in the multivariate non-parametric quickest detection algorithm proposed in Chapter 4.

In Chapter 4, we proposed the average sample power and cyclostationarity-based multivariate non-parametric quickest detection algorithm. The proposed quickest detection algorithm is assumed to be used when the Radiobot encounters an alien RF environment. We also proposed the parallel on-line quickest detection/off-line change-point detection algorithm that is used to achieve self-awareness of the detection delays and false alarm rates. The knowledge of the achieved detection delays and false alarm rates may help the Radiobot to perform self performance evaluation

in order to achieve higher level of autonomous in conjunction with machine learning techniques. We also show that the multivariate non-parametric quickest detection algorithm has a comparable computation complexity to the uni-variate case, when only the average sample power feature is used as in other existing solutions in the literature. The simulation shows that the proposed multivariate quickest detection algorithm outperforms the energy-based uni-variate case, in terms of the detection delays and the utilization of spectrum opportunities.

In Chapter 5, we proposed a cognitive radio PHY/MAC decision-making strategy for wideband bandwidth aggregation. A multi-objective optimization problem is formulated with the objectives being the communication throughput and energy consumption of the Radiobot device. The proposed multi-objective optimization problem takes into account the practical concerns on imperfect spectrum sensing, time varying channel conditions, hardware reconfiguration time delay, hardware reconfiguration power consumptions, and communication energy consumptions. The optimal wideband bandwidth aggregation problem is solved using a combination of the Hungarian algorithm and convex optimization. We showed that by self-adjusting the weighting coefficients of the objectives, the Radiobot may achieve autonomous operation. The formulation can also be easily extended to similar optimization problems with more than two objectives.

Finally, in Chapter 6, we proposed the wideband spectrum sensing scheduling solutions for cognitive radios that are equipped with reconfigurable RF front-ends. Multiple sub-band selection solutions are proposed by assuming different RF environment knowledges. The sub-band selection solutions are designed for better finding spectrum opportunities across an ultra-wideband RF environment. The proposed solutions take into account realistic hardware reconfiguration overheads. We also proposed a Q-learning based sub-band selection solution to reduce the computational complexity. Performance of the proposed solutions are compared with

a performance upper-bound of the optimal solution form the POMDP formulation. The Q-learning based sub-band selection solution is validated by showing that it can achieve good performance through numerical results in both simulated and real measured RF environments.

7.2 Future Research Directions

The work that is presented in this dissertation can be extended along several directions, focusing on either spectrum sensing or decision-making applications.

7.2.1 Channel Dynamic Model Recognition

To achieve the robustness of the Radiobot operations in heterogeneous RF environments and to improve the spectrum utilization efficiency, the suggested future work under this research direction is summarized in the following:

- Designing the general algorithm for distinguishing various stochastic models for RF channels under the assumptions of general arbitrary sensing durations and sensing intervals, and the realistic channel modeling by taking into account the channel fading, shadowing, Doppler effects, etc.
- Designing the algorithm for stochastic model parameter estimation with the consideration of the models are in general non-stationary by using time discount factors for the observation history.
- Designing the decision rule to determine the optimized (minimizing the model recognition as well as the parameter estimation errors) time discount factor for the non-stationarity of the channel dynamics.

7.2.2 Cooperative Communications of the Radiobots

The suggested future work under this research direction is summarized in the following:

- Extension of the PHY/MAC decision making for various QoS requirements in a network of Radiobots with communication cooperations such as relaying each others messages.
- Protocol for spectrum sensing cooperations, such as decentralized partial network decision fusion, with realistic channel modeling.
- Exploit spacial diversity of multiple Radiobots to perform blind signal separation (BSS) in order to better perform feature extraction and classification.
- Analysis of the tradeoff between the cooperations in spectrum sensing overhead and the spectrum efficiency, as well as the communication throughput.
- Integration of the non-supervised machine learning based algorithms to ensure the cognitive feature and to lower the decision-making computation complexities.

References

[1] P. August and M. A. Mchenry, "Nsf spectrum occupancy measurements project summary," *Spectrum*, 2005.

[2] M. A. McHenry, P. A. Tenhula, D. McCloskey, D. A. Roberson, and C. S. Hood, "Chicago spectrum occupancy measurements & analysis and a long-term studies proposal," *Proceedings of the first international workshop on Technology and policy for accessing spectrum TAPAS 06*, 2006. [Online]. Available: http://portal.acm.org/citation.cfm?doid=1234388.1234389

[3] J. Mitola III and G. Q. Maguire, Jr., "Cognitive radio: making software radios more personal," *IEEE Personal Communications*, vol. 6, no. 4, pp. 13 –18, Aug. 1999.

[4] "IEEE-USA President Commends FCC for National Broadband Plan [IEEE;USA]," *IEEE Antennas and Propagation Magazine*, vol. 52, no. 2, p. 179, April 2010.

[5] J. Wang, M. Ghosh, and K. Challapali, "Emerging cognitive radio applications: A survey," *Communications Magazine, IEEE*, vol. 49, no. 3, pp. 74 –81, march 2011.

[6] S. K. Jayaweera and C. G. Christodoulou, "Radiobots: Architecture, algorithms and realtime reconfigurable antenna designs for autonomous, self-learning future cognitive radios," University of New Mexico, Technical Report EECE-TR-11-0001, Mar. 2011. [Online]. Available: http://repository.unm.edu/handle/1928/12306

[7] M. Bkassiny, S. K. Jayaweera, Y. Li, and K. A. Avery, "Wideband spectrum sensing and non-parametric signal classification for autonomous self-learning cognitive radios," *IEEE Transactions on Wireless Communications*, pp. 2596 – 2605, Aug. 2011.

[8] S. Jayaweera, Y. Li, M. Bkassiny, C. Christodoulou, and K. Avery, "Radiobots: The autonomous, self-learning future cognitive radios," in *International Symposium on Intelligent Signal Processing and Communications Systems (ISPACS '11)*, Chiangmai, Thailand, Dec. 2011, pp. 1 –5.

[9] C. Christodoulou, Y. Tawk, and S. Jayaweera, "Cognitive radio, reconfigurable antennas, and Radiobots," in *2012 IEEE International Workshop on Antenna Technology (iWAT), Tucson, Arizona, USA*, March 2012, pp. 16 –19.

[10] Y. Li, S. Jayaweera, and C. Christodoulou, "Wideband PHY/MAC bandwidth aggregation optimization for cognitive radios," in *Cognitive Information Processing (CIP), 2012 3rd International Workshop on*, May 2012.

[11] M. Bkassiny, S. K. Jayaweera, Y. Li, and K. A. Avery, "Blind cyclostationary feature detection based spectrum sensing for Autonomous self-learning cognitive radios," in *IEEE International Conference on Communications (ICC '12), Ottawa, Canada,*, June 2012.

[12] S. Haykin, D. Thomson, and J. Reed, "Spectrum sensing for cognitive radio," *Proceedings of the IEEE*, vol. 97, no. 5, pp. 849 –877, May. 2009.

[13] T. Yucek and H. Arslan, "A survey of spectrum sensing algorithms for cognitive radio applications," *IEEE Communications Surveys Tutorials*, vol. 11, no. 1, pp. 116–130, Mar. 2009.

[14] K. Ben Letaief and W. Zhang, "Cooperative communications for cognitive radio networks," *Proceedings of the IEEE*, vol. 97, no. 5, pp. 878 –893, May 2009.

[15] J. Ma, G. Y. Li, and B. H. Juang, "Signal processing in cognitive radio," *Proceedings of the IEEE*, vol. 97, no. 5, pp. 805–823, May 2009.

[16] W. Zhang, R. Mallik, and K. Letaief, "Optimization of cooperative spectrum sensing with energy detection in cognitive radio networks," *IEEE Transactions on Wireless Communications*, vol. 8, no. 12, pp. 5761 –5766, Dec. 2009.

[17] Y. M. Kim, G. Zheng, S. H. Sohn, and J. M. Kim, "An alternative energy detection using sliding window for cognitive radio system," in *10th International Conference on Advanced Communication Technology (ICACT '08)*, vol. 1, Gangwon-Do, South Korea, Feb. 2008, pp. 481 –485.

[18] A. Dandawate and G. Giannakis, "Statistical tests for presence of cyclostationarity," *IEEE Transactions on Signal Processing*, vol. 42, no. 9, pp. 2355 –2369, Sep. 1994.

[19] B. Deepa, A. Iyer, and C. Murthy, "Cyclostationary-based architectures for spectrum sensing in IEEE 802.22 WRAN," in *IEEE Global Telecommunications Conference (GLOBECOM '10)*, Miami, FL, Dec. 2010, pp. 1 –5.

[20] Y. Zeng and Y. Liang, "Covariance based signal detections for cognitive radio," in *2nd IEEE International Symposium on New Frontiers in Dynamic Spectrum Access Networks (DySPAN '07)*, Apr. 2007, pp. 202–207.

[21] R. D. Smallwood and E. J. Sondik, "The optimal control of partially observable Markov processes over a finite horizon," *Operations Research*, vol. 21, no. 5, pp. 1071 –1088, Sept.-Oct. 1973.

[22] S. Ahmad, M. Liu, T. Javidi, Q. Zhao, and B. Krishnamachari, "Optimality of Myopic Sensing in Multichannel Opportunistic Access," *Information Theory, IEEE Transactions on*, vol. 55, no. 9, pp. 4040 –4050, Sept. 2009.

[23] Q. Zhao, B. Krishnamachari, and K. Liu, "On myopic sensing for multi-channel opportunistic access: Structure, optimality, and performance," *IEEE Transactions on Wireless Communications*, vol. 7, no. 12, pp. 5431 –5440, Dec. 2008.

[24] S. Ahmad and M. Liu, "Multi-channel opportunistic access: A case of restless bandits with multiple plays," in *Communication, Control, and Computing, 2009. Allerton 2009. 47th Annual Allerton Conference on*, Oct. 2009, pp. 1361 –1368.

[25] K. Liu, Q. Zhao, and B. Krishnamachari, "Dynamic multichannel access with imperfect channel state detection," *Signal Processing, IEEE Transactions on*, vol. 58, no. 5, pp. 2795 –2808, May 2010.

[26] J. Unnikrishnan and V. Veeravalli, "Algorithms for dynamic spectrum access with learning for cognitive radio," *IEEE Transactions on Signal Processing*, vol. 58, no. 2, pp. 750 –760, Feb. 2010.

[27] Y. Li, S. Jayaweera, M. Bkassiny, and K. Avery, "Optimal myopic sensing and dynamic spectrum access in cognitive radio networks with low-complexity implementations," *IEEE Transactions on Wireless Communications*, vol. 11, no. 7, pp. 2412 –2423, July 2012.

[28] M. Duarte and A. Sabharwal, "Full-duplex wireless communications using off-the-shelf radios: Feasibility and first results," in *2010 Conference Record of the Forty Fourth Asilomar Conference on Signals, Systems and Computers (ASILOMAR), Monterey, California, USA*, Nov. 2010, pp. 1558 –1562.

[29] J. I. Choi, M. Jain, K. Srinivasan, P. Levis, and S. Katti, "Achieving single channel, full duplex wireless communication," in *Proceedings of the sixteenth annual international conference on Mobile computing and networking*, ser. MobiCom '10. New York, NY, USA: ACM, 2010, pp. 1–12. [Online]. Available: http://doi.acm.org/10.1145/1859995.1859997

[30] M. Jain, J. I. Choi, T. Kim, D. Bharadia, S. Seth, K. Srinivasan, P. Levis, S. Katti, and P. Sinha, "Practical, real-time, full duplex wireless," in *The 17th Annual International Conference on Mobile Computing and Networking (MOBICOM), Las Vegas, Nevada, USA*, 2011, pp. 301–312.

[31] M. Knox, "Single antenna full duplex communications using a common carrier," in *2012 IEEE 13th Annual Wireless and Microwave Technology Conference (WAMICON), Cocoa Beach, FL, USA*, April 2012, pp. 1 –6.

[32] K. Chebrolu and R. Rao, "Bandwidth aggregation for real-time applications in heterogeneous wireless networks," *IEEE Transactions on Mobile Computing*, vol. 5, no. 4, pp. 388 – 403, April 2006.

[33] M. Vuran and I. Akyildiz, "A-mac: Adaptive medium access control for next generation wireless terminals," *IEEE/ACM Transactions on Networking*, vol. 15, no. 3, pp. 574 –587, June 2007.

[34] M.-F. Tsai, N. Chilamkurti, J. Park, and C.-K. Shieh, "Multi-path transmission control scheme combining bandwidth aggregation and packet scheduling for real-time streaming in multi-path environment," *IET, Communications*, vol. 4, no. 8, pp. 937 –945, 21 2010.

[35] B. Gao, Y. Yang, and J.-M. Park, "Channel aggregation in cognitive radio networks with practical considerations," in *2011 IEEE International Conference on Communications (ICC)*, June 2011, pp. 1 –5.

[36] J. Lee and J. So, "Analysis of cognitive radio networks with channel aggregation," in *2010 IEEE Wireless Communications and Networking Conference (WCNC)*, April 2010, pp. 1 –6.

[37] F. Huang, W. Wang, H. Luo, G. Yu, and Z. Zhang, "Prediction-based spectrum aggregation with hardware limitation in cognitive radio networks," in *2010 IEEE 71st Vehicular Technology Conference (VTC 2010-Spring)*, May 2010, pp. 1 –5.

[38] M. Iwamura, K. Etemad, M.-H. Fong, R. Nory, and R. Love, "Carrier aggregation framework in 3GPP LTE-advanced [WiMAX/LTE Update]," *IEEE Communications Magazine*, vol. 48, no. 8, pp. 60 –67, Aug. 2010.

[39] H. Wang, C. Rosa, and K. Pedersen, "Uplink component carrier selection for LTE-Advanced systems with carrier aggregation," in *2011 IEEE International Conference on Communications (ICC)*, June 2011, pp. 1 –5.

[40] F. Sanchez-Moya, J. Villalba-Espinosa, L. Garcia, K. Pedersen, and P. Mogensen, "On the impact of explicit uplink information on autonomous component carrier selection for lte-a femtocells," in *Vehicular Technology Conference (VTC Spring), 2011 IEEE 73rd*, May 2011, pp. 1 –5.

[41] S. Yasukawa, T. Kawamura, Y. Kishiyama, H. Taoka, and T. Nakamura, "Experimental evaluation on su-mimo transmission with closed-loop precoding in lte-advanced uplink," in *Vehicular Technology Conference (VTC Spring), 2011 IEEE 73rd*, May 2011, pp. 1 –5.

[42] Y. Chen, Q. Zhao, and A. Swami, "Distributed spectrum sensing and access in cognitive radio networks with energy constraint," *IEEE Transactions on Signal Processing*, vol. 57, no. 2, pp. 783–797, 2009.

[43] E. J. Sondik, "The optimal control of partially observable markov processes over the infinite horizon: Discounted costs," *Operations Research*, vol. 26, no. 2, pp. pp. 282–304, Mar.-Apr. 1978.

[44] Y. Pei, Y.-C. Liang, K. Teh, and K. H. Li, "How much time is needed for wideband spectrum sensing?" *IEEE Transactions on Wireless Communications*, vol. 8, no. 11, pp. 5466–5471, 2009.

[45] M. Bkassiny, S. Jayaweera, Y. Li, and K. Avery, "Wideband Spectrum Sensing and Non-Parametric Signal Classification for Autonomous Self-Learning Cognitive Radios," *IEEE Transactions on Wireless Communications*, vol. 11, no. 7, pp. 2596–2605, 2012.

[46] Y. Tawk, J. Costantine, and C. Christodoulou, "A rotatable reconfigurable antenna for cognitive radio applications," in *2011 IEEE Radio and Wireless Symposium (RWS)*, Jan. 2011.

[47] Y. Tawk, M. Bkassiny, G. El-Howayek, S. Jayaweera, K. Avery, and C. Christodoulou, "Reconfigurable front-end antennas for cognitive radio applications," *IET Microwaves, Antennas Propagation*, Jan. 2011.

[48] J. W. Kim, M. Chu, P. Jacob, A. Zia, R. Kraft, and J. McDonald, "Reconfigurable 40 ghz bicmos uniform delay crossbar switch for broadband and wide tuning range narrowband applications," *IET Circuits, Devices Systems*, vol. 5, no. 3, pp. 159–169, 2011.

[49] J. Papapolymerou, K. Lange, C. Goldsmith, A. Malczewski, and J. Kleber, "Reconfigurable double-stub tuners using mems switches for intelligent rf front-ends," *IEEE Transactions on Microwave Theory and Techniques*, vol. 51, no. 1, pp. 271–278, 2003.

[50] M. D. Holland, "A nonparametric change point model for multivariate phase-II statistical process control," Ph.D. dissertation, 2011.

[51] E. N. Gilbert, "Capacity of a burst-noise channel," *Bell System Technical Journal*, vol. 39, pp. 1253–1265, Sept. 1960.

[52] Y. Chen, Q. Zhao, and A. Swami, "Joint design and separation principle for opportunistic spectrum access in the presence of sensing errors," *IEEE Transactions on Information Theory*, vol. 54, no. 5, pp. 2053 –2071, May 2008.

[53] Q. Zhao, L. Tong, A. Swami, and Y. Chen, "Decentralized cognitive mac for opportunistic spectrum access in ad hoc networks: A pomdp framework," *IEEE Journal on Selected Areas in Communications*, vol. 25, no. 3, pp. 589 –600, Apr. 2007.

[54] Z. Lu, Y. Ma, and R. Tafazolli, "A first-order cyclostationarity based energy detection approach for non-cooperative spectrum sensing," in *Personal Indoor and Mobile Radio Communications (PIMRC), 2010 IEEE 21st International Symposium on*, Sept. 2010, pp. 554 –559.

[55] "IEEE Standard for Information Technology–Telecommunications and information exchange between systems Wireless Regional Area Networks (WRAN)–Specific requirements Part 22: Cognitive Wireless RAN Medium Access Control (MAC) and Physical Layer (PHY) Specifications: Policies and Procedures for Operation in the TV Bands," *IEEE Std 802.22-2011*, pp. 1 –680, 1 2011.

[56] H. V. Poor, *An Introduction to Signal Detection and Estimation*, 2nd ed. New York, NY, USA: Springer-Verlag, 1994.

[57] A. Sahai, N. Hoven, and R. Tandra, "Some Fundamental Limits on Cognitive Radio," in *in Forty-second Allerton Conference on Communication, Control, and Computing*, 2004.

[58] M. Bkassiny and S. K. Jayaweera, "Optimal channel and power allocation for secondary users in cooperative cognitive radio networks," in *Special Session on Advanced Radio Access Techniques for Energy-Efficient Communications in 2nd International Conference on Mobile Lightweight Wireless Systems*, Barcelona, Spain, May 2010.

[59] D. Li and X. Sun, *Nonlinear Integer Programming*, 1st ed. Springer, 2010.

[60] H. W. Kuhn, "The Hungarian method for the assignment problem," *Naval Research Logistics Quarterly*, vol. 2, pp. 83–97, Mar. 1955.

[61] L. Rabiner, "A tutorial on hidden Markov models and selected applications in speech recognition," *Proceedings of the IEEE*, vol. 77, no. 2, pp. 257 –286, Feb 1989.

[62] J. Baker, "The dragon system–an overview," *Acoustics, Speech and Signal Processing, IEEE Transactions on*, vol. 23, no. 1, pp. 24 – 29, Feb 1975.

[63] L. E. Baum and G. R. Sell, "Growth functions for transformations on manifolds," *Pac. J. Math.*, vol. 23, no. 2, pp. 211 – 227, 1968.

[64] W. Gardner, "Measurement of spectral correlation," *IEEE Transactions on Acoustics, Speech and Signal Processing*, vol. 34, no. 5, pp. 1111 – 1123, Oct. 1986.

[65] M. Bkassiny, S. K. Jayaweera, Y. Li, and K. A. Avery, "Blind cyclostationary feature detection based spectrum sensing for autonomous self-learning cognitive radios," in *IEEE International Conference on Communications (ICC '12)*, Ottawa, Canada, June 2012.

[66] F. Millioz and N. Martin, "Estimation of a white gaussian noise in the short time fourier transform based on the spectral kurtosis of the minimal statistics: Application to underwater noise," in *IEEE International Conference on Acoustics Speech and Signal Processing (ICASSP '10)*, Dallas, TX, Mar. 2010, pp. 5638 –5641.

[67] A. Sonnenschein and P. Fishman, "Radiometric detection of spread-spectrum signals in noise of uncertain power," *IEEE Transactions on Aerospace and Electronic Systems*, vol. 28, no. 3, pp. 654 –660, July 1992.

[68] B. Shent, L. Huang, C. Zhao, Z. Zhou, and K. Kwak, "Energy detection based spectrum sensing for cognitive radios in noise of uncertain power," in *International Symposium on Communications and Information Technologies (ISCIT '08)*, Vientiane, Lao PDR, Oct. 2008, pp. 628 –633.

[69] O. Setter, M. Sharir, and D. Halperin, "Constructing two-dimensional voronoi diagrams via divide-and-conquer of envelopes in space," in *Sixth International Symposium on Voronoi Diagrams (ISVD '09)*, Copenhagen, Denmark, June 2009, pp. 43 –52.

[70] W. Gardner, W. Brown, and C.-K. Chen, "Spectral correlation of modulated signals: Part ii–digital modulation," *IEEE Transactions on Communications*, vol. 35, no. 6, pp. 595 – 601, June 1987.

[71] W. A. Gardner", *Introduction to Random Processes: With Applications to Signals and Systems*, 2nd ed. "New York: McGraw-Hill", 1990.

[72] J. Parsons and A. Bajwa, "Wideband characterisation of fading mobile radio channels," *Communications, Radar and Signal Processing, IEE Proceedings F*, vol. 129, no. 2, p. 95, April 1982.

[73] M. Patzold, *Mobile Fading Channels*, 1st ed. John Wiley & Sons, Ltd, 2002.

[74] D.-S. Yoo and W. Stark, "Characterization of WSSUS channels: Normalized mean square covariance," *IEEE Transactions on Wireless Communications*, vol. 4, no. 4, pp. 1575 – 1584, July 2005.

[75] P. Hoeher, "A statistical discrete-time model for the WSSUS multipath channel," *IEEE Transactions on Vehicular Technology*, vol. 41, no. 4, pp. 461 –468, Nov. 1992.

[76] K.-W. Yip and T.-S. Ng, "Discrete-time model for digital communications over a frequency-selective Rician fading WSSUS channel," *Communications, IEE Proceedings-*, vol. 143, no. 1, pp. 37 –42, Feb. 1996.

[77] W. Gardner, A. Napolitano, and L. Paura, "Cyclostationarity: Half a century of research," *Signal Processing*, vol. 86, no. 4, pp. 639–697, Apr. 2006. [Online]. Available: http://dx.doi.org/10.1016/j.sigpro.2005.06.016

[78] H. V. Poor and O. Hadjiliadis, *Quickest Detection*. Cambridge University Press, 2008. [Online]. Available: http://dx.doi.org/10.1017/CBO9780511754678

[79] L. Lai, Y. Fan, and H. Poor, "Quickest detection in cognitive radio: A sequential change detection framework," in *2008 IEEE Global Telecommunications Conference (GLOBECOM), New Orleans, Louisiana, USA*, Dec. 2008, pp. 1 –5.

[80] S. Geirhofer, L. Tong, and B. Sadler, "A Measurement-Based Model for Dynamic Spectrum Access in WLAN Channels," in *2006 IEEE Military Communications Conference, 2006 (MILCOM)*, oct. 2006, pp. 1 –7.

[81] E. S. Page, "Continuous Inspection Schemes," *Biometrika*, vol. 41, no. 1/2, pp. 100–115, 1954. [Online]. Available: http://dx.doi.org/10.2307/2333009

[82] L. Gordon and M. Pollak, "A robust surveillance scheme for stochastically ordered alternatives," *Annals of Statistics*, vol. 23, pp. 1350 – 1375, Aug. 1995.

[83] K. Choi and J. Marden, "An approach to multivariate rank tests in multivariate analysis of variance," *Journal of the American Statistical Association*, vol. 92, no. 440, pp. pp. 1581–1590, 1997. [Online]. Available: http://www.jstor.org/stable/2965429

[84] M. Bkassiny, Y. Li, and S. Jayaweera, "A Survey on Machine-Learning Techniques in Cognitive Radios," *IEEE Communications Surveys Tutorials,*, vol. PP, no. 99, pp. 1 –24, 2012.

[85] M. Jain, J. I. Choi, T. Kim, D. Bharadia, S. Seth, K. Srinivasan, P. Levis, S. Katti, and P. Sinha, "Practical, real-time, full duplex wireless," in *Proceedings of the 17th annual international conference on Mobile computing and networking*, ser. MobiCom '11. New York, NY, USA: ACM, 2011, pp. 301–312. [Online]. Available: http://doi.acm.org/10.1145/2030613.2030647

[86] S. Geirhofer, L. Tong, and B. Sadler, "A measurement-based model for dynamic spectrum access in wlan channels," in *Military Communications Conference, 2006. MILCOM 2006. IEEE*, oct. 2006, pp. 1 –7.

[87] S. Kotz and S. Nadarajah, *Extreme value distributions: theory and applications*. Imperial College Press, 2000. [Online]. Available: http://books.google.com/books?id=b40P_o3yXuUC

[88] H. Kim and K. Shin, "Efficient discovery of spectrum opportunities with mac-layer sensing in cognitive radio networks," *Mobile Computing, IEEE Transactions on*, vol. 7, no. 5, pp. 533 –545, may 2008.

[89] J. Cavers, "An analysis of pilot symbol assisted modulation for rayleigh fading channels [mobile radio]," *Vehicular Technology, IEEE Transactions on*, vol. 40, no. 4, pp. 686 –693, nov 1991.

[90] L. Tong, B. Sadler, and M. Dong, "Pilot-assisted wireless transmissions: general model, design criteria, and signal processing," *Signal Processing Magazine, IEEE*, vol. 21, no. 6, pp. 12 – 25, nov. 2004.

[91] H. W. Kuhn, "The Hungarian method for the assignment problem," *Naval Research Logistics Quarterly*, vol. 2, no. 1-2, pp. 83–97, 1955. [Online]. Available: http://dx.doi.org/10.1002/nav.3800020109

[92] C. H. Papadimitriou and K. Steiglitz, *Combinatorial Optimization : Algorithms and Complexity*. Dover Publications, Jul. 1998.

[Online]. Available: http://www.amazon.com/exec/obidos/redirect?tag=citeulike07-20\&path=ASIN/0486402584

[93] Y.-J. Choi, J. Kim, and S. Bahk, "Downlink scheduling with fairness and optimal antenna assignment for mimo cellular systems," in *Global Telecommunications Conference, 2004. GLOBECOM '04. IEEE*, vol. 5, nov.-3 dec. 2004, pp. 3165 – 3169 Vol.5.

[94] S. Haykin, "Cognitive radio: brain-empowered wireless communications," *IEEE Journal on Selected Areas in Communications*, vol. 23, no. 2, pp. 201–220, Feb. 2005.

[95] J. Mitola, "Cognitive radio architecture evolution," *Proceedings of the IEEE*, vol. 97, no. 4, pp. 626 –641, Apr. 2009.

[96] E. Biglieri, "Effect of uncertainties in modeling interferences in coherent and energy detectors for spectrum sensing," in *IEEE International Symposium on Information Theory Proceedings (ISIT '11)*, Aug. 2011, pp. 2418 –2421.

[97] Z. Tian and G. B. Giannakis, "A wavelet approach to wideband spectrum sensing for cognitive radios," in *1st International Conference on Cognitive Radio Oriented Wireless Networks and Communications*, Mykonos Island, Greece, June 2006, pp. 1–5.

[98] Z. Tian and G. Giannakis, "Compressed sensing for wideband cognitive radios," in *IEEE International Conference on Acoustics, Speech and Signal Processing (ICASSP '07)*, vol. 4, Honolulu, HI, Apr. 2007, pp. IV–1357 –IV–1360.

[99] S. Maleki, A. Pandharipande, and G. Leus, "Two-stage spectrum sensing for cognitive radios," in *IEEE International Conference on Acoustics Speech and Signal Processing (ICASSP '10)*, Dallas, TX, Mar. 2010, pp. 2946 –2949.

[100] M. Bkassiny, S. K. Jayaweera, and K. A. Avery, "Distributed Reinforcement Learning based MAC protocols for autonomous cognitive secondary users," in *20th Annual Wireless and Optical Communications Conference (WOCC '11)*, Newark, NJ, Apr. 2011, pp. 1 –6.

[101] Y. Li, S. K. Jayaweera, M. Bkassiny, and K. A. Avery, "Optimal myopic sensing and dynamic spectrum access with low-complexity implementations," in *IEEE Vehicular Technology Conference (VTC-spring '11)*, Budapest, Hungary, May 2011.

[102] M. Bkassiny, S. K. Jayaweera, Y. Li, and K. A. Avery, "Optimal and low-complexity algorithms for dynamic spectrum access in centralized cognitive

radio networks with fading channels," in *IEEE Vehicular Technology Conference (VTC-spring '11)*, Budapest, Hungary, May 2011.

[103] C. Ghosh, S. Roy, and M. B. Rao, "Modeling and validation of channel idleness and spectrum availability for cognitive networks," *IEEE Journal on Selected Areas in Communications*, Nov. 2012.

[104] R. S. Sutton and A. G. Barto, *Reinforcement Learning: An Introduction*. Cambridge, MA: MIT Press, 1998.

[105] C. Watkins, "Learning from delayed rewards," Ph.D. dissertation, University of Cambridge, United Kingdom, 1989.

[106] Y. Reddy, "Detecting Primary Signals for Efficient Utilization of Spectrum Using Q-Learning," in *Fifth International Conference on Information Technology: New Generations (ITNG '08)*, Las Vegas, NV, Apr. 2008, pp. 360 –365.

[107] H. Li, "Multi-agent Q-learning of channel selection in multi-user cognitive radio systems: A two by two case," in *IEEE International Conference on Systems, Man and Cybernetics (SMC '09)*, San Antonio, TX, Oct. 2009, pp. 1893 –1898.

[108] A. Galindo-Serrano and L. Giupponi, "Distributed Q-Learning for Aggregated Interference Control in Cognitive Radio Networks," *IEEE Transactions on Vehicular Technology*, vol. 59, no. 4, pp. 1823 –1834, May 2010.

[109] M. L. Littman, A. R. Cassandra, and L. P. Kaelbling, "Learning Policies for Partially Observable Environments: Scaling Up," *Readings in agents*, pp. 495–503, 1998.

[110] J. Aruz, "Discrete rayleigh fading channel modeling," *Wireless Communications and Mobile Computing 2004*, vol. 4, pp. 413–425, 2004.

[111] J. C.-I. Chuang and N. Sollenberger, "Spectrum resource allocation for wireless packet access with application to advanced cellular internet service," *IEEE Journal on Selected Areas in Communications*, Aug. 1998.

[112] Y. Li and S. K. Jayaweera, "Dynamic spectrum tracking using energy and cyclostationarity-based multi-variate non-parametric quickest detection for cognitive radios," *IEEE Transactions on Wireless Communications*, vol. 12, no. 7, pp. 3522–3532, 2013.

[113] L. Luo, N. Neihart, S. Roy, and D. Allstot, "A two-stage sensing technique for dynamic spectrum access," *IEEE Transactions on Wireless Communications*, vol. 8, no. 6, pp. 3028–3037, 2009.

[114] M. Wellens and P. Mahonen, "Lessons learned from an extensive spectrum occupancy measurement campaign and a stochastic duty cycle model," in *5th International Conference on Testbeds and Research Infrastructures for the Development of Networks Communities and Workshops (TridentCom), 2009, Washington DC, USA*, 2009, pp. 1–9.

[115] M. Lopez-Benitez and F. Casadevall, "Empirical Time-Dimension Model of Spectrum Use Based on a Discrete-Time Markov Chain With Deterministic and Stochastic Duty Cycle Models," *IEEE Transactions on Vehicular Technology*, vol. 60, no. 6, pp. 2519–2533, 2011.